

Markus Gerke

**Automatic Quality Assessment of Road Databases
Using Remotely Sensed Imagery**

München 2006

**Verlag der Bayerischen Akademie der Wissenschaften
in Kommission beim Verlag C. H. Beck**

ISSN 0065-5325

ISBN 3 7696 5038 7

**Diese Arbeit ist gleichzeitig veröffentlicht in:
Wissenschaftliche Arbeiten der Fachrichtung Geodäsie und Geoinformatik der Universität Hannover
ISSN 0174-1454, Nr. 261, Hannover 2006**

Automatic Quality Assessment of Road Databases
Using Remotely Sensed Imagery

Von der Fakultät für Bauingenieurwesen und Geodäsie
der Universität Hannover
zur Erlangung des Grades
Doktor-Ingenieur (Dr.-Ing.)
genehmigte Dissertation

von

Dipl.-Ing. Markus Gerke

München 2006

Verlag der Bayerischen Akademie der Wissenschaften
in Kommission bei der C. H. Beck'schen Verlagsbuchhandlung München

ISSN 0065-5325

ISBN 3 7696 5038 7

Diese Arbeit ist gleichzeitig veröffentlicht in:
Wissenschaftliche Arbeiten der Fachrichtung Geodäsie und Geoinformatik der Universität Hannover
ISSN 0174-1454, Nr. 261, Hannover 2006

Adresse der Deutschen Geodätischen Kommission:

Deutsche Geodätische Kommission

Alfons-Goppel-Straße 11 • D – 80 539 München

Telefon +49 - (0)89 - 23 031 -0 / -1113 • Telefax +49 - (0)89 - 23 031 -1283 / -1100

E-mail hornik@dgfi.badw.de • <http://dgk.badw.de>

Prüfungskommission

Referent: Univ.-Prof. Dr.-Ing. Christian Heipke

Korreferenten: Univ.-Prof. Dr.-Ing. Helmut Mayer

Univ.-Prof. Dr.-Ing. Claus-Eberhard Liedtke

Gutachter: Univ.-Prof. Dr.-Ing. Dietmar Grünreich

Tag der mündlichen Prüfung: 09.06.2006

© 2006 Deutsche Geodätische Kommission, München

Alle Rechte vorbehalten. Ohne Genehmigung der Herausgeber ist es auch nicht gestattet,
die Veröffentlichung oder Teile daraus auf photomechanischem Wege (Photokopie, Mikrokopie) zu vervielfältigen

ISSN 0065-5325

ISBN 3 7696 5038 7

Where you end up isn't the most important thing. It's the road you take to get you there. – Tim Wile

Kurzfassung

In dieser Arbeit wird ein neuer Ansatz zur automatischen Qualitätsbewertung bestehender räumlicher Vektordaten vorgestellt. Die notwendige Referenzinformation wird mit Hilfe von Bildanalyseverfahren aus aktuellen Fernerkundungsdaten gewonnen. Der Schwerpunkt liegt auf der Qualitätsbewertung von Straßen, da diese zu den sich am häufigsten verändernden Objekten in der Landschaft zählen. Im Gegensatz zu bereits existierenden Ansätzen zur automatischen Qualitätskontrolle von Straßendaten wird hier eine durchgängige statistische Modellierung und Verarbeitung sowohl der gegebenen Straßenobjekte als auch der automatisch aus Bildern extrahierten Objekte durchgeführt.

Es wird ein geometrisch-topologisches Relationenmodell für Straßen und ihre Umgebung definiert. Die Nachbarschaftsobjekte (Kontextobjekte, z.B. Baumreihen) unterstützen die Qualitätsbewertung der Straßenvektordaten, da sie Lücken in der Straßenextraktion erklären können. Werden beispielsweise Luftbilder im Sommer aufgenommen, erschweren Bäume entlang der Straßen die Straßenextraktion, da die Straßenoberfläche nicht vollständig sichtbar ist. Die Extraktion und explizite Einbeziehung solcher Kontextobjekte tragen zur effizienten Bewertung einer bestehenden Straßendatenbank bei.

Die Modellierung der Relationen und die Konzentration auf statistische Modelle sind von großer Bedeutung für die Qualitätsbewertung von Straßendaten, denn auch den automatisch extrahierten Objekten haften Ungenauigkeiten an. Während der Bewertung werden die existierenden Relationen zwischen den Datenbankobjekten und den extrahierten Objekten mit den modellierten Relationen verglichen. Die Genauigkeitsmaße werden in diesen Vergleich einbezogen. In der Regel geben mehrere extrahierte Objekte Evidenz für ein Datenbankobjekt. Spricht ein Großteil der Gesamtevidenz bezogen auf ein gegebenes Objekt für dessen Korrektheit, und wird eine Mindestabdeckung des gegebenen Objektes mit extrahierten Objekten erreicht, so wird dieses Datenbankobjekt als richtig angenommen; es wird also akzeptiert, andernfalls wird es als falsch zurückgewiesen. Dieses Verfahren kann in einen halbautomatischen Arbeitsablauf eingebracht werden, in dem ein Operateur lediglich die vom System zurückgewiesenen Objekte überprüft.

Das Vorgehen ist in einen zweistufigen graphbasierten Ansatz eingebettet, der die Verbindungsfunktionen von Straßen ausnutzt. Im ersten Schritt erfolgt eine Straßenextraktion mit strengen Parametereinstellungen, die zu einer geringen Anzahl falsch-positiver Extraktionen führt, aber auch zur Zurückweisung von vielen korrekten Objekten. Zur endgültigen Bewertung werden die zurückgewiesenen Objekte hinsichtlich ihrer Verbindungsfunktion im Straßennetzwerk untersucht. Es wird davon ausgegangen, dass die bereits im ersten Schritt bestätigten Objekte über einen möglichst kurzen Weg im Netzwerk verbunden sind. Die erneute Untersuchung von Objekten, die im ersten Schritt verworfen wurden, hängt davon ab, ob sie eine wichtige Verbindungsaufgabe für die bereits akzeptierten Objekte übernehmen.

Es werden Beispiele der Qualitätsbewertung von Straßen in der offenen Landschaft gezeigt. Das genutzte ATKIS BasisDLM verzeichnet in der betrachteten $2 \times 8 \text{ km}^2$ großen Szene 527 Straßenobjekte. In den genutzten Orthobildern werden 25% der Straßenobjekte signifikant durch Baumreihen verdeckt. Die Ergebnisse bestätigen die Notwendigkeit einer durchgängigen statistischen Modellierung. Das entwickelte Verfahren ist in der Lage, die Qualität der gegebenen Objekte unter Einbeziehung von automatisch aus Luftbildern extrahierten Straßenobjekten und Baumreihen zu bewerten. Ungefähr 69% der Objekte wurden richtigerweise akzeptiert, 1% wurden akzeptiert, obwohl sie nicht korrekt sind. Diese falschen Entscheidungen sind hauptsächlich auf eine fehlende Qualitätskontrolle von Kreuzungsbereichen zurückzuführen. Jedoch zeigen weitere Sensitivitätsuntersuchungen, dass der gewählte zweistufige graphenbasierte Ansatz überwiegend zu einer Reduzierung falscher Entscheidungen führt.

Schlagnworte: räumliche Datenbank, Verifikation, Bildanalyse

Abstract

In this thesis a new approach to the automatic quality assessment of existing geo-spatial vector data is presented. The necessary reference information is derived automatically from up-to-date digital remotely sensed images using automatic image analysis. The focus is on the quality assessment of roads as these are amongst the most frequently changing objects in the landscape. In contrast to existing approaches for quality control of road data, a consistent statistical modelling and processing of the road data to be assessed and the objects extracted from the images is carried out.

A geometric-topologic relationship model for the roads and their surroundings is defined. The surrounding objects (context objects, such as rows of trees) support the quality assessment of road vector data as they may explain gaps in road extraction. If for instance aerial images are captured in summer, trees along roads hamper the road extraction as the road surface is not entirely visible. The extraction and explicit incorporation of those context objects contribute to an efficient assessment of a given road database.

The modelling of the relations and the concentration on statistical models are of great relevance for the assessment of the quality of road data, because the automatically extracted objects are uncertain themselves. During the assessment, existing relations between road objects from the database and extracted objects are compared to the modelled relations. The certainty measures of the objects are integrated in this comparison. Normally several extracted objects give evidence for a road database object. If the majority of the total evidence argues for the database object and if a minimum coverage of this database object with extracted objects is reached, the database object is assumed to be correct, i.e. it is accepted, otherwise it is rejected as incorrect. The algorithms may be incorporated into a semi-automatic environment, where a human operator only verifies the objects that have been rejected.

The procedure is embedded into a two-stage graph-based approach which exploits the connection function of roads. In the first phase the road extraction is carried out using a strict parameter control, leading to a relatively low degree of false-positive road extraction, but also to a high number of roads being rejected although correct. For the final assessment the rejected objects are examined regarding their connectivity in the road network. It is assumed that accepted roads from the initial phase are connected via the shortest path in the network. The further investigation of objects that have not been accepted depends on whether they fulfil an important network connection task for the already accepted objects.

Examples for the quality assessment of road data in open landscape regions are shown. The used ATKIS DLMBasis lists 527 road objects in the considered scene with a size of 2x8 km². In the orthoimage, 25% of these road objects are significantly occluded by trees. The results confirm the need for a consistent statistical modelling. The developed approach is able to reasonably assess the roads from the given database, using road and context objects which have been automatically extracted from remotely sensed imagery. Approximately 69% of the road objects have been correctly accepted, 1% has been accepted though incorrect. Those false decisions are mainly related to a lacking assessment of road junction areas. However, further sensitivity analyses show that in most cases the chosen two-stage graph-approach supports the reduction of false decisions.

Keywords: geo-spatial database, verification, image analysis

Contents

1. Introduction and background	9
1.1. Quality of geo-spatial information	9
1.2. Objectives and focus	9
1.3. Relevance	10
1.4. Organisation of this thesis	11
2. State of the art	13
2.1. Basics of geo-spatial data handling, acquisition and assessment	13
2.1.1. Object representation	13
2.1.2. Uncertainty in object capture	14
2.1.3. Roads in ATKIS DLMBasis	16
2.1.4. Shape descriptors	16
2.1.5. Topologic relations between uncertain objects	17
2.1.6. Hint Theory	21
2.2. Automatic road extraction and quality control of road databases	23
2.2.1. Road extraction without prior information from GIS	23
2.2.2. Road extraction making use of road databases	25
2.2.3. Road database verification	26
2.2.4. Discussion	26
3. A new approach to road database assessment	29
3.1. Outline	29
3.2. Model for objects and their relations	31
3.2.1. Object model	31
3.2.2. Relationship model	36
3.3. Workflow	37
3.4. Realisation	40
3.4.1. Assignment of objects and calculation of coverage	40
3.4.2. Assessment of geometric relations	41
3.4.3. Assessment of topologic relations	43
3.4.4. Combination of evidence	49
3.4.5. Graph analysis	53
3.5. Discussion	55
4. Test of approach	57
4.1. Data and model parameters	57
4.2. Test configurations	62
4.3. Results and evaluation	63
4.3.1. Assessment of geometric and topologic relations	63
4.3.2. Combination of evidence	64
4.3.3. Graph analysis and overall approach	69
5. Conclusions and outlook	85
A. Appendix	89
A.1. Distance transforms and skeletons	89
A.2. Line moments and their statistical properties	90
References	97
Curriculum vitae	102
Acknowledgement	103

1. Introduction and background

1.1. Quality of geo-spatial information

With the increasing use and dissemination of digital geo-spatial data, the question of whether the given data comply to predefined quality standards becomes more and more important. Quality comprises completeness, positional accuracy, attribute correctness and temporal correctness for each object, refer to [ZHANG and GOODCHILD 2002].

Some aspects cover *logical consistency*, for instance attribute completeness which concerns the question of whether all required attributes are stored together with an object. Those issues are not in the scope of this thesis. They are tackled without needing to incorporate a comparison to reality: it may be performed completely automatically by comparing a given data model with the data.

However, many aspects of *completeness, correctness, and accuracy* can only be checked in comparison to *reality*. It has to be verified whether for instance all objects registered in the data set are present in reality and whether their attributes are set correctly. The information on the current situation can be obtained using terrestrial measurements, but if the area to be observed is large, it becomes more economical to use remotely sensed data, i.e. aerial or satellite imagery. This kind of data is indeed the only possibility of achieving a comprehensive result in the given timeframe. Therefore, in the following, remotely sensed imagery will be referred to as reference data at a defined time, keeping in mind that of course not all components can be checked. For instance, the name of a road object cannot be verified using remotely sensed imagery.

Often the representation for both datasets is different: the given data are represented in vector format, whereas the reference is given as an up-to-date (raster) orthoimage. So, prior to comparison a similar representation for both datasets must be derived. In general, this is achieved by automatic object extraction algorithms; the result is a geometric, i.e. vectorial description of objects derived from the remotely sensed imagery. Having both datasets available in a similar representation, the subsequent steps are *verification* followed by *update* [VOSSELMAN 1996]. Verification means comparing the database objects to the reference: the geometrical accuracy, for instance position and size, can be checked using the extracted objects. The completeness and temporal aspect is only considered partly as just commission errors are identified. During the following update process, new or modified road objects not included in the database are extracted. By this means also completeness and temporal correctness are fully considered. In this thesis the term *quality assessment* is used instead of verification in order to emphasise that the proposed approach aims at a statistical description of the quality of the given geo-spatial data.

1.2. Objectives and focus

The main objective of the work described in this thesis has been to develop methods for an *automatic quality assessment* of geo-spatial data, given as a highly detailed vector data set using information automatically extracted from orthorectified aerial or satellite images.

One aspect of quality assessment concerns the question of whether the object can be found in the image and whether the required positional accuracy is achieved. Moreover, the attributes concerning geometric and semantic properties which can be identified in the image, such as the width of the road, have to be correct with respect to given tolerance intervals. The result of the assessment is an acceptance/rejection decision for each database object.

An approach has been developed which aims at linking existing information with results from automatic image analysis in a carefully balanced manner:

- information from an existing database is used as prior information guiding the extraction of objects in remotely sensed imagery,

- at the same time, the assessment of the given vector data using the results from object extraction algorithms is a primary aim of the work.

In contrast to existing approaches for quality control of geo-spatial information, a common and consistent geometric and statistic modelling and processing of the data to be assessed and the objects extracted from the images is carried out. This is necessary mainly because one does not have a real, i.e. reliable *reference* for the assessment. The only information one can use consists of automatically extracted objects, therefore a means has been developed to reasonably consider the evidence given by those extracted objects concerning the correctness and precision of given road database objects. This aspect is the main innovative component of this thesis.

A probabilistic and an Evidential approach, namely the so-called Hint Theory, are applied in this thesis to combine the evidence from the observed data in order to obtain the final assessment result. One key issue here is that an extracted object often does not give evidence for the whole object from the database. This is because depending on the used model for object extraction, the definition of start and end points for objects may not be identical. Moreover, if the object is not entirely observable, for example due to bad radiometric conditions, extracted objects are split. Thus, ignorance has to be considered during inference. In contrast to the probabilistic theory, a central feature of the Evidential approach is the ability to handle ignorance explicitly. Therefore, one further objective of the thesis is to analyse whether the exploitation of this property leads to more reliable assessment results.

The focus of this thesis is on *roads*. They are sufficiently complex to illustrate the methods, while being important enough from a practical point of view. More specifically, the German *ATKIS¹ DLMBasis* is used as the given data source. However, the methods to be developed can be transferred to other linear object classes (e.g. rivers, railway tracks etc.) as well as to vector data from other sources.

Furthermore, the approach has been developed for *open landscape* areas, because these regions have two key advantages: a) sophisticated and also practically relevant road extraction algorithms are available, b) the modelling of relationships between roads and context objects, i.e. neighbouring objects, is of limited complexity. Concerning context objects being incorporated into the assessment, the main attention is on *rows of trees* as mainly these are hampering automated road extraction from remotely sensed imagery in open landscape regions.

The development of approaches to automatic road and context *object extraction* from remotely sensed imagery is not subject to this thesis; thus, existing implementations are used. Because of their possible complexity, a geometric assessment of *road crossings* is also not intended, however their position with respect to the adjacent roads is evaluated implicitly.

Questions concerning coordinate system transformations including unknown scale or orientations between given objects are not treated. Therefore, all objects are assumed to be given in the same coordinate system.

1.3. Relevance

The handling of imprecision in geo-spatial data in general is increasingly gaining attention. One issue concerns the incorporation of information on the quality in GIS analyses and visualisation tasks: if such an information is available, it can be used adequately. On the other hand it is obvious that the data constitutes the most valuable component of a geo-spatial information system. This means quality control aids conservation of value and is therefore very important from an economic point of view.

The approach to automatic road database assessment presented in this thesis addresses several aspects. The interaction between existing vector data and extracted objects is modelled statistically and geometrically in a consistent way. On the one hand, the existing geo-spatial data is used as prior information for an automatic object extraction process. On the other hand, the approach is able to generate a quality indication for the existing data. From a scientific point of view the realised strategy of using and assessing prior information is a very important research task in the fields of image analysis and data fusion. From a practical and economical view the automated quality assessment is interesting as today quality control is done almost completely manually. This workflow can be supported and arranged more efficiently when

¹Authoritative Topographic Cartographic Information System

the presented approach is incorporated into a semi-automatic environment. Here, a human operator only verifies or corrects the objects rejected automatically.

1.4. Organisation of this thesis

The next chapter consists of two main sections. The first introduces the basics of geo-spatial data handling, such as object representation and the identification of influences on the data capture. The modelling and representation of road objects in the ATKIS DLMBasis is described in Section 2.1.3. In the succeeding sections, approaches for shape description and for topologic relations between uncertain objects are introduced. Furthermore, the Hint Theory is shortly reviewed. The second main section of Chapter 2 gives an overview on existing approaches to automatic road extraction and quality control of road databases. The concluding discussion in Section 2.2.4 leads up to Chapter 3, where the new approach to road database assessment is presented. In the outline (Section 3.1) requirements for the new approach are formulated and its components and related algorithms are described. The modelling of objects and relations between them is subject to Section 3.2. The workflow as implemented in the approach is then presented, followed by Section 3.4 on the realisation of the algorithms. The third chapter concludes with a discussion of the presented approach. Chapter 4 reports on extensive tests, including an evaluation of the obtained results. In Chapter 5 finally the conclusions and outlook are given.

2. State of the art

2.1. Basics of geo-spatial data handling, acquisition and assessment

2.1.1. Object representation

In this thesis objects of different origin and representations are treated. ATKIS objects are represented in continuous (Euclidean) space, whereas objects used for verification are captured from remotely sensed imagery, i.e. their origin is discrete space. This section shortly introduces both kinds of spatial object representation and means for conversion between them. The emphasis is on elongated objects as these are addressed in this work.

Object representation in Euclidean space

In Euclidean space \mathbb{R}^2 objects are normally represented in the form of *vector models*. In vector models a *point* carries the geometric information [BARTELME 2005]. Points are defined as coordinate pairs (x, y) in the 2D case at hand. The choice of the coordinate system is important for practical applications, but of minor interest here. Later in this work it is assumed that all objects are given in the same system. One-dimensional objects are represented as *lines* in the vector model. Curvilinear objects can be modelled by arbitrary polynomials, but normally such features are approximated as lists of *vertices*, i.e. points connected by straight *line segments*, resulting in a *linestring*. Similarly, *area* objects are modelled in the vector approach. The boundary of area objects is also represented as a concatenation of single line segments (polygons); the first and the last node are identical, resulting a closed object boundary.

This model has a close connection to graph theory [BARTELME 2005], which plays an important role in this thesis, for instance in the graph-based optimisation of the quality assessment. An important concept in graph theory is topology. *Edges* terminate at *nodes*; at any node several edges can start or end, respectively. The *node degree* indicates the number of edges terminating at the node. Bordered areas are represented as *meshes*; every edge has two adjacent meshes. The geometry of these components is of secondary importance; topology is invariant against many geometric transformations. In Figure 2.1 a simple object is sketched. Mesh no. 0 represents the outer infinitely large region. Two topologic interpretations of the object are possible. Variant 1: all points 1 – 5 are interpreted as nodes in the graph, thus resulting in 5 edges. Variant 2: the points 1, 2, 4 can be interpreted as vertices as they do not have a special topologic meaning (their node degree is 2), therefore only points 3 and 5 are nodes. The resulting edge composed of edges *C, D, A, B* in the figure is called *loop*.

Object representation in discrete space

The smallest element in a discrete object representation is a cell, usually in a regular lattice in \mathbb{Z}^2 . According to the main application area, image processing, those elements are called *pixels*. In contrast to points of the Euclidean geometry the pixels are not infinitesimally small, but have a minimum *raster size*. The individual pixels are addressed by their column and row number in a matrix. The raster size is the limiting factor for discrete object representation: details smaller than one pixel cannot be resolved. In the application at hand, binary images are used only to separate the object from the background.

Transformation between spatial representations

One way to interpret the transformation from vector to raster representation is as an intersection between the vector data and the lattice: all raster cells being intersected by the vector data are labelled as belonging to the object. From signal processing stems the condition that any interval having a length x_{min} to be transferred to the raster grid needs to be sampled with more than two pixels (*sampling or*

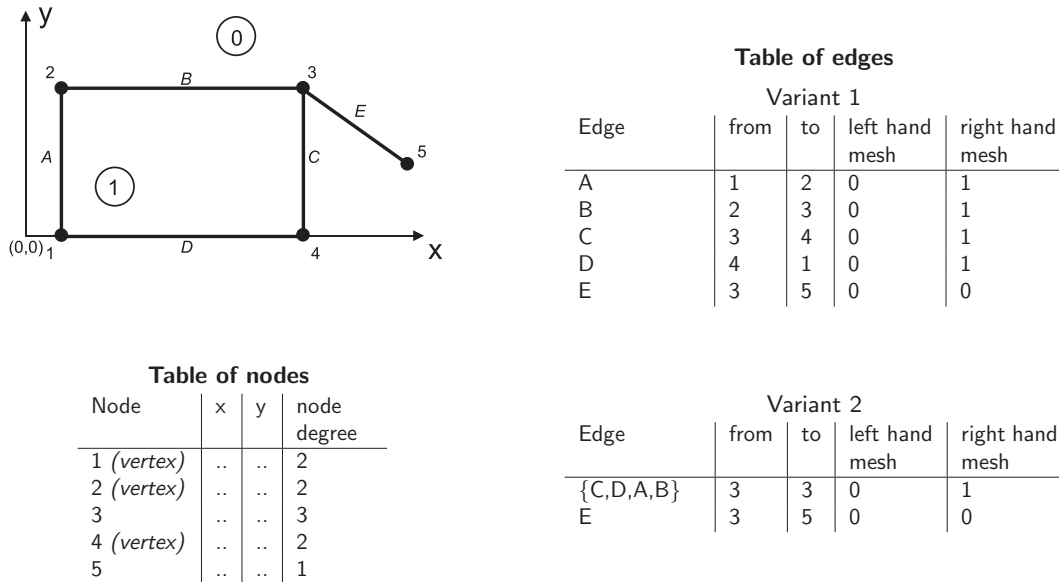


Figure 2.1.: Vector representation of an object with two topologic interpretations

Nyquist theorem). Thus the condition $a < 0.5 \cdot x_{min}$ must hold for the raster size a . The transformation from raster to vector representation is often realised based on the description of the object's boundary in \mathbb{R}^2 . Several methods are known to enhance the result, depending also on object type and application, refer to [HAKE et al. 2002, BARTELME 2005].

Elongated objects: definitions

Only elongated objects are considered in this thesis: objects to be assessed, i.e. road objects from a geo-spatial database, and objects giving evidence, namely extracted roads and rows of trees. Compared to arbitrarily shaped objects, the limitation to elongation enables a more straightforward geometric and topologic comparison between individual objects.

The objects of interest X are defined as point sets in \mathbb{R}^2 and have the following topologic properties [WORBOYS and BOFAKOS 1993, WINTER 1996]:

They are *regularly closed*: $\overline{X^o} = X$, where \overline{X} denotes the closure and X^o denotes the interior. This definition assures that no single points or lines are part of X . "... Intuitively, one may view a closed regular set as an open set (its interior) covered with a tight skin; each point in the interior is completely surrounded by other points in the set..." [REQUICHA 1977].

They are *singularly connected*. Connection means: two points of X are connected by a path lying entirely in X . Singular connection means: X is contractible to one single point.

They are *elongated*: the condition: $C(X) \gg 1$ must hold for the compactness of X . The compactness is calculated as follows [HARALICK and SHAPIRO 1993]: $C(X) = \frac{|\partial X|^2}{4|X^o|\pi}$, where $|\partial X|$ denotes the length of the boundary and $|X^o|$ denotes the area of the object.

In Figure 2.2 some example objects are shown. Objects (a-c) are valid as they are regularly closed, singularly connected and elongated. Object (d) is regularly closed and singularly connected, but not elongated (it is a circle: $C(X) = 1$). Object (e) is not singularly connected and not regularly closed. Object (f) is not singularly connected.

2.1.2. Uncertainty in object capture

In [GLEMSER 2001], the capture of an object can be classified into three individual steps: object modelling, abstraction and measurement. Any of these steps is influenced by uncertainties which will be discussed below.

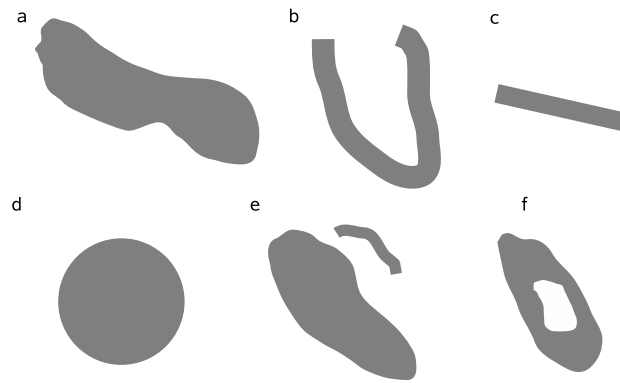


Figure 2.2.: Examples of objects (a-c): valid (matching all properties), (d-f): invalid

The first step in spatial data capture consists in *modelling* the real world. This modelling is application dependent: how is a real world object to be captured? Which properties are of interest, which can be neglected, in which scale, i.e. by which details should the spatial objects be represented? Here instructions for the capture are required; the ATKIS object catalogue (refer to Section 2.1.3), giving object models for several scales, is an example. The influences on the uncertainty cannot be given formally, as they depend on the chosen model. During modelling the real world is generalised since not all details of the world can be represented in the model. The intermediate result after modelling is called *virtual object* as up to this step no specific object has been dealt with.

The next step in object capture consists in a further *abstraction*, where a (human) operator decides which parts of a real world object belong to a certain object class. As this abstraction depends on the operator, it introduces fuzziness. The *measurements* taking place on these abstracted objects propagate the uncertainty, resulting in imprecise measurements.

Similar to WINTER [1998] the following definitions are given:

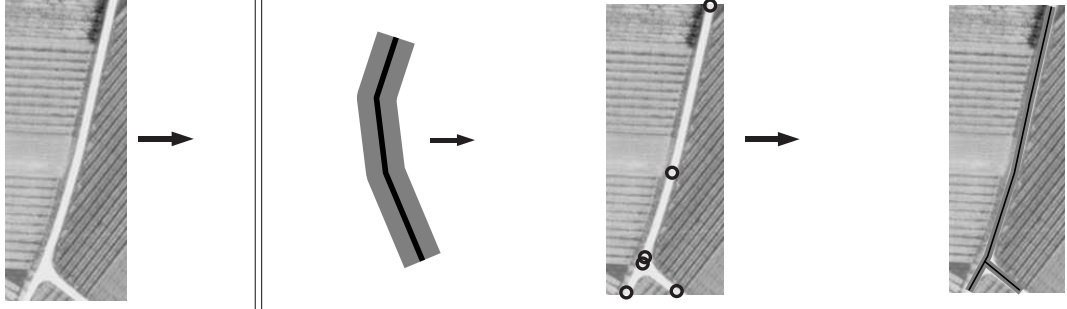
The difference between a continuous world and a generalisation and abstraction of this world is called the *fuzziness of concepts*

The deviation of a continuous random variable from its mean value is called the *imprecision of the variable*

The term fuzziness used in this context should not be linked with the Fuzzy Theory [ZADEH 1965]. The Fuzzy Theory provides a mathematical framework for the representation of uncertain knowledge. In this thesis the fuzziness is modelled by probability density functions. However, in Section 2.1.5 the possibility to model the uncertainty inherent in geo-spatial data by means of a Fuzzy approach is discussed.

Table 2.1 summarises the steps and gives an idea of how to model their impact statistically, i.e. with which type of density function. The example illustrates the capture of a road object for the ATKIS DLMBasis from an aerial image. It is important to note that the assumed distributions present an ideal view of the world, i.e. the normal (Gaussian) distribution and the uniform distribution. Yet, most experiments and experiences in the field of surveying, photogrammetry, and remote sensing show that the assumption of Gaussian distributions for geometric measurements is reasonable. If a measure is assumed to take values within a certain range but no further information is available, it is common to use the uniform distribution.

The parameters for the distributions depend on the used input data and the algorithm (in case of automatic procedures) or on the experience and skills of the human operator extracting the information. Often it is not feasible to derive these values empirically and thus they are estimated from experience and parameters of the measurement devices. WINTER [1998] suggests asking experts in order to obtain a reasonable estimation for the fuzziness inherent in the abstraction. It should be noted that systematic errors are not considered here.



	Modelling	Abstraction	Measurement
<i>Description</i>	Modelling of object: medial axis	Selection of points to be captured	Measurement of points
<i>Impact on uncertainty</i>	Defined Tolerance: Position of points $\pm 3m$	Fuzziness	Imprecision
<i>Type of possible density function</i>	Uniform distribution	Mix of normal and uniform distribution	Normal distribution

Table 2.1.: Influences on the uncertainty during data capture: roads for ATKIS DLM Basis

2.1.3. Roads in ATKIS DLM Basis

Object-based digital landscape models (DLM) are important components of the Authoritative Topographic Cartographic Information System (ATKIS) of Germany [ADV 1989, ADV 2006]. The ATKIS DLM Basis contains the data of the finest scale. Its content is approximately equivalent to topographic maps 1:25,000, but in contrast to those maps the data contained in the DLM Basis are not subject to cartographic generalisation. Of course, a certain portion of generalisation is applied during data capture as explained in Section 2.1.2, but the important issue is that shapes as well as positions are in essence faithfully represented.

The road network is part of the traffic layer (Road Traffic). The main classes of interest for this thesis are *Road* and *Path*. The class *Road* subsumes road objects, which are mainly used for car and transportation traffic, *Path* comprises road objects of minor importance, for instance leading to fields. In the following text, the term *road object* is used as a general term for both classes roads and paths. Road objects in ATKIS are geometrically described by their medial axis and average width, which is given as an attribute. The required precision (planimetric accuracy) for a road object is defined as $\pm 3m$. In the literature a concrete definition of this value is not given. In the context of this thesis this value is interpreted as a *buffer* around the real-world object. The attribute *width* is defined in intervals of $3m$. Here, this value is assumed to be the 99%-confidence interval of a Gaussian probability density function, thus a standard deviation $G_{\sigma W} = 1m$ is set for the width.

The official instructions given in the object catalogue define several rules for the object generation. A new Road Traffic object has to be generated if the type, or class of a road, or attributes change. The road network topology is not relevant for object generation. However, the network topology is specified by requiring that adjacent road objects must share the same nodes. This does not hold for crossovers and underpasses, as these do not necessarily constitute network junctions. Network edges are bounded by nodes having a node degree different from 2. One ATKIS road object consists of at least one line segment. Thus, the mapping from one object to an edge in the network is possible using the assignments between ATKIS road objects and segments on the one hand and between network edges and segments on the other hand.

2.1.4. Shape descriptors

To give an exhaustive and unambiguous definition of an object's shape is very difficult or even impossible. Unlike the definition of topologic relations between objects which will be given in the next section, the shape can be described in several ways, depending on the given data, application and intention.

One possibility is given by features describing the objects' geometric properties, such as extent, spread, eccentricity, smoothness, and so on. In literature several means of defining those features are given. The most commonly used shape descriptors are (invariant) *Fourier descriptors* or (invariant) *geometric moments* [HARALICK and SHAPIRO 1993]. In this thesis the focus is on elongated objects. The shape of such objects can be represented by their skeletons (refer to Appendix A.1). Therefore, it is reasonable to define shape descriptors for linestrings.

Invariant geometric moments have been studied in the context of object recognition. In [TEH and CHIN 1988] details on several kinds of moment invariants are given. Line moments are used e.g. in [SARDANA et al. 1994, LAMBERT and GAO 1995]. An interesting property of moments is given by the *moment uniqueness theorem* [HU 1962], which expresses that the infinite set of moments uniquely determines the object, and vice-versa. This also holds for line moments [LAMBERT and GAO 1995].

The line moments, their statistical properties and examples are given in Appendix A.2. Their application for the assessment of geometric relations is described in Section 3.4.2.

2.1.5. Topologic relations between uncertain objects

Topologic relations describe the relative position of two objects, not considering their metric; they are invariant with respect to many geometric transformations. A significant contribution to this field has been given by EGENHOFER and FRANZOSA [1991]. For two objects (regions) in \mathbb{R}^2 , being singularly connected and regularly closed, a set of eight topologic relations can be distinguished (refer to Fig. 2.3). The scheme

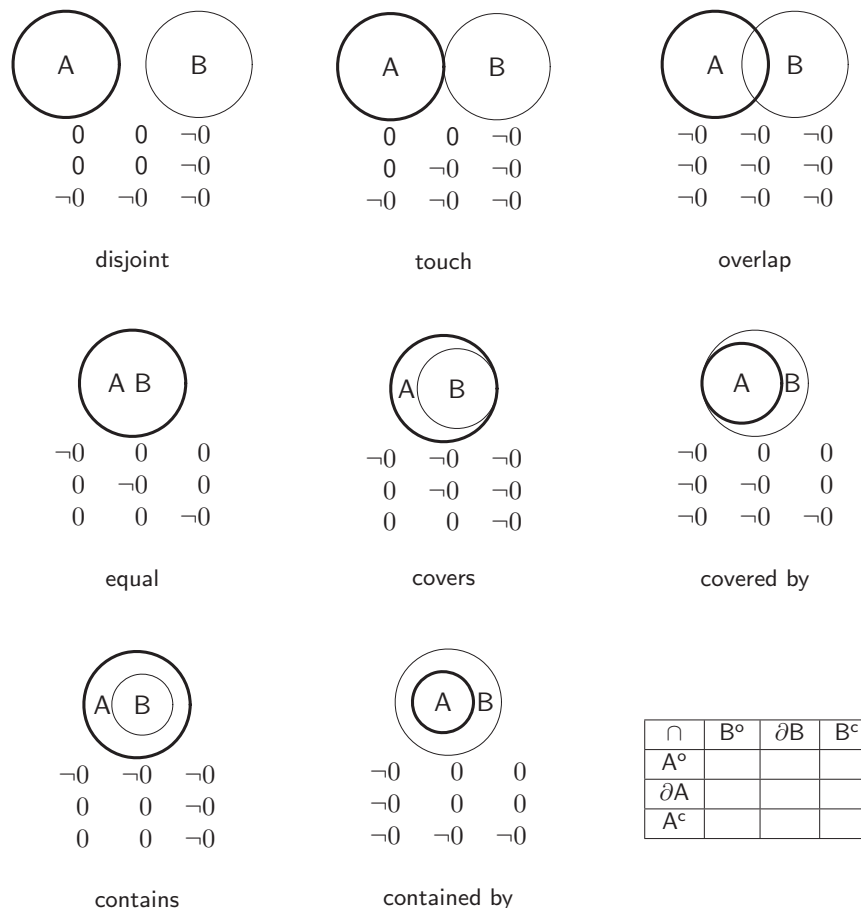


Figure 2.3.: Eight possible topologic relations between two regions A and B and the 9-intersection matrix

for this analysis is called *9-Intersection*. The 9 intersection sets between the exteriors (c), the boundaries (∂), and the interiors ($^\circ$) of the respective objects are calculated; they can be empty or not. Usually the intersection sets are represented as a matrix as shown in the lower right field in Figure 2.3. Within

the 3×3 matrix $2^9 = 512$ combinations are possible, but Egenhofer and Franzosa could exclude most combinations due to geometric constraints. Only the shown eight relations remain for regularly closed and singularly connected regions. In [EGENHOFER and HERRING 1990] the relations between regions, lines and points are investigated. For instance, two line objects may undergo 33 relations. In this thesis, however, the examination of topologic relations between elongated objects, defined in Section 2.1.1, is of interest, as in case of roads the whole surface area needs to be considered, not only the medial axis. The approaches described in the following are also valid for elongated objects, as these are regularly closed and singularly connected.

The transition from one relation to another cannot happen arbitrarily, but has to follow the edges in the *conceptual neighbourhood graph (cng)* (Fig. 2.4).

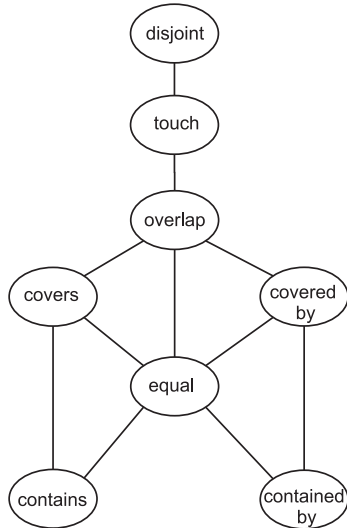


Figure 2.4.: Conceptual neighbourhood graph (cng)

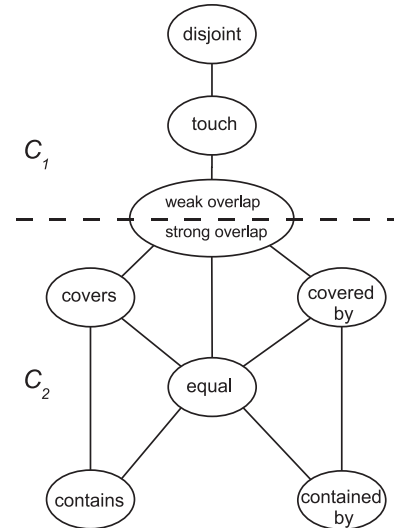


Figure 2.5.: Partitioned cng

The assessment of topologic relations between uncertain objects has been extensively treated in literature. In [WORBOYS 1998] objects T represented in discrete space are composed of two sets: set L of pixels, which is definitely part of T (lower approximation) and set U of pixels where the membership to T is not certain (upper approximation). Based on this representation some tests are defined, aiming at a qualitative statement concerning the topologic relation of two objects. The *compatibility* describes whether the two objects correspond regarding the upper and lower approximations. A connection operator allows qualitative statements such as *Both objects are definitely disjoint*; *Both objects are possibly connected* or *Both objects are definitely connected*. In [CLEMENTINI and DI FELICE 1996] the 9-Intersection is extended for uncertain objects. Instead of using an infinitely small boundary of an object, the boundary is supposed to have a certain dimension, representing the uncertainty. As a consequence the number of possible relations increases from 8 to 44, and the cng is extended accordingly.

The application of fuzzy logic [ZADEH 1965] to spatial object analysis has been treated by several authors, e.g. by ALTMANN [1994], BOXER [1997] and BLOCH [1999]. The former work is briefly introduced here. Objects are modelled in \mathbb{Z}^2 , the value assigned to a cell represents the degree to which that cell is part of an object (*fuzzy region*). Based on this model a fuzzy distance set between two regions is calculated, which is intersected with a fuzzy prototype for a relation (for instance *disjoint*). Finally, this intersection leads to a fuzzy value indicating the possibility that both regions undergo the prototyped relation.

The approaches introduced so far have the disadvantage that geometric uncertainties are represented only approximately. A simple buffer approach as used in [WORBOYS 1998, CLEMENTINI and DI FELICE 1996] actually represents a uniform distribution. The question is how more realistic distributions like the Gaussian may be mapped; an adequate means is not readily available. A similar problem arises using fuzzy approaches: due to the required quantification the transition from probabilistic measures to fuzzy regions leads to a loss of information.

In [WINTER 1996] another idea is pursued. The geometric uncertainties inherent in geo-spatial data are not modelled directly in the geometric representation: the geometry which is obtained during the

acquisition and which can be seen as an appropriate estimate of the mean value is kept. In order to obtain a measure for the displacement of two objects, a distance transform is applied. From the minimum and maximum distance the eight topologic relations as introduced above are computed. During this step the statistic properties of the objects are considered. This approach will be described in more detail as it will be used in this thesis.

It is presumed that the uncertainties of an object are small compared to the object size. Given this restriction, WINTER [1996] proves that two objects which undergo the topologic relation *touch*, considering their uncertainty, may not have the relations $\{equal, covers/covered\ by, contains/contained\ by\}$. Therefore, the *cng* is partitioned into two clusters: C_1 and C_2 , refer to Figure 2.5. The relations in C_1 are: $\{disjoint, touch, weak\ overlap\}$, and in C_2 : $\{strong\ overlap, contains/contained\ by, covers/covered\ by, equal\}$. The decision whether C_1 or C_2 applies is made according to the overlapping factor OF , refer to Equation 2.1.

$$OF = \frac{|A^o \cap B^o|}{\min(|A^o|, |B^o|)} \quad \begin{array}{l} \text{Rel} = \textit{weak overlap} : OF \leq 0.5 \\ \text{Rel} = \textit{strong overlap} : OF > 0.5. \end{array} \quad (2.1)$$

WINTER [1996] defines *certain* and *uncertain* intersection sets. For objects having a relation in cluster C_1 , e.g. *weak overlap* the area which is covered by both objects is uncertain: the relations *touch* and *disjoint* are also possible (the joint area vanishes). Vice versa, in C_2 the area which is not covered by both objects is uncertain. The definitions are given with equations 2.2 and 2.3, where P and Q are certain sets and O the respective uncertain set.

$$\text{Rel} \in C_1 : \begin{cases} P = A^o \cap B^c, \\ Q = A^c \cap B^o, \\ O = \mathbb{R}^2 \setminus P, Q, \end{cases} \quad (2.2) \quad \text{Rel} \in C_2 : \begin{cases} P = A^c \cap B^c, \\ Q = A^o \cap B^o, \\ O = \mathbb{R}^2 \setminus P, Q. \end{cases} \quad (2.3)$$

In Figure 2.6 examples for those sets are shown. The motivation for the application of skeletons will be given now. As can be seen from the definition of the uncertain intersection sets, they are closely related

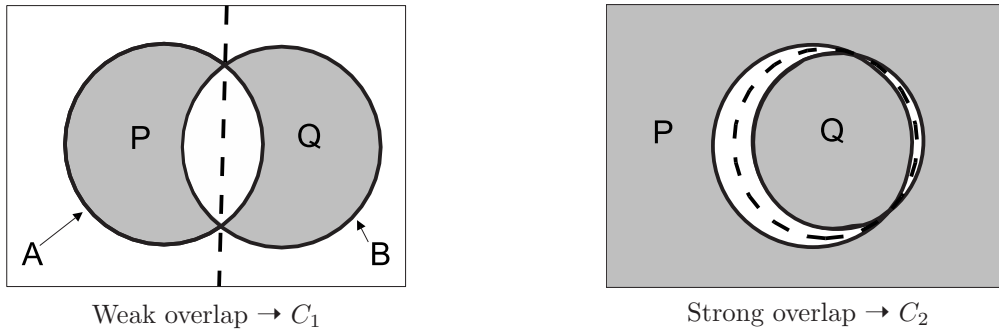
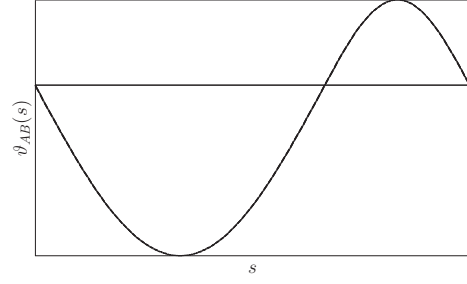


Figure 2.6.: Certain intersection sets P, Q (grey areas), uncertain intersection sets O (white areas) in C_1, C_2 and their skeleton S_1, S_2 (dashed lines) of left hand object A and right hand object B

to the existing topologic relation between the objects. Applying a morphologic distance transform along the skeleton (refer to Appendix A.1), a measure for the distance between the certain intersection sets P and Q can be obtained. The distance d is set up as a function of the arc length s of the skeleton, having no sign per definition. The skeletons are named S_1 and S_2 respectively, according to the existing relation cluster. WINTER [1996] defines a new function $\vartheta_{AB}(s)$, where s represents the arc length. The absolute value of $\vartheta_{AB}(s)$ equals d and the sign depends on whether the respective skeleton point at s is inside or outside the border of region A , refer to equation 2.4.

In Figure 2.7 the function $\vartheta_{AB}(s)$ for the right hand skeleton in Figure 2.6 is shown. As the majority of S_2 is inside A , ϑ is mostly negative. The skeleton S_2 is closed per definition, whereas S_1 may have

$$\vartheta_{AB}(s) = \begin{cases} d, & \text{if } s \in A^c \\ -d, & \text{if } s \in A^o \\ 0, & \text{if } s \in \partial A \end{cases} \quad (2.4)$$

Figure 2.7.: Distance transform along S_2 (Fig. 2.6)

open-ends in $A^c \cap B^c$. Those open-ends are poles of the morphological distance which is restricted due to the limitation of O by clipping \mathbb{R}^2 to image size. For further analyses WINTER [1996] defines classes for the morphologic distance (refer to Eqn. 2.5).

$$\Omega_\vartheta = \{\omega_-, \omega_0, \omega_+\} \text{ with } \begin{cases} \vartheta_{AB}(s) \in \omega_-, & \text{if } \vartheta_{AB}(s) < 0 \\ \vartheta_{AB}(s) \in \omega_0, & \text{if } \vartheta_{AB}(s) = 0 \\ \vartheta_{AB}(s) \in \omega_+, & \text{if } \vartheta_{AB}(s) > 0 \end{cases} \quad (2.5)$$

The minimum and maximum distances of $\vartheta_{AB}(s)$ ($\rightarrow (\vartheta_{\min}, \vartheta_{\max})$) are then assigned to the classes in Ω_ϑ : $\omega_{\min}, \omega_{\max}$. WINTER [1996] proves that the triplet $\{C_i, \omega_{\min}, \omega_{\max}\}$ has equivalences to the eight topologic relations defined in [EGENHOFER and FRANZOSA 1991]. An extension can be found in the modification of *overlap*, which is split into *weak overlap* and *strong overlap*. In Table 2.2 these equivalences are shown.

Relation	C_i	ω_{\min}	ω_{\max}
<i>disjoint</i>	C_1	ω_+	ω_+
<i>touch</i>	C_1	ω_0	ω_+
<i>weak overlap</i>	C_1	ω_-	ω_+
<i>strong overlap</i>	C_2	ω_-	ω_+
<i>covers</i>	C_2	ω_-	ω_0
<i>covered by</i>	C_2	ω_0	ω_+
<i>contains</i>	C_2	ω_-	ω_-
<i>contained by</i>	C_2	ω_+	ω_+
<i>equal</i>	C_2	ω_0	ω_0

Table 2.2.: Equivalence of the triplet $\{C_i, \omega_{\min}, \omega_{\max}\}$ and the topologic relations

Uncertainty is not modelled geometrically, but introduced into the distance measure. WINTER [1996] defines probability density functions for the three classes in Ω . These functions reflect the modelled fuzziness of abstraction and the imprecision of measurement (refer to Section 2.1.2). The fuzziness of abstraction is modelled by a uniform distribution function D_β (parameter: radius β , derived from the left and right boundary) which is convolved with a Gaussian function G_{σ_β} (parameter: variance σ_β^2). This leads to a joint function $p(\underline{\mu} = \mu_\vartheta | \omega_i) = D_\beta * G_{\sigma_\beta}$ for the probability that a measured distance μ_ϑ matches class ω_i , with $i = \{-, 0, +\}$. The domain of the density function $p(\mu_\vartheta | \omega_0)$ is defined only by the fuzziness of abstraction. WINTER [1996] calls this the concept *IsZero*, emphasising the outstanding influence of the abstraction. The density functions $p(\mu_\vartheta | \omega_-)$ and $p(\mu_\vartheta | \omega_+)$ are bounded by the borders of the given finite space where the skeleton is defined. In practical applications a minimum bounding rectangle containing both objects is used.

The imprecision of measurement is modelled in a rather simple way: the measurement process is assumed to follow a Gaussian distribution and, therefore, the imprecision of the boundary points is characterised by the standard deviation σ_A and σ_B , respectively. A variance propagation for σ_ϑ is applied: $\sigma_\vartheta^2 = \sigma_A^2 + \sigma_B^2$. This value is the parameter of the Gaussian density function describing the random measurement error

ε : $p_\varepsilon = G_{\sigma_\vartheta}$. The convolution of $p(\mu_\vartheta|\omega_i)$ with p_ε leads to a new (final) function for the probability that a distance measure ϑ belongs to a certain class ω_i : $p_{\vartheta|\omega_i}(\vartheta) = (p_\varepsilon * p_{\mu|\omega_i})(\vartheta)$.

Finally, the posterior probability $P(\omega_i|\vartheta)$ can be calculated using Bayes' theorem [KOCH 1997]:

$$P(\omega_i|\vartheta) = \frac{P(\vartheta|\omega_i) P(\omega_i)}{\sum_{\omega_j \in \Omega_\vartheta} P(\vartheta|\omega_j) P(\omega_j)}, \quad (2.6)$$

where $P(\vartheta|\omega_i) = P(\vartheta = \vartheta|\omega_i) = p_{\vartheta|\omega_i}(\vartheta)\Delta\vartheta$. The factor $\Delta\vartheta$ is the sample size from the distance transform. It is eliminated in the Bayesian summation formula. The prior probabilities $P(\omega_i)$ are derived from the borders of the uniform distribution (the ratio of the length of ω_i and the total length of Ω_ϑ). This is a reasonable method, because the intervals have to be chosen to be finite and the skeleton is also defined in finite space. The multiplication of the respective $P(\omega_i|\vartheta_{\min})$ and $P(\omega_i|\vartheta_{\max})$ according to the equivalences in Table 2.2 leads to a probability for the individual relations.

2.1.6. Hint Theory

The background of the Evidence Theory (E-T) is the assessment of incomplete knowledge by means of degrees of belief (lower probability) and degrees of plausibility (upper probability). The roots of E-T can be found in [DEMPSTER 1967], whereas the actual origin of E-T is known to be set by Shafer in [SHAFER 1976]. The degree of belief (often called credibility) expresses to what extent information can be trusted. The degree of plausibility specifies to what extent there is no disagreement regarding a piece of information. Further information regarding E-T can be found in [SHAFER and PEARL 1990]; an introduction to the Dempster-Shafer-Theory is given in [GORDON and SHORTLIFFE 1990].

In this thesis the Hint Theory (H-T), an approach to the E-T, is used. There is no significant conceptual difference between both theories, but the H-T provides a more comprehensive compilation of the original work by Dempster and Shafer. The fundamentals of the H-T can be found in [KOHLAS and MONNEY 1995]. In H-T a so-called frame of discernment Θ is defined, which contains all possible answers to a certain question. A hint \mathcal{H} is defined as the quadruple $\mathcal{H} = (\Omega, P, \Gamma, \Theta)$. Here $\Omega = (\omega_1, \omega_2 \dots \omega_m)$ represents the set of all possible interpretations of the information contained in the hint. One of these interpretations must be the correct one, but it is unknown which one. Each interpretation allows restricting the possible answers to a non-empty subset $\Gamma(\omega_i)$ of Θ . These sets $\Gamma(\omega_i)$ are called the focal sets of the hint. The precision of every interpretation ω_i is represented in its probability $p_i \in P$. The probabilities for the interpretations given by one hint must sum up to 1. The interesting fact about such a hint is that it does not need to give evidence to all possible answers – the explicit formulation of ignorance is possible.

Using a hint, a hypothesis $H \subseteq \Theta$ can be judged. The measure to what extent the hint provides a hypothesis is called *support* and is calculated as follows:

$$sp(H) = \sum_{\omega:\Gamma(\omega)\subseteq H} p(\omega) \quad (2.7)$$

In the terminology of Shafer this value is called belief. Kohlas and Monney stress that the term support in this case is the better choice, as it refers only to the support given by one single hint. The overall belief in the hypothesis may be larger. The *plausibility* is the sum of all support provided by the hint and not directly assigned to the negation of H , denoted as H^c :

$$pl(H) = \sum_{\omega:\Gamma(\omega)\cap H \neq \emptyset} p(\omega) = 1 - sp(H^c) \quad (2.8)$$

It corresponds to our perception that always $sp(H) \leq pl(H)$. These interpretations of support and plausibility are identical to Dempster's theory of upper and lower probability [KOHLAS and MONNEY 1995, Ch. 3.3].

The normal case is that there is more than one hint referring to a question. Those independent hints are combined applying *Dempster's Rule*, which leads to a new hint:

$$\mathcal{H}_{c1\dots n} = (((\mathcal{H}_1 \oplus \mathcal{H}_2) \oplus \mathcal{H}_3) \oplus \mathcal{H}_4 \dots) \oplus \mathcal{H}_n. \quad (2.9)$$

The probability k that n hints $\mathcal{H}_1 \dots \mathcal{H}_n$ are contradictory is given by

$$k = \sum \left\{ \prod_{i=1}^n p(\omega_i) : \cap_{i=1}^n \Gamma_i(\omega_i) = \emptyset \right\}. \quad (2.10)$$

This probability must be different from 1, because there must exist at least one possible combined interpretation. The combined focal sets associated to ω are the combination of all focal sets associated to ω_i :

$$\Gamma(\omega) = \cap_{i=1}^n \Gamma_i(\omega_i), \Gamma(\omega) \neq \emptyset. \quad (2.11)$$

The respective probability is

$$p(\omega) = \left(\prod_{i=1}^n p(\omega_i) \right) / (1 - k). \quad (2.12)$$

There exist some approaches in the field of image analysis using E-T for handling evidence, also exploiting the possibility of considering ignorance. For example in [LOHMANN 1991, TUPIN et al. 1999, ROTTENSTEINER et al. 2005] the results of several image segmentation operators are combined using E-T: every image operator gives evidence for one certain feature class to a certain confidence. In [QUINT 1997, TÖNJES 1999] E-T is used to balance hypotheses in knowledge-based image interpretation systems.

Example The following example is taken from [KOHLAS and MONNEY 1995], but has been slightly modified. Consider the question whether the gas tank of your car is empty or sufficiently filled (for example to reach the next filling station at least). Thus, let $\Omega = \{e, f\}$, e for empty and f for sufficiently filled. The gas gauge reads empty. This information is a hint, which has two possible interpretations: first, one can assume that the gauge is functioning correctly (ω_1 : gas gauge ok). In this case the tank indeed is empty, i.e. $\Gamma(\omega_1) = \{e\}$. Secondly, one can take into account the possibility that the gas gauge is broken (ω_2 : gas gauge broken). Under this interpretation nothing at all can be inferred about the question: $\Gamma(\omega_2) = \{\Theta\}$, since e and f remain possible. Note that the alternative interpretation ω_2 does not allow to infer the complementary answer to the first one. The probability of the first interpretation represents the reliability of the gas gauge, i.e. the probability that, at an arbitrary time, the gauge is functioning correctly. The probability of the second interpretation is simply the complement to 1 of the first one. The reliability of the gas gauge is supposed to be 99%, thus $p(\omega_1) = 0.99$ and $p(\omega_2) = 0.01$.

The second hint is related to the mileage counter. Knowing the car's consumption, one can compute the distance d one is able to drive with a completely full tank. On the other hand, each time the car is refueled, the driver usually resets the mileage counter to zero but sometimes he forgets to do it. Suppose that the mileage counter currently indicates a distance close to zero. This information can be represented by a hint with two different interpretations. In the first interpretation ω'_1 , it is supposed that the mileage counter was indeed reset to zero at the last tank filling. The interpretation ω'_2 assumes that the counter started to count from zero because of some other reasons. In that case nothing can be inferred about the current status. These observations imply that the focal sets corresponding to ω'_1 and ω'_2 are $\{f\}$ and $\{\Theta\}$, respectively. From experience one can suppose that on the average seven times out of ten the mileage counter is indeed reset to zero at tank filling, thus $p(\omega'_1) = 0.70$ and $p(\omega'_2) = 0.30$.

The first hint gives:

$$\begin{aligned} \Gamma(\omega_1) &= \{e\} & , & \quad p(\omega_1) = 0.99 \\ \Gamma(\omega_2) &= \{\Theta\} & , & \quad p(\omega_2) = 0.01 \end{aligned}$$

and the second one gives:

$$\begin{aligned} \Gamma(\omega'_1) &= \{f\} & , & \quad p(\omega_1) = 0.70 \\ \Gamma(\omega'_2) &= \{\Theta\} & , & \quad p(\omega_2) = 0.30 \end{aligned}$$

In order to obtain final support and plausibility values for the unknowns, both hints need to be combined. The probability k for contradictory hints is:

combination	focal set	probability
(ω_1, ω'_1)	empty (contradiction)	$0.99 \cdot 0.7 = 0.693$

The remaining three combinations lead to the focal sets:

combination	focal set	probability
(ω_1, ω'_2)	e	$0.99 \cdot 0.3 / (1 - 0.693) = 0.967$
(ω_2, ω'_1)	f	$0.01 \cdot 0.7 / (1 - 0.693) = 0.023$
(ω_2, ω'_2)	Θ	$0.01 \cdot 0.3 / (1 - 0.693) = 0.010$

Finally, the support and plausibility values are:

$$\begin{aligned} sp(e) &= 0.967 & pl(e) &= 0.977 \\ sp(f) &= 0.023 & pl(f) &= 0.033 \\ sp(\Theta) &= 0.010 \end{aligned}$$

The information from the first hint is almost entirely assigned to the first interpretation, i.e. to the unknown "empty tank". Although the majority of the second hint is not in favour of this unknown, the ignorance contained in this hint is relatively large. Therefore, the final support values are quite comprehensible. A maximum support rule would result in the decision that the tank is empty.

However, the incorporation of ignorance into the calculation of a final inference result in this example leads to the same result as a simple maximum probability decision: the probability that the tank is empty (according to the first observation, gas gauge ok) is larger than the probability that the mileage counter has been set to zero, which implies a full tank. Whether the explicit incorporation of ignorance shows significant differences in the approach presented in this thesis will be analysed in detail in Chapters 3 and 4.

2.2. Automatic road extraction and quality control of road databases

In this section an overview on contributions to the field of automatic road extraction from remotely sensed imagery for acquisition and verification of GIS databases is given. Three research lines can be identified:

- A) approaches for automatic road extraction not using prior information about the road objects to be extracted (refer to Section 2.2.1),
- B) approaches using existing road-databases as prior information to support the subsequent road extraction (refer to Section 2.2.2),
- C) approaches aiming at a verification of existing road data (refer to Section 2.2.3).

The description of all three research lines is important for this thesis, in order to understand the challenges, and also the possibilities, for an efficient quality assessment approach.

In the introduction the term *quality assessment* has been defined in the context of this thesis. The term emphasises that, in contrast to existing research work, the approach developed here aims at a consistent statistical modelling of the involved objects. Consequently, the approaches categorised as type C) are termed *verification* approaches.

2.2.1. Road extraction without prior information from GIS

Approaches to road extraction which do not incorporate any prior information from a geo-spatial database address questions such as: what is possible by fully automatic road extraction? What road models and tools can be used in what circumstances?

In [FISCHLER et al. 1981] a quite simple road model is used for aerial images of low resolution (1 to 2 m): roads are modelled as lines, their surface is assumed to be homogeneous and the width of roads needs to be approximately constant. The strategy is to apply two types of road extraction operators: operator 'type I' is designed to reliably detect roads, i.e. the number of false positives is minimised, but some roads

are not extracted. Operator 'type II' extracts most roads, but also finds instances of other objects. The task then is to combine the results of these two algorithms in order to find an optimised road network. A graph-based approach, applying the A*-Algorithm [DUDA and HART 1973], is introduced linking the reliable output of 'type I' operator through 'type II' objects. This early work already shows that a strategy combining data-driven and model-driven procedures seems to be beneficial. Also a first attempt was made to exploit the topologic network function of roads. Even though FISCHLER et al. [1981] do not use the global network function of roads, they efficiently link reliably extracted roads.

WIEDEMANN [2002] extends the above approach. He models roads as linear objects in aerial or satellite imagery with a resolution of about 1 to 2 m. The underlying line extractor is the one introduced in [STEGER 1998]. The initially extracted lines are evaluated by fuzzy values according to attributes, such as length, straightness, constancy in width and in grey value. The final step is the grouping of the individual lines in order to derive topologically connected and geometrically optimal paths between seed points. The decision of whether extracted and evaluated lines are grouped into one road object is made corresponding to a collinearity criterion, allowing for a maximum gap length and a maximum direction difference. A so-called detour factor is used to exploit the global network properties of roads: the extracted preliminary road network is compared to an optimised road network which is derived by graph analysis. At places where a significant detour exists, the road extraction operator is applied again, using more tolerant parameters.

The approaches presented in [FISCHLER et al. 1981] and [WIEDEMANN 2002] are designed for open landscapes, mainly because objects disturbing the given line-based road model are not considered. This aspect is addressed in [RUSKONÉ 1996], where local context objects such as trees, extracted by a supervised multispectral classification, are used to explain gaps in the extracted road network. One deficit of this approach is the disregard of the scale-space behaviour of roads, as introduced below. The explicit incorporation of rows of trees into road extraction in open landscape areas is presented in [STRAUB et al. 2000, BUTENUTH et al. 2003]. Results show that such a strategy significantly enhances the quality of road extraction concerning the completeness of the extracted road network.

In [MAYER 1998] and [BAUMGARTNER et al. 1999] road networks are modelled as hierarchical networks considering also the scale-space behaviour. The linear scale-space in association with image information was basically analysed in [KOENDERINK 1984] and [LINDBERG 1994]. In coarse resolution images road objects appear as bright lines, having a limited curvature and a nearly constant width. Such a model is not very sensitive towards objects on the roads such as cars or different road surfaces. In fine resolution more components like road markings are visible and area-based segmentation methods are applied for the road extraction [BAUMGARTNER 2003]. The last-mentioned approach is again limited to open landscape areas.

In [HINZ 2004] the road models are enhanced and expanded concerning the context for built-up areas: buildings and high vegetation are included in the model to limit the search space and to explain gaps in the road extraction caused e.g. by shadows and occlusions. Hinz also introduces an extraction algorithm for vehicles to be able to collect more evidence for roads. Redundant information is used for the verification of hypotheses (interior evaluation). By these means, hypotheses are verified with information originating from objects extracted in the same resolution level. Experiments show that the approach increases the reliability of the road network extraction.

Recently, road extraction from high resolution satellite imagery has received considerable interest. In [DIAL et al. 2001] and [GIBSON 2003], results from multispectral classification, edge detection and a texture classifier are combined to extract roads in IKONOS imagery. Each operator is applied in different scales of the image. Examples are given for urban and suburban areas in the US. One has to keep in mind that the grid-like structure of the road network in these areas makes automatic road extraction easier. The algorithms introduced in [DOUCETTE et al. 2004] and [BACHER and MAYER 2005] follow similar ideas. They show that the incorporation of spectral information leads to a more robust and efficient road extraction.

A different approach is pursued by road trackers: given a starting point and direction, they follow the road in the image [MCKEOWN and DENLINGER 1988, HEIPKE et al. 1994, BAUMGARTNER et al. 2002] exploiting the property that the road is bordered by parallel edges and that the area between these edges needs to be homogeneous. The tracker predicts and estimates the subsequent road segments based on the given reference segment until a stop criterion, e.g. insufficient parallelism of edges, is reached. Some

authors apply active contours [KASS et al. 1988, BLAKE and ISARD 1998]. These energy minimising methods aim at finding the best road representation considering geometric constraints on the road shape on one the hand and radiometric constraints due to the property that roads appear as local extrema in optical imagery on the other hand. In [ROCHERY et al. 2004], gaps in an initially extracted road network are closed applying such a method. In [STOICA et al. 2004] a statistical approach based on Markov random fields is introduced. A road network is modelled using Gibbs points processes. The total energy, composed of the data energy, defined by the road model and the image energy, is minimised to find reasonable road model parameters. One advantage of this approach is that the road model can be evaluated by simulation.

The extraction of roads in forest areas is not mentioned here, as the identification of road objects in densely vegetated areas using optical imagery is a quite hopeless venture. In recent research, however, road extraction from multiple aspect SAR (Synthetic Aperture Radar) data shows some good results, even in forest areas [HEDMAN et al. 2005].

2.2.2. Road extraction making use of road databases

A general overview on approaches for object extraction making use of existing GIS data is given in [BALTSAVIAS 2004]. The use mainly consists in limiting the search space and in pre-defining road model parameters.

One motivation for using prior information for road extraction is given by the insufficient modelling of roads. Particularly in road junction areas, some components of the road model, for example the assumption that roads are bordered by parallel edges and have a constant width, are often not valid. In those cases, areas of interest or direction information derived from the prior information can support the extraction algorithms. Yet, the risk of misinterpreting the possibly wrong information from the existing database needs to be minimised, for instance through the application of constraints which restrict the influence of the prior knowledge on the final extraction result.

In [DOUCETTE et al. 1999] the information from a coarse resolution road database is used to initialise road extraction based on a Neural Network approach, i.e. the database information is used to provide input samples. Additionally, the network topology is used to enhance the extraction. In [BORDES et al. 1997] a road database is used to specify the type of road and attributes such as the width. This information is consulted to define hypotheses for the appearance of roads. Features extracted by means of image analysis are then used to evaluate these hypotheses. Similar to [DOUCETTE et al. 1999] the representation of the database objects is very coarse, i.e. derived from 1:100,000 map data, but good enough for limiting the search space and making assumptions on the appearance of the objects due to the type given in the database. In [WALLACE et al. 2002] another approach is applied: as the underlying system is designed to extract also other linear object classes than roads, it carries out a linear object extraction at first and then classifies these objects according to additional knowledge, derived from a database.

In [ZHANG and BALTSAVIAS 2002, ZHANG 2004] the Swiss project ATOMI (Automated reconstruction of Topographic Objects from aerial images using Map Information) is introduced. Its goal is to enhance the geometric accuracy of road objects given in the topographic vector database 1:25,000 by means of automatic image extraction algorithms. The given vector data is generalised as it was captured by digitisation from maps. Similar to BORDES et al. [1997] the database information is used to limit the search space in aerial images and to bias the extraction algorithms via the known attributes. In contrast to BORDES et al. [1997], ZHANG [2004] defines a more sophisticated model which also incorporates context objects, such as vegetation. The demands on the data are high: stereo colour images are needed as well as a high resolution digital surface model.

Traditional pixel-based classification methods are pursued for instance in [SOLBERG 1992] and [WALTER 2000]. The former uses the existing rasterised official Norwegian topographic map, scale 1:50,000, to support the extraction of road pixels from SPOT imagery. Walter utilises the ATKIS DLMBasis as training information for a maximum likelihood classification of aerial imagery. The main deficit of these raster-based approaches is that the linear properties of roads are not exploited. Thus, the often required linear representation needs to be derived in a post processing step, which can only rely on the extracted segments. This procedure normally results in road objects not being necessarily coincident with the imagery.

2.2.3. Road database verification

With the advent of highly detailed and accurate vector data sets such as the ATKIS DLMBasis an automated quality control applying a direct comparison between given objects and extracted objects has become possible. The information can be advantageously exploited for the task given in this thesis. Such vector data are available for example in Germany (ATKIS DLMBasis), in France (BDTopo), or in Great Britain (OS Mastermap).

In [DE GUNST 1996] a very detailed road model (focusing on highways) is formulated for verification. Similar to BORDES et al. [1997], input data from a road database is used to define the search space for the road extraction. The extraction starts with the detection of road markings which are then grouped to carriageways. This approach relies on relatively precise data, as the only inconsistencies being detected are changes in the road properties such as additional carriageways, the width being different from the one registered in the database, and new exits.

The verification of the ATKIS DLMBasis is treated in [PLIETKER 1997]. Lines are extracted in high resolution images (0.3 to 0.5m per pixel) and then grouped. If these lines correspond to the given vector data according to the direction and the distance between them, the vector data is assumed to be correct. If this does not give enough evidence, the next step consists in analysing the region surrounding the line for homogeneity. If this still does not give enough evidence, the neighbourhood of the object is analysed concerning possible disturbing objects, such as forests. The latter information is gathered from the database, not from the imagery. If disturbing objects are identified, the initial steps are applied again, considering the possible occlusions as explanations for gaps in road extraction. After this object-based verification, the given network topology is exploited: if a rejected object is connected to two accepted objects, a new connection hypothesis is created assuming a possible change of attributes or position. Unfortunately, there are no results given for this approach.

In the German WiPKA-QS¹ project [BUSCH et al. 2004, GERKE et al. 2004] road objects from the DLMBasis are verified. The road extraction approach is the one introduced in [WIEDEMANN 2002], thus the verification system is restricted to open landscape areas. Knowledge from the database is mainly used in two ways: firstly, the landscape objects contained in the database are employed to define global context regions, i.e. open landscape, urban, forest. Secondly, road objects define the region of interest for road extraction (considering the nominal positional accuracy of $\pm 3\text{m}$) and support the grouping of extracted lines, as they are also used as seed lines. The given road objects are compared to the extracted ones applying the buffer approach presented in [WIEDEMANN et al. 1998]. The uncertainty of extracted objects and the allowed tolerance of the given objects is represented by a buffer surrounding the objects. Values for completeness and correctness are then derived by an analysis of the intersection sets of these buffers. The developed procedure is embedded in a two-stage graph-based approach, which exploits the connection function of roads and leads to a reduction of false alarms in the verification. Results show that the approach works well in open landscape areas when the impact from disturbing context objects is limited.

2.2.4. Discussion

The overview on road extraction algorithms which do not use prior information on roads from a GIS shows that several aspects are tackled. In all presented approaches the model for road extraction is designed for the appearance of roads in different regions (global context regions). The consideration of background objects interfering with the extraction, i.e. local context objects, requires sophisticated object modelling and extraction algorithms, both regarding road objects and the local context objects. The consideration of local context objects is more important and even indispensable in urban areas compared to open landscape.

In the context of this thesis it is important to achieve a high reliability and efficiency. The goal is to extract as many correct objects as possible and at the same time to minimise the false extractions. One promising means of improving on this is to incorporate topologic information about road networks. Another way to enhance the reliability is to calculate interior evaluation measures, computed for example using redundant information.

¹Wissensbasierter Photogrammetrisch-Kartographischer Arbeitsplatz zur Qualitätssicherung (Knowledge-based Photogrammetric-Cartographic Workstation for Quality Control)

The exploitation of scale space behaviour, the use of methods such as snakes or the application of road trackers show that extensive research has been undertaken during the last decades. Developments in optical sensor technology for satellites, delivering images with a resolution on the ground of 1m or better, are also considered in new publications as well as the increasing exploitation of spectral information.

In summary, the introduced approaches show that *sophisticated road extraction algorithms exist*, at least for open landscape areas.

The presented research studies incorporating existing road databases into the road extraction strategy only make limited use of vector data, because often no information on its precision and up-to-dateness is available. Another reason is that the used data is of low quality in the first place, for instance being represented in a small scale, i.e. being substantially generalised. However, even the (vague) knowledge about the existence and geometry of roads gives valuable hints for an enhanced road extraction compared to the approaches not using prior information.

The overview on approaches on road database verification reveals that no approach exists which allows for an exhaustive and reliable quality control of road vector data. DE GUNST [1996] shows results using simulated vector data instead of information from an existing database. GERKE et al. [2004] use a buffer approach for the verification, which in general does not reflect the quality very well, additionally the shape and position cannot be assessed separately. Nevertheless, GERKE et al. [2004] demonstrate the usefulness of the consideration of road network information for the verification. PLIETKER [1997] shows some interesting components for road database verification, for example the incorporation of context objects and the exploitation of network topology. However, information on context objects from the possibly outdated database may lead to errors and finally, the uncertainty inherent in the data is not considered at all. Since no results are given, the approach cannot be judged thoroughly.

The automatic extraction of the most prominent type of context object in open landscape – trees and rows of trees – is also tackled widely in literature. Depending on the available image data different strategies are pursued. If height data from lidar or from stereo imagery is available, the detection of single trees is reliably feasible [STRAUB 2003]. Generally, rows of objects can be obtained from individual objects by introducing geometric and topologic constraints [GERKE 2002]. Another method to find rows of trees is based on a preceding segmentation of forest areas in images. In [BUSCH et al. 2004] the scene is segmented into built-up, industrial, grassland, cropland and forest areas applying a multi-scale, multi-spectral segmentation approach [GIMEL'FARB 1996]. This supervised algorithm segments an input image into regions of similar properties concerning texture and colour measures of different scales.

Rows of trees can be separated from forest areas by applying geometric constraints (refer to the definition of elongated objects in Section 2.1.1). The incorporation of prior knowledge from the database can also be helpful: if objects of the class rows of trees are contained in the database, they can be used for the restriction of the search space. Moreover, information on global context regions may be utilised to exclude forest areas.

Finally, the findings regarding the existing research on road database verification can be summarised as follows:

- Most of the existing approaches on road database verification lack an adequate modelling of the relations between road and context objects, although recent work in road extraction shows that the incorporation of context objects can give valuable evidence for road objects.
- The statistic properties of the input data are not sufficiently modelled and considered: the common and consistent modelling of the uncertainties and fuzziness during data capture is essential for a successful quality assessment of a given road database.
- Road network topology is incorporated in some approaches and was found to be a valuable means of enhancing the overall results.
- In particular, algorithms for the automatic extraction of road objects and rows of trees from remotely sensed imagery in open landscape areas exist. The results delivered by them constitute adequate input information for the quality assessment of road objects from geo-spatial databases.

In this thesis all these findings are considered in order to develop a new approach to road database quality assessment.

3. A new approach to road database assessment

3.1. Outline

According to the definitions given in Section 1.1, quality assessment deals with the comparison of given road vector data to objects being automatically extracted from an up-to-date orthorectified remotely sensed image. The aspects to be checked are the positional accuracy of the road objects and attribute values obtainable from this data source, particularly the road width. Only commission errors can be identified by this assessment process, whereas the detection of omissions is subject to update, which is not further tackled in this thesis. The result of the quality assessment is an acceptance/rejection decision for each database object.

The discussion in the preceding chapter shows that existing approaches have significant deficits and allows to formulate requirements which a new approach to road database quality assessment from remotely sensed imagery should meet. It needs to

- make use of **extracted road and local context objects**,
- incorporate the **existing road database** into the extraction algorithms, but avoid significant influence of the assessment result by this prior information,
- model the **geometric and topologic relations** between the road objects and local context objects,
- model the **statistical properties** of the incorporated objects,
- **assess in a sound statistical manner** whether an existing ATKIS road object and the extracted objects are in accordance with the modelled relations,
- **collect and balance evidence** given by the extracted objects and finally **infer** the quality of the given road vector data, and
- exploit the road **network topology**.

In this thesis the ATKIS DLMBasis is explicitly used as an example for road databases, however, as pointed out in the introductory chapter, the methodologies developed are not restricted to it.

In Figure 3.1 the components of the developed approach and their connections are sketched. In the following text, all components are described in more detail.

Input data

ATKIS vector data time t_0 : This component contains the road vector data from the DLMBasis which is to be assessed and at the same time used as prior information for object extraction. Additionally, information on global context regions may be obtained from the database.

Sensor data time t_1 : The input information for the object extraction algorithm consists of orthorectified aerial or satellite images. Road vector data and images are assumed to be given in the same coordinate system.

Models

Object model: The object model used refers to two main issues. Firstly, a geometric model is defined considering that all objects incorporated into the assessment are elongated objects and that different geometric representations are necessary for the assessment. Secondly, as objects from different data sources and extraction algorithms are combined, the different levels of precision and certainty have to

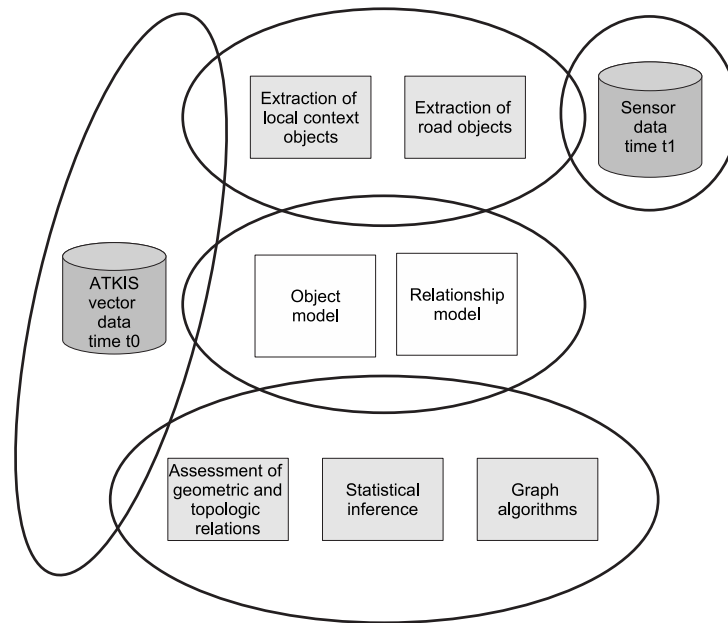


Figure 3.1.: Components for the quality assessment of ATKIS DLMBasis road database objects

be considered in statistical modelling. This modelling also includes the uncertainty propagation for conversions of geometric representations.

Relationship model: Objects from a highly detailed vector database such as the ATKIS DLMBasis have not undergone cartographic generalisation. Thus, topologic and geometric relations between database objects and objects extracted from imagery can be described directly. The use of these relations between roads and context objects advances the assessment, e.g. by including the explanation of gaps in road extraction. In this thesis, the relationship model particularly describes the relations for roads and trees in open landscape areas.

Algorithms

Extraction of road objects: Road objects are extracted from the given sensor data. Additional input information is the road vector data from the database and information on global context regions. The extraction results in a geometric description of road objects, including statistical measures.

Extraction of local context objects: Similar to the extraction of road objects, these algorithms produce a geometric description of local context objects from given sensor data, also including statistical measures. Depending on the available vector database, additional prior information is incorporated.

Assessment of geometric and topologic relations: Based on the extracted objects, each given road vector object is assessed: to what extent, i.e. probability, do the existing geometric and topologic relations between a given ATKIS road object and the extracted objects comply with the modelled one? In this assessment the object specific statistical measures have to be considered adequately.

Statistical inference: The combination of the evidence for an ATKIS road object is accomplished using a statistic inference algorithm, resulting in an acceptance/rejection decision for this object.

Graph algorithms: The network topology is exploited to increase reliability and efficiency of the overall quality assessment results.

In the following sections, the object and the relationship model are defined (Section 3.2). Afterwards, the workflow for the quality assessment of road databases is described in detail (Section 3.3), the realisation of the algorithms is given in Section 3.4. Finally, this chapter concludes with a discussion of the new approaches in Section 3.5.

3.2. Model for objects and their relations

3.2.1. Object model

The requirements for the object modelling are derived from the outline of the approach given above. The model should

- be applicable to all three types of objects being incorporated: ATKIS DLMBasis road objects, extracted road objects, and local context objects,
- allow an adequate geometric description for the assessment of topologic and of geometric relations,
- consider the uncertainties inherent in geo-spatial data, and
- allow the conversion between representations, also including a propagation of uncertainties.

Below, firstly the geometric modelling for the representations *Pointset*, *Medial axis* and *Border lines* is defined, followed by the description and modelling of uncertainties relevant for this thesis, finally the conversion of the representations including uncertainty propagation is presented.

Geometric modelling

All considered objects – extracted objects and AKTIS road objects – are elongated, therefore the approach described in this thesis only deals with this type of objects.

The model provides three geometric representations:

- *Pointset*: a representation of the area covered by the object
- *Medial axis*: the skeletonisation of the object. The definition of the medial axis differs from literature, see below
- *Border lines*: an explicit description of the object's contour

Additionally, the attribute *width* is part of the object definition. Depending on the given data, it is assigned to the whole object as a constant or implicitly given as a variable difference measure between the border lines along the medial axis.

All representations may be defined both in discrete and Euclidean space. However, some definitions made here and subsequently on statistical modelling are explicitly given in one of both spaces. Two representations are of particular importance for the assessment (refer to Fig. 3.2): the pointset \textcircled{S} of the object will be used to assess topologic relations and the medial axis M to assess shapes and orientations. The border lines are necessary for the definition of the medial axis.

The skeleton as described in Appendix A.1 has deficits for elongated objects. The skeleton is not completely placed in the centre of the long-side borders: near the cross-sides of such an object the skeleton is split (see dashed lines in Figure 3.2¹). However, for objects considered here, such a splitting is not desired. Consider for example a road object where the medial axis should touch both cross-sides at their centre. Moreover, branches attached to the axis do not comply with the usual model of a road axis.

Therefore, in this thesis a modified definition for the medial axis is developed. In the remainder the term *skeleton* refers to the definition presented in the appendix and the term *medial axis* refers to the definition given in the following.

¹In order to avoid too many details in the figure, additional branches of the original skeleton are not shown.

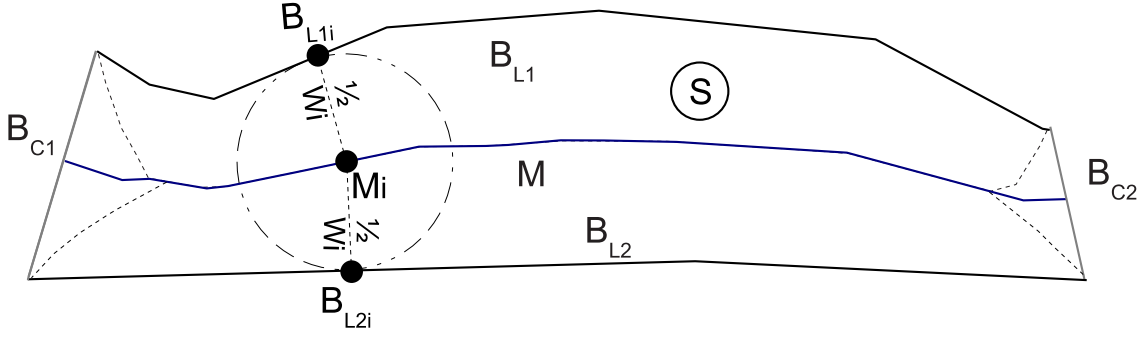


Figure 3.2.: Object model: pointset \textcircled{S} , borders $B_{L1,2}$, $B_{C1,2}$ and medial axis M (continuous line), main branches of the skeleton according to definition in appendix: dashed line. The width W_i is assigned to M_i .

The long-side borders of an object are explicitly given by B_{L1} and B_{L2} . These borders are optionally connected by two cross-side borders B_{C1} and B_{C2} , refer to Figure 3.2. Definitions for the borders are often given by object extraction operators, particularly by road extraction algorithms. If only a pointset is available, the separation of the long-side borders can be derived by a method described later.

The medial axis M is defined in Euclidean space as follows: a point $M_i \in M$ is the centre of a circle with radius $\frac{W_i}{2}$ which touches the points $B_{L1i} \in B_{L1}$ and $B_{L2i} \in B_{L2}$. The medial axis ends at the centres of the cross-side borders B_{C1} and B_{C2} . W_i is the width at M_i .

The definition is similar to interpretations of a skeleton, for example the *grassfire process* (refer to Appendix A.1), but in this case the two fire fronts lit at B_{L1} and B_{L2} can only meet the opposite fire front, avoiding junctions and branches of the medial axis. Since the cross-side borders are not lit, the intersection of the fire fronts from B_{L1} and B_{L2} will finally propagate to B_{C1} and B_{C2} .

Algorithms for the conversion between representations will be defined below.

Statistical modelling

This section addresses the question of how uncertainties in data capture can be modelled for the problem tackled in this thesis. The influences on uncertainty are modelled similarly to approaches in the literature given in Section 2.1.2. In Section 2.1.5 it is pointed out and shown that the consideration of statistic measures in further calculations is more realistic and flexible than a geometric representation. Therefore, in the following uncertainties are not represented explicitly in the geometric description, for instance in a buffer approach.

The notation *uncertainty* is used without a differentiation between *fuzziness* and *imprecision*, i.e. it is understood as a generic term.

The influences on the uncertainty, i.e. Modelling, Abstraction, and Measurement, defined in Section 2.1.2 are incorporated, but an additional influence is considered, which is related to the following issue. The model for the object capture from remotely sensed imagery also comprises the mapping of objects from object space to image space, i.e. a transformation is carried out. For this approach it is assumed that the respective parameters are known accurately enough. Yet, rows of trees, being 3D-objects, are also incorporated into the assessment of database road objects. For the proposed approach these need to be given in their projection in 2D (footprints). Some algorithms extract 3D-objects from imagery, where the height of objects above the terrain was not considered during orthogonal projection. This can lead to an offset in the x-y-plane, i.e. in the orthoimage. The resulting translation of the object's position in 2D has to be considered in the statistical modelling. In order to simplify the modelling, the 3D-object is assumed to have a constant height. For the case of aerial images and central perspective projection Equation 3.1 can be found in [KRAUS 1993].

$$\Delta R = \frac{H}{c \cdot 1/\rho + \tan \alpha}, \quad (3.1)$$

with ΔR : shift in the $x - y$ -plane in the object coordinate system, H : height of the object, c : camera constant, ρ : distance of object from the nadir point in the image (normal case) and α : ground slope at the object, related to the employed surface description.

In Table 3.1 the *statistical components* of the model are introduced. Besides the three components already defined in Section 2.1.2 the *Mapping* from object to image space as described above is added. For each component the probability density function (PDF) is given, including the following notations: D_X is the radius of a uniform distribution and $G_{\sigma X}$ the standard deviation of a Gaussian distribution.

Additionally, the fourth and fifth columns indicate whether the respective component has an impact on the geometric and/or the topologic relation between objects. One can see that two components do not have an influence on the geometric relations: *Object modelling* and *Mapping object \rightarrow image*. The geometric relations are not influenced by the object modelling, because it results in a constant position offset, which does not modify the shape and the orientation of the object as pointed out in Section 2.1.3 on the road database of the ATKIS DLMBasis. The mapping from object to image space does also have no impact on the shape and orientation of the respective object, because the 3D-object is assumed to have a constant height and a limited length. Therefore, the unknown translation can also be set constant for the whole object.

The last two columns indicate which component has an impact on which type of object, i.e. on either ATKIS DLMBasis road database objects or on extracted objects. The modelling has only an impact on ATKIS objects (refer to the nominal values given in Section 2.1.3). The influences of the other components cannot be modelled explicitly as generally no quantitative information on the data capture is available. On the other hand, the extracted objects are assumed to be captured from imagery and thus all related components influence the statistical modelling. The object modelling is not considered here, as it is normally impossible to quantify it. However, it is implicitly contained in the other three components.

Component	PDF and its parameter		Impact on ... relation		Concerns ... objects	
	Normal	Uniform	Geometric	Topologic	ATKIS	Extracted
Object modelling		D_{M_o}	no	yes	yes	no
Mapping object \rightarrow image		D_O	no	yes	no	yes
Abstraction	$G_{\sigma A}$	D_A	yes	yes	no	yes
Measurement	$G_{\sigma C}$		yes	yes	no	yes

Table 3.1.: Statistical components of the object model

The actual values for the statistical parameters depend on many factors and cannot be given generally – they even can be zero (refer to Section 2.1.2). If for example rows of trees are extracted from an orthorectified aerial imagery, where the original exterior and interior orientation parameters are known and the tree heights can be reasonably estimated, the translation can be calculated and thus the planimetric position can be corrected. Then, D_O is approximately zero and thus the offset can be neglected. If however such information is not available, D_O needs to be estimated based on the available knowledge of image acquisition and tree type. An exception is the object modelling of ATKIS road database objects: the nominal accuracy is $\pm 3m$, i.e. D_{M_o} is fixed to $D_{M_o} = 3m$.

To simplify the statistical modelling, the following assumptions are made:

- uncertainty is assigned to every point $P_i \in \textcircled{S}$
- uncertainty is assumed to be identical for every point $P_i \in \textcircled{S}$ and in both coordinate directions
- points of the borders are a subset of \textcircled{S} and therefore have the same uncertainty as every other P_i

These assumptions are reasonable, as the objects considered are captured from digital imagery. If information on any systematic effects is available, for instance for distortions of the optical system, these are normally corrected in the processing.

In the following, the conversion between geometric representations is described including an uncertainty propagation of the statistical components.

Derivation of medial axis from given borders

Geometric representation conversion: The derivation of M from the given $B_{L1,2}$ and $B_{C1,2}$ is realised by applying distance transforms to B_{L1} and B_{L2} in discrete space (refer to Appendix A.1). Points on M are defined at raster cells inside \textcircled{S} where the value of both distance transforms are identical, i.e. at raster cells which have the same distance to B_{L1} and B_{L2} . The medial axis terminates at B_{C1} and B_{C2} . In the case that these borders are not defined, the long-side borders are directly connected by identical points and thus the medial axis terminates at those connection points.

Uncertainty propagation: Any point M_i on M has a certain precision, depending on the given statistical parameters of the border. As pointed out above, a constant translation of the object due to the unknown and possibly wrong mapping from object to image space has no influence on the shape and orientation. Therefore, it does not need to be considered during error propagation for M .

Generally, the precision of M_i can be obtained by applying variance propagation. To simplify the propagation the following assumption is made: the long-side borders are modelled as partly parallel, therefore M_i can be interpreted as the centre between the points B_{L1i} and B_{L2i} . The assumption of partly parallel borders is reasonable for the considered objects roads and rows of trees. Furthermore, the variances of the border points are identical ($\sigma_{P_i}^2$), therefore the variance of M_i is

$$\sigma_{M_i}^2 = 0.5 \cdot \sigma_{P_i}^2. \quad (3.2)$$

The points on the borders follow a mixture of a uniform and a normal distribution. Thus, after the variance propagation as explained here, the information on the probability distribution function is lost. However, the PDF is necessary for some statistical computations, carried out later for the assessment of geometric relations. One reasonable means of overcoming this deficit is to assume a certain PDF, being aware of the fact that this can lead to some imprecision when used for the statistical calculations. In [KUTTERER and SCHÖN 2004] this problem is addressed in conjunction with data interpretation methodologies. It is shown that if the influence of the uniform distribution compared to the Gaussian is small, the difference between the quantiles from the joint Gaussian PDF and the quantiles from the originally convolved PDFs is relatively small.

According to Table 3.1 the only remaining component which is uniformly distributed in the given case is the fuzziness of abstraction with the parameter D_A , i.e. the radius of the uniform distribution. All other components are assumed to follow the Gaussian distribution. The test data used in this thesis (refer to Chapter 4) is supposed to be representative for most practical cases. Using the parameters defined for rows of trees (Tab. 4.3), the maximum difference between the quantiles from the joint Gaussian PDF and the quantiles from the originally convolved PDFs is only 1%. Thus, it is reasonable to use a Gaussian PDF for the medial axis.

The variance of a uniform distribution is defined as $\sigma^2 = D_X^2/3$. Considering the respective variances, the final variance for points on the medial axis is

$$\sigma_{M_i}^2 = 0.5 \cdot \sigma_{P_i}^2 = 0.5 \cdot \left(G_{\sigma^2 A} + \frac{D_A^2}{3} + G_{\sigma^2 C} \right), \quad (3.3)$$

with $G_{\sigma A}$, D_A : standard deviation of a Gaussian distribution and radius of uniform distribution for fuzziness of abstraction and $G_{\sigma C}$: standard deviation for imprecision of measurement.

If desired, the variance of the width at point M_i (W_i) can be calculated as follows: the width can be interpreted as the distance between B_{L1i} and B_{L2i} , therefore

$$\sigma_{W_i}^2 = 2 \cdot \sigma_{P_i}^2 = 4 \cdot \sigma_{M_i}^2. \quad (3.4)$$

If the mean value of all $W_i, i = 1 \dots n$ is calculated, the variance of the mean (W) is

$$\sigma_W^2 = \frac{1}{n-1} \sigma_{W_i}^2. \quad (3.5)$$

Derivation of borders given medial axis and width

Geometric representation conversion: If M and a constant width W are given, the long-side borders are constructed through a parallel translation of the M_i , perpendicular to M . The distance for this translation is $0.5 \cdot W$. The cross-side borders are defined by a straight line between the end points of the long-side borders.

Uncertainty propagation: Similar to the case above, the uncertainty of the mapping from object to image space is assumed to have no influence on the uncertainty of the border. As the border points are derived by a simple shift of the M_i by $0.5 \cdot W$, their variances, given the medial axis and the width, are

$$\sigma_{P_i}^2 = \sigma_{M_i}^2 + 0.25 \cdot \sigma_W^2 = \left(G_{\sigma^2 A} + \frac{D_A^2}{3} + G_{\sigma^2 C} \right) + 0.25 \cdot G_{\sigma^2 W}. \quad (3.6)$$

This is a simplified model since the amount of shift in x - and y -direction also depends on the orientation of the medial axis at point M_i . However, as the uncertainty in both coordinate directions is assumed to be identical, this simplification is reasonable.

Determination of long-side borders for a given pointset

If only a pointset of an elongated object is given, the long-side borders B_{L1} and B_{L2} have to be determined geometrically. In that case no cross-side borders are considered.

Geometric representation conversion: The basic idea is as follows: given an elongated object, the longest linestring derived from its skeleton is part of the medial axis. This procedure ensures that branches along the axis are not considered. Yet, this longest linestring includes undesired branches at its ends, pointing towards convex corners of the object. These branches have to be identified and adequate points on the border, representing end points of the medial axis, have to be found. The medial axis is constructed as follows:

- Derive the skeleton of \textcircled{S} , refer to Figure 3.3.
- Find junctions of the skeleton, i.e. nodes with a degree larger than 2 (depicted by squares in Figure 3.3).
- Find the longest linestring inside the skeleton: it is given by the maximum shortest path between the junctions (the hatched squares in Figure 3.3 are the endpoints of the longest linestring). The longest linestring is obtained by the A*-Algorithm [DUDA and HART 1973].
- Extend the skeleton at the endpoints of the longest linestring towards the border. The points, where the border is split, i.e. where B_{L1} and B_{L2} meet, are given by the intersection points of this extension and the border (points in Figure 3.3).

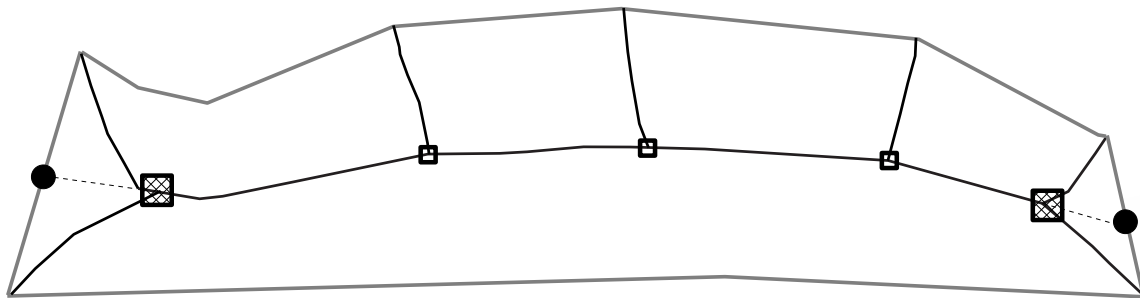


Figure 3.3.: Construction of intersection points of long-side borders. Continuous black line: skeleton, squares: junctions of the skeleton, hatched squares: endpoints of the longest linestring inside the skeleton, dashed line: straight extension of the skeleton at junction, circles: points, where the long-side borders meet.

Uncertainty propagation: As the points of the borders are assumed to be a subset of \textcircled{S} , their statistical measures are identical to those of \textcircled{S} . Therefore, a propagation is not necessary.

Derivation of pointset from borders

Geometric representation conversion: The pointset \textcircled{S} is implicitly given by the borders: it is the area enclosed by the borders B_{L1} and B_{L2} (optionally also B_{C1} and B_{C2}). By definition adjacent borders share the same endpoints, therefore \textcircled{S} is closed.

Uncertainty propagation: As the points of the borders are assumed to be a subset of \textcircled{S} , their statistical measures are identical to those of \textcircled{S} . Therefore, a propagation is not necessary.

3.2.2. Relationship model

The relationship model describes geometric and topologic relations between an ATKIS DLMBasis road object, the local context objects and the extracted road objects (refer to Figure 3.4). The shown model is restricted to open landscape areas and the object class *row of trees* is an example for local context objects, thus the connection type *generalisation* is used in the shown model. The object classes are connected through *associative* links, and the modelled relations are interpreted as attributes of the association. This notation has been chosen according to UML¹.

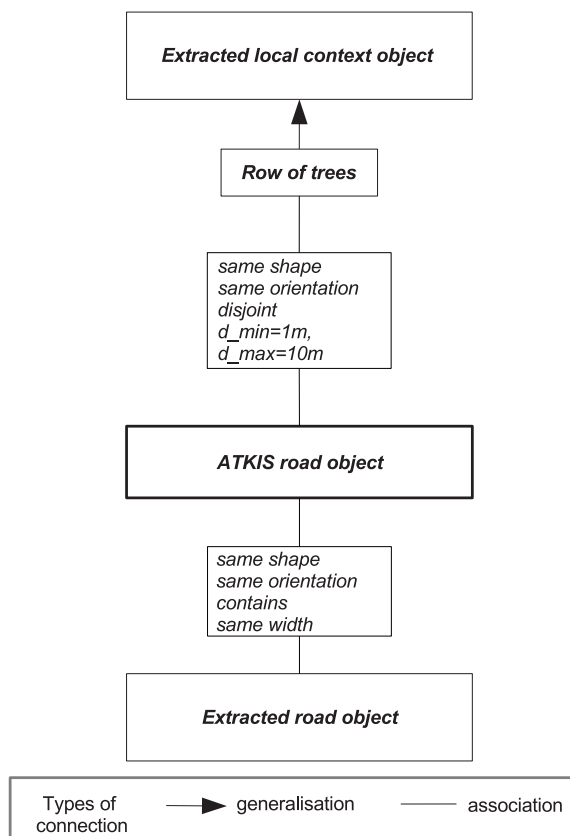


Figure 3.4.: Relationship model

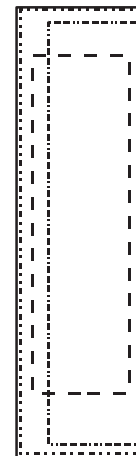


Figure 3.5.: Road database object (continuously drawn box) and three possible relations to extracted road objects (dashed boxes): *contains*, *cover*, *equal*

In contrast to many other definitions given in literature, here *geometry* does not comprise the position of an object, but the *shape and orientation*. The relative position of objects is modelled by *topology*. The absolute position is of minor importance here, because georeferencing is assumed to be correct.

¹Unified Modeling Language [AMBLER 2005]

The geometric relations *same shape* and *same orientation* express the fact that the shapes of an ATKIS road object and the respective extracted object need to be identical and that both objects must have an identical orientation, but a tolerance value δ_i for the angle between two objects is introduced.

Topologic relations are important for this thesis because for example rows of trees – more precisely the trunks of the trees – must be located outside the road given in ATKIS, whereas an extracted road, i.e. the surface of the road, must be identical to or at least within the ATKIS road. The topologic relations considered are *disjoint* and *contains*. The latter one is defined relative to the ATKIS object, i.e. the ATKIS road object *contains the extracted object*. Concerning extracted road objects, this is a minimal requirement: normally one would request the identities of an extracted road object and an ATKIS road object. But as all considered objects are elongated, such a requirement would be too strict. If for example two objects are identical, but one of the objects is shorter than the other, the relation *equal* becomes less probable. Thus, the relation *contains* is given in the model. However, the probability that the relations *equal* and *cover* exist between the respective objects are also calculated and supports the required relation *contains*, refer to section 3.4.3. In Figure 3.5 an example for valid configurations according to the model is sketched: a road object from the ATKIS DLMBasis (bordered by a continuous line) and extracted road objects, given in three possible relations to the ATKIS road object, i.e. *contains*, *cover*, *equal*, bordered by dashed lines.

Besides this qualitative topologic relation one may define side conditions. For *disjoint* it can be desirable to give a minimum and a maximum distance (d_{min}, d_{max}). Due to security reasons, a row of trees must have a minimum distance to the road and it is also expected that trees having a distance to the road larger than a certain value cannot explain gaps in the road extraction, i.e. they do not cover the road in aerial imagery. For *contains* an *same width* of objects may be required additionally. The relations between the *ATKIS road object* and the *local context object* and the respective values in the given relationship model are defined by experience and common knowledge. An alternative way to find the measures would be to incorporate official specifications, for instance from road construction.

Freestanding trees are not considered here, as only elongated objects are taken into account. The treatment of points and arbitrarily shaped regions is not in the scope of this thesis.

3.3. Workflow

The process of road database assessment as proposed in this thesis consists of three main parts: *Initial object assessment*, *Graph analysis* and *Final object assessment*. This partitioning makes the network exploitation aspect explicit. To shorten the following text, the term *Phase 1* is used for the *Initial object assessment*, while *Phase 2* is employed for the *Final object assessment*. Phase 1 aims at a very reliable result. This means, the number of falsely accepted road objects (false positives) should be very small. As a consequence, the total number of accepted road objects will be quite low. In the Graph analysis part the network function of the road net is exploited, and local context objects are also incorporated. The idea is to identify those roads which have been rejected in Phase 1 but which perform important network functions, i.e. connect reliably extracted road network components. If local context objects give hints regarding the correctness of those important road objects, they will be accepted, otherwise they will be subject to a second assessment in Phase 2. In that phase road extraction is applied a second time, but the algorithm is modified to extract more tolerantly. The use of these tolerant parameters for the whole scene in Phase 1 would usually lead to an unacceptably high number of false positives. Only the support given by topological considerations allows the application of more tolerant parameters. Phases 1 and 2 are related to single road objects of the ATKIS DLMBasis, whereas in the Graph analysis the transition to network edges is performed.

The workflow is sketched in Figure 3.6. The individual components are briefly introduced and justified in the following, while the respective methodologies are described in detail in the next sections. The following components are involved:

Extraction of road objects: As pointed out in the discussion regarding existing work on road extraction and on road database verification (Section 2.2.4), the road extraction algorithm should incorporate the existing road vector data – in the case of ATKIS DLMBasis, the individual road objects. How this

information is used depends on the specific algorithm. Yet, the influence of the prior information on the final assessment result needs to be restricted. The road extraction algorithm must also offer the possibility to adapt its behaviour concerning the sensitivity, i.e. to set different parameters for Phase 1 and Phase 2. An example is given in Chapter 4, where the approach proposed in [WIEDEMANN 2002] is used for testing purposes.

Extraction of local context objects: Whether prior knowledge is incorporated in the extraction of local context depends on the available data, however, the remarks on the restriction of the influence on the final result given above for roads are also valid here. In this thesis, automatically extracted rows of trees obtained by means of the approach of GIMEL'FARB [1996] are used as well as manually digitised rows of trees. Details are given in Chapter 4.

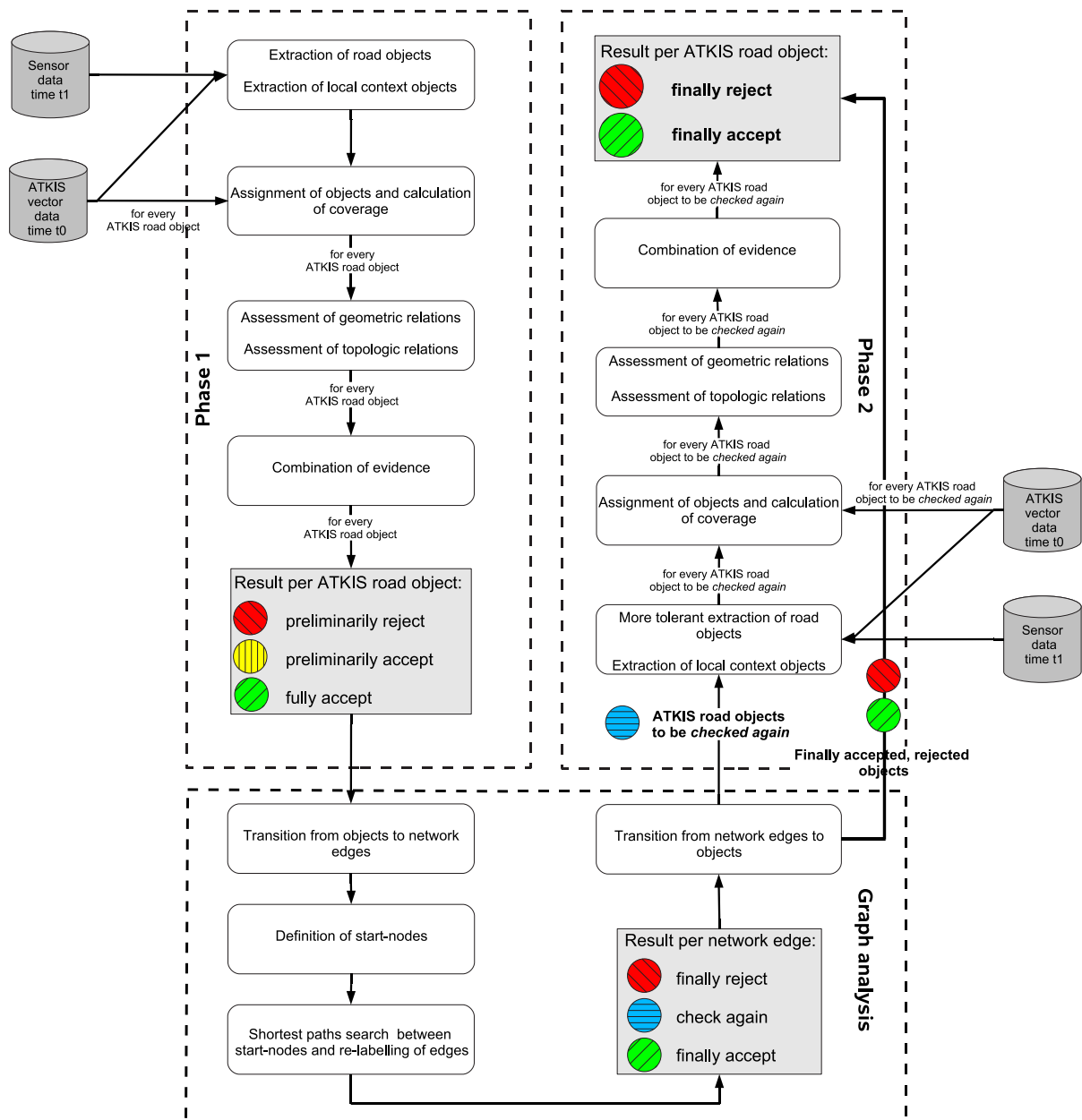


Figure 3.6.: Workflow of processes

Assignment of objects and calculation of coverage: The objects extracted in the preceding steps are assigned to the individual road objects from the ATKIS DLMBasis. Three issues are related:

1. The computation time is reduced, since in the following assessment steps only those extracted objects are considered which have a direct connection to an ATKIS road object. Whether this connection is given depends on the modelled topologic relation between the class of the extracted object and the ATKIS road object, but is also influenced by the uncertainty measures assigned to the objects. Consider for example an extracted road object (modelled to be *contained* in the ATKIS road object and having the *same width*): according to the given uncertainty measures, *buffers of interest* enclosing the objects are defined. All extracted road objects being placed completely outside this buffer are not considered for the assessment of the respective ATKIS object.
2. Some objects assigned to a given ATKIS road object need to be clipped if they extend considerably beyond the ATKIS object, i.e. some parts of these objects cannot give evidence regarding the correctness of the road object,
3. During this assignment the relative *coverage* of the extracted object and the ATKIS road object is obtained. This coverage is of importance for the calculation of the evidence concerning the coincidence of the modelled and the actual relations between both objects.

Assessment of geometric relations and Assessment of topologic relations: Here, the probabilities that the geometric and topologic relations between a given ATKIS road object and every assigned extracted object correspond to the model are calculated.

Combination of evidence: The goal is the combination of the individual evidence given by the algorithms defined in the above components regarding one ATKIS road object. To attain one objective of this thesis, namely to compare a traditional probabilistic and the Evidential approach, both of them are applied for this task. This leads to a maximum probability or a maximum support decision regarding the correctness of the object, respectively.

Depending on the phase, the ATKIS road objects are then labelled as *preliminarily reject*, *fully accept*, *preliminarily accept (Phase 1)* or *finally reject*, *finally accept (Phase 2)*. The main difference between both phases consists in how local context objects are incorporated into the assessment, e.g. if in Phase 1 only the extracted road objects together with local context objects give enough evidence for the correctness of an ATKIS road object, the latter is labelled *preliminarily accept*.

Graph analysis: Here, those ATKIS road objects not having been fully accepted in Phase 1, but which fulfil an important network function are selected. They are either accepted directly or checked again in Phase 2, where less restrictive parameters for road extraction are applied. The decision between those two options depends on whether local context objects give evidence concerning the correctness of the ATKIS road database object.

The approach to road network topology exploitation is based on the assumption that a road network connects any two points (called *start-nodes* below) in a way minimising travel time and distance. In the absence of knowledge about travel time, only distance is considered. In other words, the shortest path between two start-nodes is searched for, based on the ATKIS DLMBasis road database. Although it is not certain whether the network given in the database is fully correct, it can be used to formulate such connection hypotheses.

The procedures employed are shortly introduced below, a more detailed description is given in Section 3.4.5.

- Transition from objects to network edges: the assessment result per ATKIS road object is transferred to edges of the road network. This is important to be able to reasonably analyse the network function of the assessed roads.
- Definition of start-nodes: nodes connected to edges, which after the initial assessment are assumed to be highly reliable are labelled as start-nodes.
- Shortest path search between start-nodes and re-labelling of edges: The shortest paths between start-nodes are identified. The edges are labelled afterwards according to the following rules: if a

preliminarily rejected edge is part of a shortest path, it is labelled as *check again*. If a preliminarily accepted edge is part of a shortest path, it is labelled as *finally accept*. All remaining preliminarily rejected or accepted edges are labelled as *finally reject* as it is assumed that they do not fulfil an important network function. The possible transitions between the single assessment results are given in Figure 3.7.

- Transition from network edges to objects: the labels from the edges are transferred to the ATKIS road objects. The objects being labelled as *check again* are prepared to be processed again in Phase 2, the remaining objects, i.e. objects being labelled *finally accept* and *finally reject*, are not checked again.

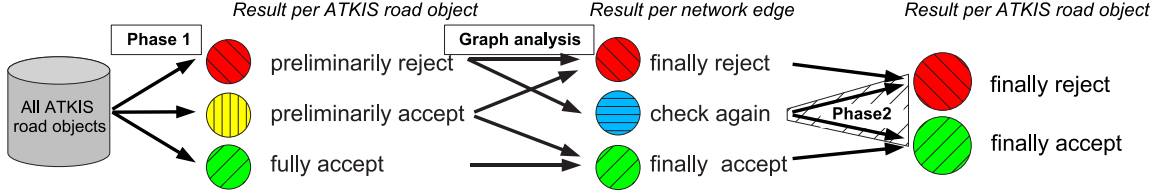


Figure 3.7.: Possible transitions between assessment results concerning the three parts Initial object assessment (Phase 1), Graph analysis, Final object assessment (Phase 2)

In the figures the colours of a traffic light are used to indicate the decisions. In [FÖRSTNER 1996] the so-called traffic light paradigm is formulated. It should be pointed out that the given indication differs slightly from the interpretation given in the named paradigm. In the latter, the colours are interpreted as the outcome of a quality assessment, derived from an interior evaluation by an automatic image interpretation operator. Only the decisions from Phase 2 can be interpreted in this regard; in Phase 1 the colours yellow and red only represent preliminarily results.

3.4. Realisation

3.4.1. Assignment of objects and calculation of coverage

According to the preceding section, in the components of Phase 1 and 2 only individual ATKIS road objects are considered. In the following text the notation A is used for such an object.

The task of the *assignment and calculation of coverage*-component is to find those N extracted road objects and local context objects (or parts of them) $E_i, i=1 \dots N$, which might give evidence concerning the question of whether A maintains the relations modelled in the relationship model. Additionally, the respective amount of coverage $qcov_i$ is calculated. This value becomes important when the evidence given by E_i is combined (refer to Section 3.4.4). It is used as a weighting factor indicating the influence E_i has on the overall assessment of A .

A *buffer of interest* is calculated for every object by applying a morphologic dilation on the pointset representation \textcircled{S} . The radius of the circular structuring element used for the dilation depends on the uncertainty measures assigned to the individual object: the radii of the uniform distributions are considered as well as the 99%-quantiles of the respective Gaussian distributions. If a maximum distance d_{max} is given for the topologic relation *disjoint*, it is also taken into account for the dilation radius. The dilation radius can be interpreted as a *snapping distance*. All extracted objects and local context objects whose buffer of interest intersects the buffer of interest of A are considered as being assigned to A , i.e. they become part of the set $E_i, i = 1 \dots N$. A special case exists when the road objects from the ATKIS DLMBasis have been incorporated into the road extraction algorithm: then the assignment is explicitly given.

All extracted road objects and local context objects E_i being assigned to A according to the buffer of interest are further examined. The projections of E_i onto A ($= A'_i$) in Figure 3.8 are interesting in two different aspects. Firstly, objects reaching beyond A are clipped, refer to E_1 in the figure. The finally assigned parts are labelled E'_i . Secondly, the relative coverage $qcov_i$ is calculated by

$$qcov_i = \frac{|A'_i|}{|A|}, \quad (3.7)$$

where $||$ denotes the length of the medial axis.

It is important to point out that $qcov_i$ is a stochastic variable, since it is a function of uncertain objects. However, as it can be safely assumed that the uncertainty of the objects is small against the length of the medial axis, $qcov_i$ is treated as an error-free function. Moreover, the uncertainty measures given for E_i or A remain the same for E'_i or A'_i even if the objects have been clipped.

The *total coverage* is given by the length of the union of all projected objects, relative to the length of A :

$$total\ coverage = \frac{|\cup_{i=1}^N A'_i|}{|A|}. \quad (3.8)$$

Besides A'_i and E'_i , the following abbreviations will be used:

A : ATKIS road object

ERO : extracted road object

LCO : local context object

cov_ERO : total coverage of A with $EROs$

cov_LCO : total coverage of A with $LCOs$

cov_ERO_LCO : total coverage of A with $EROs$ and $LCOs$

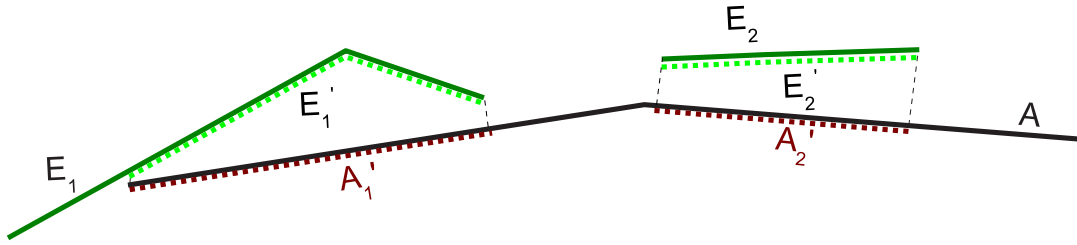


Figure 3.8.: Assignment of objects E_1 and E_2 to A . E_1 is clipped. The assigned objects are E'_1 and E'_2 . The projections on A , A'_1 and A'_2 , are used to compute $qcov_1$ and $qcov_2$.

3.4.2. Assessment of geometric relations

In this component the probability P_{g_i} is calculated. It expresses to what extent the ERO or the LCO E'_i and the respective projection onto the ATKIS road object (A'_i) maintain the modelled geometric relations *same shape* and *same orientation*. Only A'_i is considered here and not the complete ATKIS object A . It is assumed that any object E'_i only gives evidence regarding the quality of an ATKIS object for the covered section of A , namely A'_i .

The probability P_{g_i} consists of two components: $P_{g-shape_i}$, expressing to what extent the shapes of E'_i and A'_i are identical and P_{g-ori_i} concerning the identity of the orientation of both objects. The final probability is (assuming independence) the product of both measures:

$$P_{g_i} = P_{g-shape_i} \cdot P_{g-ori_i}. \quad (3.9)$$

The medial axis representation is used for the calculation of both components. According to Section 3.2, the uncertainty inherent in the medial axis is modelled by a Gaussian distribution. Its parameter, the variance G_σ^2 , is either given directly by the object extraction operator or from error propagation. In the case that a uniform distribution is assumed for the fuzziness of abstraction (parameter D_A) for the medial axis, it needs to be approximated by a Gaussian, refer to Section 3.2. As mentioned in Section 2.1.3 concerning the road database of the ATKIS DLMBasis and in the modelling Section 3.2, the modelled uncertainty inherent in ATKIS road objects is interpreted as a constant shift and therefore not considered for the assessment of geometric relations. Thus, in the remainder of this section the medial axis of A is assumed to be error-free.

The components $P_{g-shape_i}$ and P_{g-ori_i} are defined as follows:

Two objects, represented by their medial axis, are supposed to have a *same shapes* if their *local* course is identical.

Two objects, represented by their medial axis, are assumed to have *same orientation* if their *global* course is identical.

Figure 3.9 illustrates the definitions, simulating a portion of uncertainty.

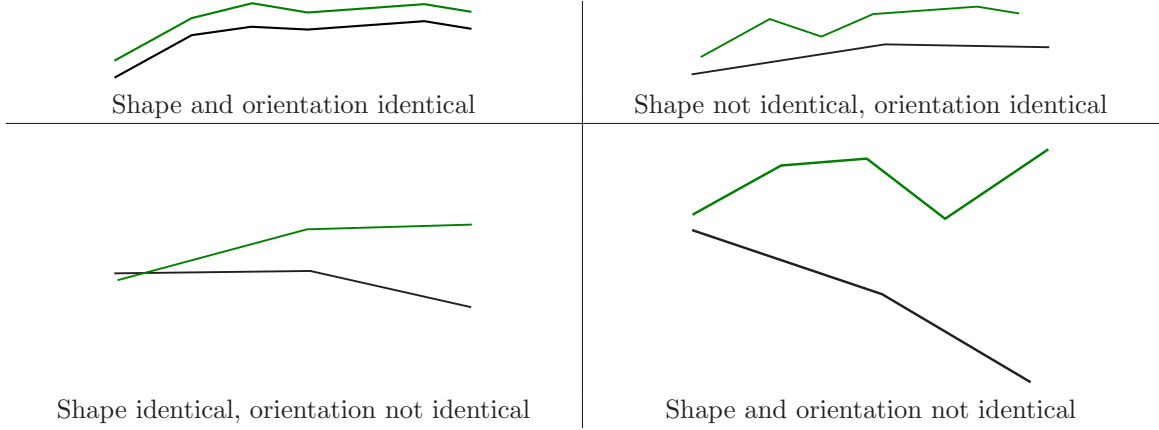


Figure 3.9.: Four examples for the identity of shape and orientation of two linestrings

Assessment of identity of shape: The basic idea of comparing the shape of two objects as pursued in this thesis is that if the shapes of these objects are identical, the translation and rotation invariant line moments up to a certain order need to be identical, too. This is based on the moment uniqueness theorem, refer to Section 2.1.4: since an object can be represented by an (infinite) set of moments, two objects are identical, if their moments (up to a certain order) are identical. The use of *translation and rotation invariant* moments is allowed since a unique coordinate system is requested. The utilisation of translation invariant moments permits to assess the relative position of the objects using topology which is flexible concerning the definition of neighbourhood relations. Furthermore, the use of *rotation invariant* moments offers the possibility to assess *shape* and *orientation* separately: if the moments were not invariant to rotation, the orientation of the objects would be checked implicitly. This is not desired as the relationship model allows the explicit incorporation of a tolerance into the orientation assessment. Finally because the coordinate system is identical for all objects, the moments used here do not need to be and are not scale invariant.

When the uncertainties of the objects are considered, the comparison of the moments can be expressed in terms of a statistical test. The choice of the maximum regarded order can be seen in this context. Depending on the uncertainties and the actual shape, moments above a certain order are not significantly different from zero, refer also to the example in Appendix A.2 (Fig. A.4 and Tab. A.1). By various experiments undertaken with real and simulated data it was found that moments of an order higher than eight are not significant within this application. Therefore, the maximum order applied here is $o_{max} = 8$. Moreover, the moments of the first and second order are used for the calculation of the centre of gravity and the orientation, and are thus implicitly considered in the moments of higher orders. For this reason, the minimum order used for the comparison of translation and rotation invariant moments is $o_{min} = 3$.

The probability P_{pq} that the translation and rotation invariant moments $\mu'_{pq A_i'}$ and $\mu'_{pq E_i'}$ of two objects A_i' and E_i' are equal is expressed by the probability that the difference of both moments is zero. The difference is $D_{pq} = \mu'_{pq A_i'} - \mu'_{pq E_i'}$ and its variance is $\sigma_{D_{pq}}^2 = \sigma_{\mu'_{pq E_i'}}^2$ since A_i' is assumed to be error-free. If translated to a standard normal distribution with the test statistic $\tilde{D}_{pq} = D_{pq}/\sigma_{D_{pq}}$, the probability P_{pq} for $\tilde{D}_{pq} = 0$, is [NIEMEIER 2002]:

$$P_{pq} = F(y_{1-\alpha/2} - \tilde{D}_{pq}) - F(y_{\alpha/2} - \tilde{D}_{pq}), \quad (3.10)$$

with $y_{1-\alpha/2}$ and $y_{\alpha/2}$: boundaries of the confidence interval (quantiles of the standard normal distribution). Here the probability of error $\alpha = 0.01$ is chosen. F is the normal distribution function. In Figure 3.10 the fact that P_{pq} equals the area under the density function of \tilde{D}_{pq} between the confidence boundaries is illustrated.

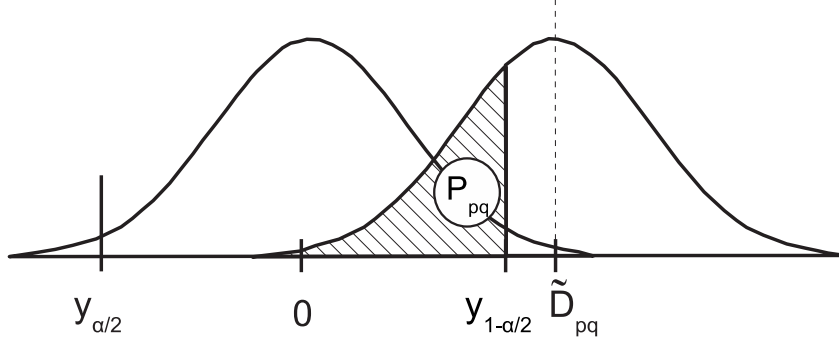


Figure 3.10.: Calculation of P_{pq}

Finally, the probability $P_{g-shape_i}$, considering all moments with order o from o_{min} to o_{max} is

$$P_{g-shape_i} = \prod_{o=o_{min}}^{o_{max}} \prod_{q=0}^o P_{pq} \text{ with } p = o - q. \quad (3.11)$$

Assessment of identity of orientation: An overall orientation of both objects ($t_{E'_i}$ and $t_{A'_i}$) is calculated, taking into account the variance of the assigned Gaussian density function derived by variance propagation: the orientation is given by the endpoints of the medial axis, while the variance is propagated using every single line segment. The difference of both orientations Δ_t is computed including its variance $\sigma_{\Delta_t}^2$. This difference must be inside the boundaries defined by the maximum tolerance value δ_t – refer to the relationship model in Section 3.2.2. Therefore, the calculation of P_{g-ori_i} , constituting the probability that both orientations are identical, is similar to the determination of P_{pq} , except for the fact that the boundaries are shifted by $\delta_t/2$ (with $\tilde{\Delta}_t = \Delta_t/\sigma_{\Delta_t}$ as test statistic):

$$P_{g-ori_i} = F\left(\left(y_{1-\alpha/2} + \frac{\delta_t}{2}/\sigma_{\Delta_t}\right) - \tilde{\Delta}_t\right) - F\left(\left(y_{\alpha/2} - \frac{\delta_t}{2}/\sigma_{\Delta_t}\right) - \tilde{\Delta}_t\right). \quad (3.12)$$

In the case that no tolerance for the orientation is defined, i.e. $\delta_t = 0$, the test reduces to the question whether the difference is zero, which is quite reasonable.

3.4.3. Assessment of topologic relations

This section describes the computation of the probability P_{t_i} , expressing to what extent both objects A'_i and E'_i maintain the modelled topologic relation.

As pointed out in Section 2.1.5, the approach to the assessment of topologic relations between uncertain regions by WINTER [1996] allows to flexibly model and adequately incorporate different impacts on the uncertainty inherent in geo-spatial objects. However, three main issues need to be tackled in order to be able to apply this method for the task at hand:

1. The side condition of given d_{min} , d_{max} for the relation *disjoint* needs to be handled.
2. The requirement that the object size is large compared to the uncertainty does not hold for every case here. Consider for example a row of trees: according to the relationship model the trunks are modelled. They have a quite small diameter compared to the fuzziness of abstraction D_A , or the fuzziness due to the unknown translation offset D_O .

3. The side condition *same width* has to be checked.

A solution for these issues is developed in the following.

1. Incorporating the side conditions d_{min}, d_{max} for the relation *disjoint*: If in the relationship model the topologic relation between two objects is modelled as *disjoint*, but at the same time a minimum d_{min} and a maximum distance d_{max} are required, the distance classes $\omega_-, \omega_0, \omega_+$ need to be extended. The class ω_0 then represents the zone between both objects, i.e. the minimum and maximum distance of the distance transform between both objects need to be within this class. This class is not interpreted as *IsZero* anymore. However, formally the same algorithm given by WINTER [1996] can be applied, considering a modified interpretation introduced in the following. The borders of the distance classes ω_- and ω_+ need to be modified accordingly¹:

$$\Omega_{\vartheta} = \{\omega_-, \omega_0, \omega_+\} \text{ with } \begin{cases} \vartheta_{AE} \in \omega_-, & \text{if } \vartheta_{AE} < d_{min} \\ \vartheta_{AE} \in \omega_0, & \text{if } d_{min} \leq \vartheta_{AE} \leq d_{max} \\ \vartheta_{AE} \in \omega_+, & \text{if } \vartheta_{AE} > d_{max}. \end{cases} \quad (3.13)$$

If no side condition is given, i.e. $d_{min} = d_{max} = 0$, the definition of the borders becomes equivalent to the one given by WINTER [1996].

The modified equivalence of the triplet $\{C, \omega_{min}, \omega_{max}\}$ and the modelled topologic relations are listed in Table 3.2. Note that the modelled relation *contains* substitutes the original relations *contains*, *covers* and *equal*, as it is allowed that the boundaries of the respective objects overlap. Special attention has to be paid if the side condition *same width* is given for *contains*. It cannot be checked by means of the distance function and will be addressed later.

Rel.	Cluster	Modelled Relation	Side Cond.?	$\omega_{min}[d_{min}, d_{max}]$	$\omega_{max}[d_{min}, d_{max}]$	Original Relation
C_1		disjoint	no	$\omega_+[0, 0]$	$\omega_+[0, 0]$	disjoint
C_1		disjoint	yes	$\omega_0[d_{min}, d_{max}]$	$\omega_0[d_{min}, d_{max}]$	–
C_2		contains	no/yes	$\omega_-[0, 0]$	$\omega_-[0, 0]$	contains
C_2		contains	no/yes	$\omega_-[0, 0]$	$\omega_0[0, 0]$	covers
C_2		contains	no/yes	$\omega_0[0, 0]$	$\omega_0[0, 0]$	equal

Table 3.2.: Equivalence of $\{C, \omega_{min}, \omega_{max}\}$ and modelled topologic relations

For the definition of probability density functions for the distance classes the definitions from the statistical modelling in Section 3.2.1 are taken into account. Here, the notation for the parameters of the uniform distributions is slightly modified: $D[a, b]$ constitutes a uniform distribution with left and right boundaries a and b . As defined earlier, $G_{\sigma X}$ is the standard deviation of a Gaussian distribution. The density functions $p(\underline{\mu} = \mu_{\vartheta} | \omega_i)$ for the conditional probability that a measured distance μ_{ϑ} matches class ω_i are given by the following definitions (for the notation of the parameters refer to Table 3.1 in Section 3.2.1)²:

Contribution of an ATKIS road object A :

$$\begin{aligned} p_A(\underline{\mu} = \mu_{\vartheta} | \omega_-) &= D[\vartheta_{min.poss.} - D_{Mo}, d_{min} + D_{Mo}], \\ p_A(\underline{\mu} = \mu_{\vartheta} | \omega_0) &= D[d_{min} - D_{Mo}, d_{max} + D_{Mo}], \\ p_A(\underline{\mu} = \mu_{\vartheta} | \omega_+) &= D[d_{max} - D_{Mo}, \vartheta_{max.poss.} + D_{Mo}]. \end{aligned} \quad (3.14)$$

The contribution of an extracted object E is given by a convolution of PDFs according to the modelled influences:

$$\begin{aligned} p_E(\underline{\mu} = \mu_{\vartheta} | \omega_-) &= D[\vartheta_{min.poss.} - D_O, d_{min} + D_O] * D[\vartheta_{min.poss.} - D_A, d_{min} + D_A] * G_{\sigma A} * G_{\sigma C}, \\ p_E(\underline{\mu} = \mu_{\vartheta} | \omega_0) &= D[d_{min} - D_O, d_{max} + D_O] * D[d_{min} - D_A, d_{max} + D_A] * G_{\sigma A} * G_{\sigma C}, \\ p_E(\underline{\mu} = \mu_{\vartheta} | \omega_+) &= D[d_{max} - D_O, \vartheta_{max.poss.} + D_O] * D[d_{max} - D_A, \vartheta_{max.poss.} + D_A] * G_{\sigma A} * G_{\sigma C}. \end{aligned} \quad (3.15)$$

¹To simplify the notation in the following, the indices A and E are used for the objects instead of A'_i, E'_i .

²To simplify the notation the term $p(\underline{\mu} = \mu_{\vartheta} | \omega_i)$ is used in the following, although the imprecision of the boundary points (separately modelled by p_{ϵ} in section 2.1.5) is already incorporated here.

The final density functions are obtained by a further convolution:

$$\begin{aligned}
 p(\underline{\mu} = \mu_{\vartheta} | \omega_{-}) &= p_A(\underline{\mu} = \mu_{\vartheta} | \omega_{-}) * p_E(\underline{\mu} = \mu_{\vartheta} | \omega_{-}), \\
 p(\underline{\mu} = \mu_{\vartheta} | \omega_0) &= p_A(\underline{\mu} = \mu_{\vartheta} | \omega_0) * p_E(\underline{\mu} = \mu_{\vartheta} | \omega_0), \\
 p(\underline{\mu} = \mu_{\vartheta} | \omega_{+}) &= p_A(\underline{\mu} = \mu_{\vartheta} | \omega_{+}) * p_E(\underline{\mu} = \mu_{\vartheta} | \omega_{+}).
 \end{aligned}
 \tag{3.16}$$

These formulas are also valid in the case that no side condition for *disjoint* is given, i.e. $d_{min} = d_{max} = 0$. The variables $\vartheta_{min.poss.}$ and $\vartheta_{max.poss.}$ denote the theoretical extreme values of ϑ . They describe the size of the finite space where the skeleton is defined. In practical applications they are derived from the maximum diameter of the minimum bounding rectangle containing both objects.

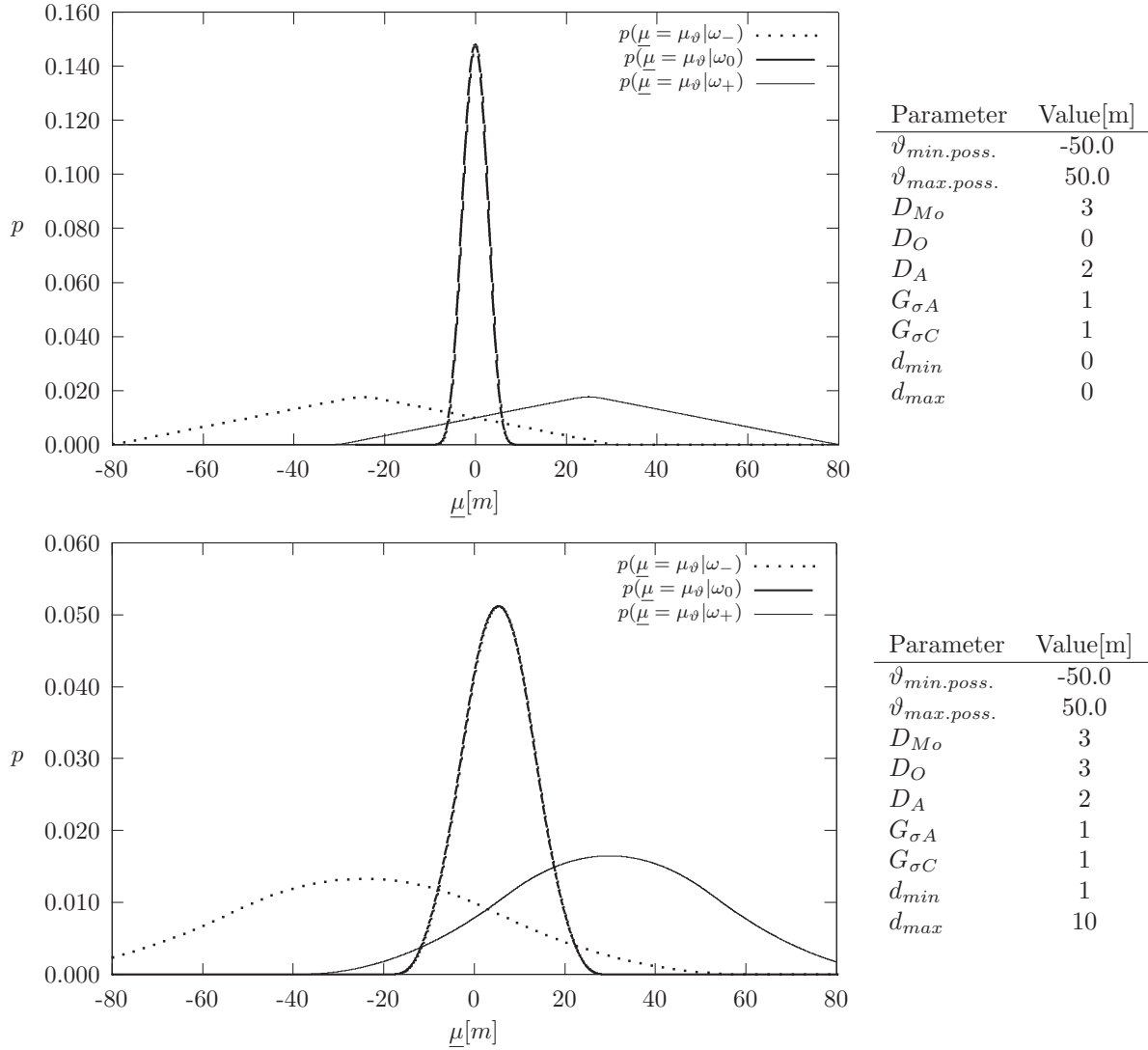


Figure 3.11.: Density functions for distance classes. Top: typical parameters for an *extracted road object*, bottom: typical parameters for a *row of trees* (note that the vertical scale of both plots differs).

In Figure 3.11 two examples are given. The parameters for the density functions are shown on the right hand side. For the upper example a typical parameter setting for an extracted road object has been chosen: no side conditions d_{min}, d_{max} are given (the topologic relation is *contains*) and the fuzziness from mapping D_O is assumed to be zero. In contrast, in the lower example d_{min} and d_{max} are set, i.e. it implies the relation *disjoint* with side condition and D_O is larger than zero. It comprises a realistic parameter setting for a row of trees extracted from orthoimages, where the heights of the trees have not been incorporated into the orthorectification.

Concerning the resulting density functions in Figure 3.11, some observations can be made: $p(\underline{\mu} = \mu_{\vartheta}|\omega_-)$ and $p(\underline{\mu} = \mu_{\vartheta}|\omega_+)$ for the upper example are approximately triangular functions – the radii of the uniform distributions of the A and E -object are identical and due to the large overall radius the influence of the Gaussian is small. On the other hand, the influence of the Gaussian on $p(\underline{\mu} = \mu_{\vartheta}|\omega_0)$ is significant compared to the uniform distribution. In the lower plots the additional uniform function for the extracted object leads to a flattening of $p(\underline{\mu} = \mu_{\vartheta}|\omega_-)$ and $p(\underline{\mu} = \mu_{\vartheta}|\omega_+)$. The given d_{min} and d_{max} lead to an increased size of the uniform distribution for ω_0 , representing the desired space in-between roads and rows of trees.

2. Violation of size constraint: If the constraint defined by WINTER [1996] that the uncertainties of an object are small compared to its extent is violated, one issue becomes important: the decision of whether two objects undergo relations in cluster C_1 or C_2 cannot be made using the overlapping factor, refer to Equation 2.1 in Section 2.1.5. In the application at hand, the relation cluster is explicitly given by the type of object E'_i : the topologic relation is defined by the relationship model. The only interesting questions here are whether this relation holds for the objects A'_i and E'_i and what the respective probability is.

As pointed out in Section 2.1.5, the skeleton S_2 is closed per definition and S_1 may have open ends only in $A^c \cap E^c$. This restricts the possible configurations of A and E . In case C_1 is implied, i.e. the relation *disjoint* (with or without side condition d_{min}, d_{max}) is requested, the certain zones P and Q must not be empty sets in Figure 3.12. On the left hand side an invalid configuration is shown as E is completely contained in A , and therefore Q is empty. The other two configurations are valid. The same condition on non-empty sets P and Q is given for C_2 , i.e. the relation *contains*. The left hand side of Figure 3.13 shows an invalid configuration since A and E are disjoint and Q vanishes. The examples for invalid configurations show that in these cases the distance function along the skeleton of the disconnected uncertain set O cannot be used as a measure for the distance between the certain sets P and Q , since Q is empty.

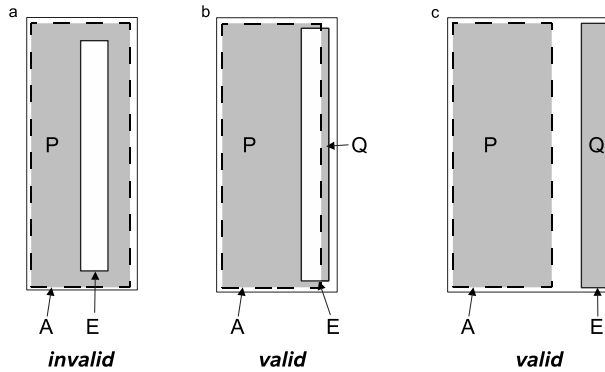


Figure 3.12.: Configurations of A and E in C_1 , e.g. *disjoint* (white area: uncertain set O), a: invalid; b,c: valid.

Consequently, it is not possible to assess the topologic relation between A and E if they do not satisfy the given conditions. For an *extracted road object*, this means it needs to at least overlap with the ATKIS road object in order to give evidence regarding its correctness. On the other hand, *rows of trees* must not be completely contained inside the ATKIS road object. In the practical application these conditions are mostly satisfied.

The priors $P(\omega_i)$ are estimated from the confidence interval of the distributions:

$$\begin{aligned}
 P(\omega_-) &= \frac{|\omega_-|}{\sum |\omega_i|}, \\
 P(\omega_0) &= \frac{|\omega_0|}{\sum |\omega_i|}, \\
 P(\omega_+) &= \frac{|\omega_+|}{\sum |\omega_i|},
 \end{aligned} \tag{3.17}$$

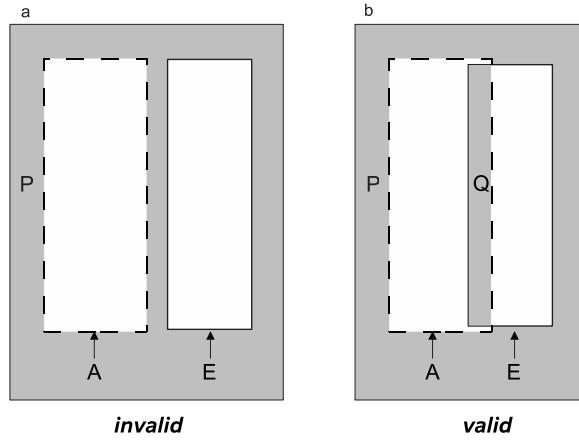


Figure 3.13.: Configurations of A and E in C_2 , e.g. *contains* (white area: uncertain set O), a: invalid; b: valid.

where $||$ denotes the length of the 99% confidence-interval of ω_i .

The application of the methodology as developed in [WINTER 1996] considering the conditions given above and the modified density functions leads to P_{t-top_i} , i.e. the probability that the modelled topologic relation between A'_i and E'_i holds.

3. Assessment of side condition *same width*: If the side condition *same width* is given for the relation *contains*, the same methodology as for the calculation of P_{pq} , namely for the probability that two moments are identical, is pursued: the difference of the widths must be zero. $P_{t-width_i}$ is the probability that this difference is zero. The difference is $D_W = W_A - W_E$, its variance $\sigma_{DW}^2 = \sigma_{WA}^2 + \sigma_{WE}^2$, the test statistics $\tilde{D}_W = D_W / \sigma_{DW}$ and the probability $P_{t-width_i}$ for $\tilde{D}_W = 0$ is:

$$P_{t-width_i} = F(y_{1-\alpha/2} - \tilde{D}_W) - F(y_{\alpha/2} - \tilde{D}_W), \quad (3.18)$$

where F is the normal distribution function and $y_{\alpha/2}$ are the quantiles of the standard normal distribution.

The final probability that the modelled topologic relation holds for A'_i and E'_i is then

$$P_{t_i} = P_{t-top_i} \cdot P_{t-width_i}. \quad (3.19)$$

Examples: In the following two examples are given. Example 1 refers to the parameters for an extracted road object given in the upper part of Figure 3.11, while the second example uses the parameters for a row of trees defined in the lower part of that figure.

Example 1: For an extracted road object the modelled relation is *contains* and thus relation cluster C_2 is implied. Here a configuration as shown in Figure 3.13, right hand side, is assumed and the side condition *same width* is given. For the necessary additional parameters the following values are assumed: width of A : $W_A = 6m$, standard deviation of a Gaussian distribution: $G_{\sigma W_A} = 2m$, and accordingly for the extracted object: $W_E = 3m$, $G_{\sigma W_E} = 1m$.

The minimum and maximum values of the distance transform of O lead to the following result (estimated from the figure and the given parameters):

$$\begin{aligned} \vartheta_{\min} &= -5m, \\ \vartheta_{\max} &= +2m. \end{aligned}$$

From the density functions in Figure 3.11 (top) one obtains:

ω_i	$P(\vartheta_{\min} \omega_i)$	ω_i	$P(\vartheta_{\max} \omega_i)$
ω_-	0.012	ω_-	0.009
ω_0	0.025	ω_0	0.116
ω_+	0.008	ω_+	0.011

The priors are

$$\begin{aligned} P(\omega_-) &= 0.47, \\ P(\omega_0) &= 0.06, \\ P(\omega_+) &= 0.47, \end{aligned}$$

leading to the posteriors (refer to equation 2.6):

ω_i	$P(\omega_i \vartheta_{\min})$	ω_i	$P(\omega_i \vartheta_{\max})$
ω_-	0.517	ω_-	0.259
ω_0	0.138	ω_0	0.425
ω_+	0.345	ω_+	0.316

Using the Table 3.2 of equivalences, the probabilities for the individual relations as shown in Table 3.3 are derived. The sum of these values leads to a total probability that the modelled relation *contains* hold: $P_{t-top_i} = 0.413$.

Relation	P
<i>contains</i>	$0.517 \cdot 0.259 = 0.134$
<i>covers</i>	$0.517 \cdot 0.425 = 0.220$
<i>equal</i>	$0.138 \cdot 0.425 = 0.059$

Table 3.3.: Final probabilities, example 1

It is assumed that the side condition *same width* is given. The difference of the widths is $D_W = 6 - 3 = 3m$, its variance is $\sigma_{D_W}^2 = 2^2 + 1^2 = 5m^2$ and $\tilde{D}_W = D_W/\sigma_{D_W} = 3/\sqrt{5}$, the probability $P_{t-width_i}$ for $\tilde{D}_W = 0$ is: $P_{t-width_i} = 0.89$.

The final probability P_{t_i} is then $P_{t_i} = P_{t-top_i} \cdot P_{t-width_i} = 0.368$.

Example 2: In this example the relation *disjoint* with given d_{min} and d_{max} and further parameters as listed in Figure 3.11, bottom, is assessed. When a configuration as shown in the centre of Figure 3.12 is assumed, the following values are found:

$$\begin{aligned} \vartheta_{\min} &= -2m, \\ \vartheta_{\max} &= +1m. \end{aligned}$$

From the lower density functions in Figure 3.11 one obtains:

ω_i	$P(\vartheta_{\min} \omega_i)$	ω_i	$P(\vartheta_{\max} \omega_i)$
ω_-	0.010	ω_-	0.010
ω_0	0.034	ω_0	0.045
ω_+	0.007	ω_+	0.008

The priors are

$$\begin{aligned} P(\omega_-) &= 0.48, \\ P(\omega_0) &= 0.13, \\ P(\omega_+) &= 0.39, \end{aligned}$$

leading to the posteriors:

ω_i	$P(\omega_i \vartheta_{\min})$	ω_i	$P(\omega_i \vartheta_{\max})$
ω_-	0.419	ω_-	0.344
ω_0	0.354	ω_0	0.419
ω_+	0.227	ω_+	0.237

This leads to $P_{t-top_i} = 0.354 \cdot 0.419 = 0.148$. As the side condition *same width* is not given here, this is the final probability: $P_{t_i} = P_{t-top_i}$.

3.4.4. Combination of evidence

The objective of the combination of evidence is to find a quality indication for the ATKIS road object A depending on the present phase incorporating the results from the assessment algorithms.

Every extracted object E'_i , $i=1 \dots N$, being assigned to an ATKIS road object A allows a conclusion $\xi_i = 1$, which states that E'_i and the respective part of A , A'_i , maintain the modelled geometric and topologic relations. The probability of whether $\xi_i = 1$ is true (P_i^+) or false (P_i^-) is assumed to depend on the collected measures.

The probability that the modelled geometric relation holds (P_{g_i}) gives the main evidence: if it is likely that the shape and the orientation of both objects comply with the model, P_i^+ will be correspondingly large, and vice versa: the smaller P_{g_i} , the larger P_i^- will be.

The measures P_{t_i} and $qcov_i$ describe the impact an extracted object E'_i has on the assessment of A'_i : the larger these values are, the larger the evidence given by P_{g_i} . Therefore, these two measures are interpreted as weighting factors α_i . Under the additional assumption that no other influences exist these considerations lead to:

$$\begin{aligned}
 \alpha_i &= P_{t_i} \cdot qcov_i, \\
 P_i^+ &= P_{g_i} \cdot \alpha_i, \\
 P_i^- &= (1 - P_{g_i}) \cdot \alpha_i.
 \end{aligned} \tag{3.20}$$

The incorporation of P_{g_i} and $(1 - P_{g_i})$ in both, P_i^+ and P_i^- implies a threshold of 0.5: if $P_{g_i} > 0.5$, the evidence given by the object E'_i is in favour of P^+ , otherwise P^- is larger than P^+ .

At first glance it may seem incorrect that P_i^- is proportional to P_{t_i} and not to $(1 - P_{t_i})$. Referring to Section 3.4.1 on the assignment of objects, the modelled topologic relation in conjunction with the uncertainty of the objects was considered as a sort of snapping distance. In this respect, the value P_{t_i} can be interpreted as a measure for the snapping quality and thus $(1 - P_{t_i})$ is not of interest. In order to be able to assess the whole ATKIS road object A , all $\xi_1 \dots \xi_N$ need to be combined. Two hypotheses are defined for this purpose:

H^+ : the whole ATKIS road object is correct given the observed data, i.e., the modelled relations hold for the extracted objects and the ATKIS road object, and

H^- : the whole ATKIS road object is not correct given the observed data, i.e., the modelled relations do not hold for the extracted objects and the ATKIS road object.

An approach combining all conclusions $\xi_1 \dots \xi_N$ related to, i.e. giving evidence for, an ATKIS road object A must consider all the individual probabilities and finally infer the quality of A , permitting an overall assessment conclusion, i.e. confirm H^+ or H^- . One issue is that the evidence given by every object, P_i^+ and P_i^- , does not necessarily describe the quality of the whole object, i.e. $(P_i^+ + P_i^-) \leq 1$. Only the part of A which is covered by E'_i , i.e. A'_i , with the probability that the topologic relation holds, P_{t_i} , is affected. Therefore, $(1 - \alpha_i)$ can be seen as the ignorance which is contained in the observation obtained by E'_i .

One task pursued in this thesis is to analyse whether the explicit incorporation of ignorance – using the Evidential framework – leads to different and particularly more realistic results compared to a probabilistic approach, where ignorance is not considered conceptually. Thus, in the following algorithms for both approaches are given. The outcomes are probabilities or support and plausibility values, respectively, for H^+ and H^- . In the overall strategy, the separation of evidence from extracted road objects (ERO) and local context objects (LCO) is a key issue. Therefore, depending on the phase, evidence fusion is done either using only the objects of a specific object class ERO or LCO, or for all objects, regardless of the class. However, in the formulas given below, again the term E'_i is used in order to simplify the notation.

Whether the road database object A is accepted depends on a maximum probability/maximum support decision. H^+ is confirmed, if

$$P(\xi_1 + \dots + \xi_N | H^+) > P(\xi_1 + \dots + \xi_N | H^-), \text{ or } sp(H^+) > sp(H^-), \text{ respectively.} \quad (3.21)$$

Additionally, a required minimum total coverage cov_req needs to be reached for the road database object A to be confirmed. This is important to assure that a major part of A was assessed. An alternative way would be to demand a given minimum probability or minimum support for the correctness of H^+ , i.e. $P(\xi_1 + \dots + \xi_N | H^+) \geq P_{min}$ or $sp(H^+) \geq sp_{min}$ with $P_{min}(P_{gmin}, P_{tmin}, cov_req) = sp_{min}(P_{gmin}, P_{tmin}, cov_req)$.

Such a procedure requires knowledge of the joint probabilities which do not only depend on the quality of the extracted object, but also on its individual geometric properties. In general these values are not known. Therefore, the proposed maximum probability/maximum support condition seems to be a quite sensible means instead.

A separate consideration of EROs and LCOs is necessary, therefore cov_ERO and cov_LCO are distinguished. The decisions concerning the quality indication depending on Phase 1 and 2 are shown in Figure 3.14 and 3.15, respectively. A closer look at the motivations for the decisions is taken in the next section on graph analysis.

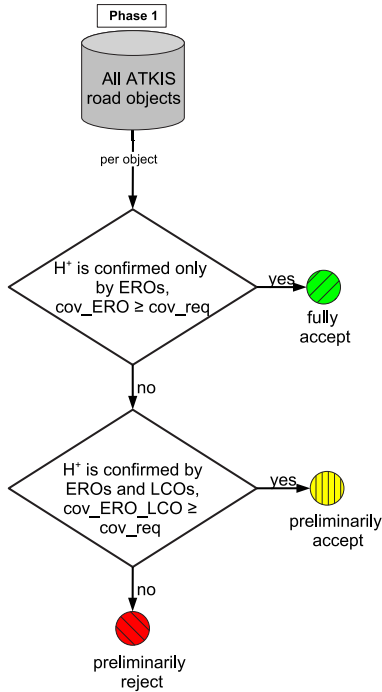


Figure 3.14.: Decisions after combination of evidence, Phase 1

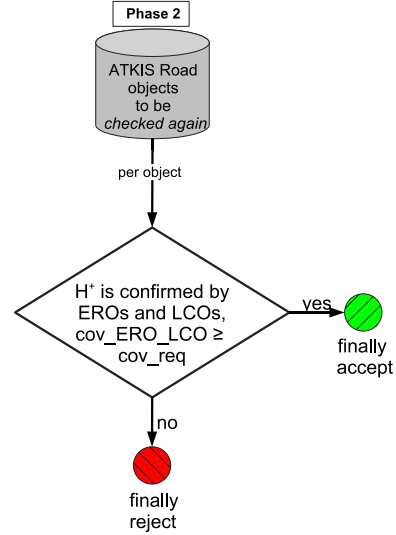


Figure 3.15.: Decisions after combination of evidence, Phase 2

Probabilistic Approach

The conditional probabilities for the correctness of the statement $\xi_i = 1$ are assumed to be given by P_i^+ and P_i^- and the weighting factor α :

$$\begin{aligned} P(\xi_i = 1 | \theta_1 = H^+) &= P_i^+ = P_{g_i} \cdot \alpha_i, \\ P(\xi_i = 1 | \theta_2 = H^-) &= P_i^- = (1 - P_{g_i}) \cdot \alpha_i. \end{aligned} \quad (3.22)$$

The ξ_i are assumed to be independent:

$$P(\xi_i, \xi_k | \theta_j) = 0 \quad \forall i \neq k, \quad (3.23)$$

therefore, the combined probability for the correctness of θ_1 and θ_2 can be derived through the addition of the individual probabilities:

$$P(\xi_1 + \dots + \xi_N | \theta_j) = \sum_{i=1}^N P(\xi_i | \theta_j). \quad (3.24)$$

The assumption of independence is a quite optimistic estimation, because it may be expected that there is a certain correlation between objects extracted by the same algorithm from the same imagery. However, as every extracted object gives evidence for H^+ and H^- , the influence of possible correlations on the probability for both hypotheses may be assumed to be identical, and thus has no impact on the final maximum probability decision.

The chosen quality indication depends on whether the condition

$$P(\xi_1 + \dots + \xi_N | \theta_1 = H^+) > P(\xi_1 + \dots + \xi_N | \theta_2 = H^-) \quad (3.25)$$

is satisfied. The condition expresses the formulated maximum probability rule: is there more evidence in favour or against the correctness of A ?

In order to ensure that a majority of the road database object A is covered by extracted objects, a given minimum total coverage `cov_req` needs to be attained, refer also to the preceding text.

Evidential Approach

Here, the frame of discernment Θ contains both hypotheses: $\Theta = \{H^+, H^-\}$. Any given conclusion $\xi_i = 1$ is interpreted as a hint \mathcal{H}_i , refer to Table 3.4.

Ω	Γ	P
ω_i^+	$\{H^+\}$	$P_i^+ = P_{g_i} \cdot \alpha_i$
ω_i^-	$\{H^-\}$	$P_i^- = (1 - P_{g_i}) \cdot \alpha_i$
ω_i^Θ	Θ	$1 - \alpha_i$

Table 3.4.: Hint \mathcal{H}_i

The last interpretation (ω_i^Θ) represents the ignorance. By applying Dempster's Rule all hints referring to an ATKIS object are combined into an overall hint:

$$\mathcal{H}_{c1\dots N} = (((\mathcal{H}_1 \oplus \mathcal{H}_2) \oplus \mathcal{H}_3) \oplus \mathcal{H}_4 \dots) \oplus \mathcal{H}_N. \quad (3.26)$$

Finally, the support sp and plausibility pl for both hypotheses can be derived:

$$\begin{aligned} sp(H^+) &= p(\omega_{c1\dots N}^+), \\ sp(H^-) &= p(\omega_{c1\dots N}^-), \\ pl(H^+) &= 1 - sp(H^-), \\ pl(H^-) &= 1 - sp(H^+). \end{aligned} \quad (3.27)$$

Similar to the probabilistic approach, the final quality indication depends on the fulfilment of the condition that $sp(H^+) > sp(H^-)$ and the attainment of a given minimum total coverage.

Comparison

The above equations are further analysed in order to compare the behaviour of the probabilistic and the evidential approach. The interesting question is: in what circumstances are the final quality indications from the probabilistic approach and from the Evidential approach contradictory, i.e. has the ignorance being explicitly modelled in the Evidential approach a significant impact on the result? The attainment of a given minimum total coverage applies to both approaches in the same way, therefore it does not need to be taken into account for the comparison.

Suppose, two extracted objects are given and assigned to A . The combination of evidence is both commutative and associative for both approaches. Therefore, the following is valid for an arbitrary number of objects being assigned to A .

The maximum probability constraint $P(\xi_1 + \xi_2|H^+) > P(\xi_1 + \xi_2|H^-)$ can be expressed as

$$\begin{aligned} P(\xi_1 + \xi_2|H^+) &> P(\xi_1 + \xi_2|H^-) \\ \Leftrightarrow P_{g_1} \cdot \alpha_1 + P_{g_2} \cdot \alpha_2 &> (1 - P_{g_1}) \cdot \alpha_1 + (1 - P_{g_2}) \cdot \alpha_2 \\ \Leftrightarrow 2 \cdot (P_{g_1} \cdot \alpha_1 + P_{g_2} \cdot \alpha_2) &> \alpha_1 + \alpha_2. \end{aligned} \quad (3.28)$$

Applying the Evidential approach, the combination of the two hints considering the maximum support constraint leads to

$$\begin{aligned} sp(H^+) &> sp(H^-) \\ \Leftrightarrow p(\omega_{e12}^+) &> p(\omega_{e12}^-) \\ \Leftrightarrow \frac{P(\omega_1^+) \cdot P(\omega_2^+) + P(\omega_1^+) \cdot P(\omega_2^\ominus) + P(\omega_1^\ominus) \cdot P(\omega_2^+)}{1 - k} &> \frac{P(\omega_1^-) \cdot P(\omega_2^-) + P(\omega_1^-) \cdot P(\omega_2^\ominus) + P(\omega_1^\ominus) \cdot P(\omega_2^-)}{1 - k}, \end{aligned}$$

$k = P(\omega_1^+) \cdot P(\omega_2^-) + P(\omega_1^-) \cdot P(\omega_2^+)$ and the probability measures given in Table 3.4 finally lead to

$$2 \cdot (P_{g_1} \cdot \alpha_1 + P_{g_2} \cdot \alpha_2) - \alpha_1 \cdot \alpha_2 \cdot (P_{g_1} + P_{g_2} - 1) > \alpha_1 + \alpha_2. \quad (3.29)$$

This is an interesting result, because both Inequations 3.28 and 3.29 are equal, except for the term $(-\alpha_1 \cdot \alpha_2 \cdot (P_{g_1} + P_{g_2} - 1))$ on the left side. Since the term $(\alpha_1 + \alpha_2)$ is isolated in both inequations the following inequation for contradicting final quality indications can be formulated:

$$\begin{aligned} 2 \cdot (P_{g_1} \cdot \alpha_1 + P_{g_2} \cdot \alpha_2) &\leq \alpha_1 + \alpha_2 \leq 2 \cdot (P_{g_1} \cdot \alpha_1 + P_{g_2} \cdot \alpha_2) - \alpha_1 \cdot \alpha_2 \cdot (P_{g_1} + P_{g_2} - 1) \\ \Leftrightarrow 0 &\leq \alpha_1 + \alpha_2 - 2 \cdot (P_{g_1} \cdot \alpha_1 + P_{g_2} \cdot \alpha_2) \leq -\alpha_1 \cdot \alpha_2 \cdot (P_{g_1} + P_{g_2} - 1). \end{aligned} \quad (3.30)$$

If this inequation is satisfied, the final quality indications are contradictory.

Using Inequation 3.30 four different scenarios are created to analyse possible occurring contradictions. To simplify the notation the term T_1 is used for $(\alpha_1 + \alpha_2 - 2 \cdot (P_{g_1} \cdot \alpha_1 + P_{g_2} \cdot \alpha_2))$ and the term T_2 substitutes $(-\alpha_1 \cdot \alpha_2 \cdot (P_{g_1} + P_{g_2} - 1))$.

Scenario I $P_{g_1} \approx P_{g_2} \approx 1$: This scenario simulates that based on P_g , i.e. the probability that the geometric relations are in accordance with the model, both extracted objects strongly confirm H^+ . As will be seen the actual size of α_i is not of interest for this examination. In this scenario the following approximations are valid:

$$\begin{aligned} T_1 &\approx -\alpha_1 - \alpha_2 < 0 \quad \text{and} \\ T_2 &\approx -\alpha_1 \cdot \alpha_2. \end{aligned} \quad (3.31)$$

According to Inequation 3.30 a contradiction appears if $T_1 > T_2$, because $T_1 < 0$:

$$\begin{aligned} -\alpha_1 - \alpha_2 &> -\alpha_1 \cdot \alpha_2 \\ \Leftrightarrow \alpha_1 + \alpha_2 &< \alpha_1 \cdot \alpha_2. \end{aligned} \quad (3.32)$$

Since $0 \leq \alpha_i \leq 1$ Inequation 3.32 cannot be satisfied, i.e. in the given scenario the final quality indications from the probabilistic and from the Evidential approach cannot be contradictory. The values α_i are not of interest for the final decision. Thus, the ignorance being modelled as $(1 - \alpha_i)$ has no impact on the result.

Scenario II $P_{g_1} \approx P_{g_2} \approx 0$: In this scenario a strong confirmation of H^- is simulated, i.e. the hypothesis that A is not correct is supported by both extracted objects. In this case

$$\begin{aligned} T_1 &\approx \alpha_1 + \alpha_2 > 0 \quad \text{and} \\ T_2 &\approx \alpha_1 \cdot \alpha_2. \end{aligned} \quad (3.33)$$

According to Inequation 3.30 contradiction appears if $T_1 < T_2$, because $T_1 > 0$:

$$\alpha_1 + \alpha_2 < \alpha_1 \cdot \alpha_2. \quad (3.34)$$

Again, this is not possible.

In scenarios I and II both extracted objects strongly support the same hypothesis. It was shown that in those cases the size of α_i and thus the ignorance is not relevant for the final quality indication. Both methodologies to combine evidence result in the same maximum probability, or maximum support decision, respectively. In the remaining scenarios conflicting and undetermined evidence is assumed.

Scenario III $P_{g_1} \approx 0, P_{g_2} \approx 1$: This scenario simulates that both extracted objects are strongly conflicting concerning the confirmation of H^+ and H^- . In this case

$$\begin{aligned} T_1 &\approx \alpha_1 - \alpha_2 \quad \text{and} \\ T_2 &\approx -\alpha_1 \cdot \alpha_2 \cdot \tau \quad \text{with} \quad \tau = (P_{g_1} + P_{g_2} - 1) \rightarrow 0. \end{aligned} \quad (3.35)$$

Here, contradiction appears if the following inequation is satisfied:

$$0 < \alpha_1 - \alpha_2 < -\alpha_1 \cdot \alpha_2 \cdot \tau. \quad (3.36)$$

No general statement can be made regarding this inequation, because the sign of τ depends on the given values of P_{g_1} and P_{g_2} .

Scenario IV $P_{g_1} \approx P_{g_2} \approx 0.5$: Here, both objects give undetermined evidence regarding the correctness of A . Both terms T_1 and T_2 tend towards zero in this case. Therefore, a similar situation as for Inequation 3.36 related to the previous scenario occurs. Whether the combination of evidence using the probabilistic and the Evidential approach results in contradictory quality indications for A depends on the actual values of P_{g_i} and α_i .

Summary: It was shown with these four assumed scenarios that in case both extracted objects give strong evidence for the same hypothesis based on the probability P_{g_i} , a contradictory quality indication cannot be expected from both combination approaches. The ignorance, modelled by $(1 - \alpha_i)$, is not relevant in those cases.

In case of conflicting or undecided evidence, the final result and the question if the results are contradictory depends on the actual values obtained from the geometric and topologic assessment. From a theoretical point of view the ignorance plays a certain role. Whether it has a significant impact on practical applications will be analysed in Chapter 4.

3.4.5. Graph analysis

The steps to road object assessment described in the preceding sections are related to individual road objects; the road network has not been incorporated so far. The exploitation of road network topology is based on the requirement that road objects having been accepted in Phase 1 need to be connected to each other. To restrict the number of possible connections and according to the assumption that road objects link places on short paths, the criterion to be fulfilled is that the distance between objects is minimised. The further treatment of objects not having been accepted in Phase 1 depends on whether they are part of the shortest distance between accepted objects and on the amount of evidence given by local context objects in Phase 1.

In the following the procedures for graph analysis outlined in Section 3.3 are described in more detail.

1. Transition from objects to network edges: In the ATKIS DLMBasis the topology of the road network is implicitly given, as adjacent road objects share the same node points, refer to Section 2.1.3. Yet, the assignment of road objects to edges of the network is not directly possible, because it is not guaranteed that objects are split at junctions. Therefore, firstly the quality indications (termed *label* in the following) are transferred from the objects to their individual line segments. Afterwards, the transition to network edges is accomplished, as the assignment of line segments to network edges is known. The

relations between ATKIS road objects, line segments and network edges are shown in Figure 3.16. On the left hand part, bottom, some ATKIS road objects are sketched: A_1 to A_4 , the straight line segments are given by S_1 to S_6 in the centre, and the network edges A to E are shown in the upper drawing. In the right hand part of the figure the links between the components are shown. A typical example for the problem of the assignment between the components is given by ATKIS road object A_3 : it consists of the three line segments S_3 , S_4 and S_6 and represents two network edges, namely C and E . The explicit mapping from A_3 to network edges C and E is not possible, the labels of A_3 need to be transferred at first to the named segments and then from these segments to both edges.

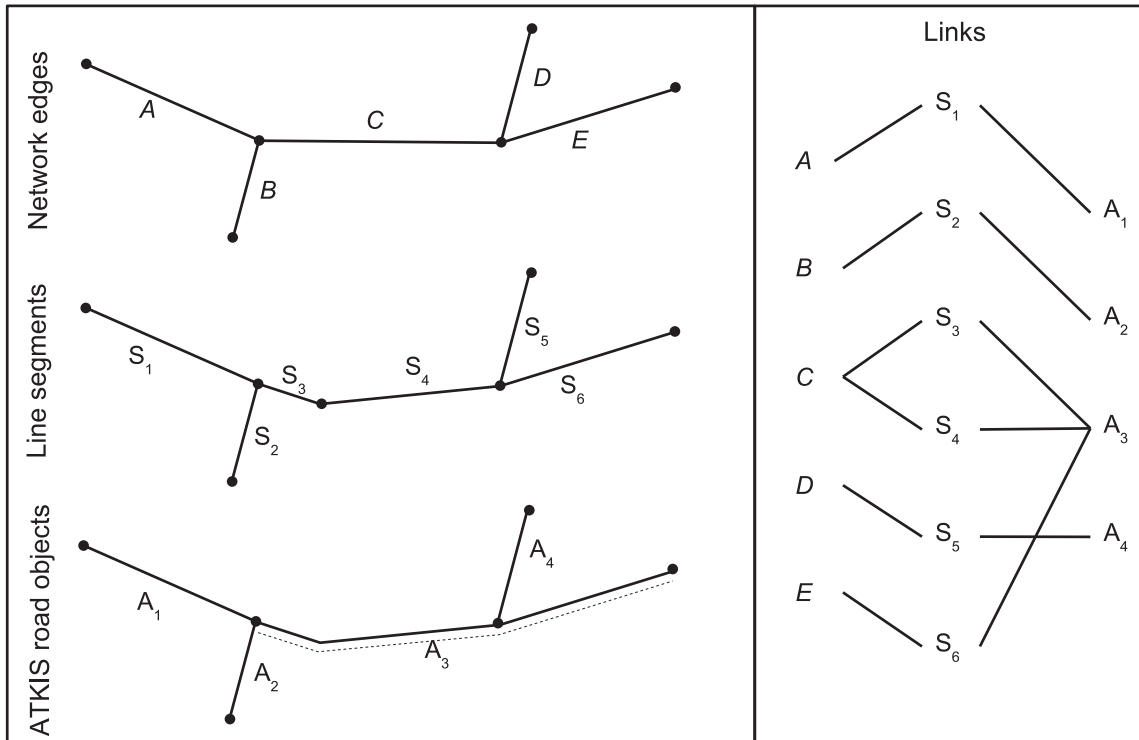


Figure 3.16.: Relations between ATKIS road objects, line segments and network edges

For the transition of labels some constraints need to be considered:

- A minimum total coverage cov_req is necessary for every segment and every edge. Otherwise, the label will be set to *finally reject*.
- If the segments assigned to an edge have mixed labels *preliminarily reject* as well as *preliminarily accept*, the more pessimistic label is chosen for the edge, i.e. *preliminarily reject*.

2. Definition of start-nodes: The start-nodes for the search of shortest paths are identified according to the label of adjacent edges: a start-node must have at least one adjacent edge, which has been *fully accepted* in Phase 1. This is a sufficient criterion to find the shortest paths between accepted objects. However, as only network edges not having been accepted in Phase 1 will be eventually chosen for Phase 2 and in order to minimise the computing time, a start-node must also have at least one adjacent edge, labelled *preliminarily reject* or *preliminarily accept*.

3. Shortest path search between start-nodes and re-labelling of edges: The shortest paths between all start-nodes are searched using the A*-Algorithm [DUDA and HART 1973]. The weight of the edges equals the total length of the assigned line segments.

The subsequent re-labelling of the edges applies the following rules:

- *Preliminarily rejected edges* (edges of the ATKIS road database, which have neither been confirmed by extracted road objects nor by local context objects) which are part of a shortest path between start-nodes are chosen for an additional check in Phase 2 and labelled *check again*. The network function of those edges is assumed to give enough evidence to check them again, applying a road extraction with more tolerant parameters.
- *Preliminarily accepted edges* (edges of the ATKIS road database, which have not been confirmed by extracted road objects alone, but in conjunction with the available local context objects) which are part of a shortest path between start-nodes are labelled as *finally accepted*. This rule is motivated by the assumption that the local context objects are able to explain existing gaps in the road extraction.
- All remaining edges not being part of a shortest path between start-nodes are assumed not to have any important network function and are thus *finally rejected*.

4. Transition from network edges to objects: This procedure is similar to 1. Firstly, the line segments obtain the labels from the edges they are linked to. Secondly, according to the assignment between line segments and ATKIS road objects, the latter obtain the labels from the line segments. For an overview on possible transitions between the assessment results, refer to Figure 3.7 on page 40.

3.5. Discussion

Concluding the chapter on the new approach to road database assessment, the properties, advantages and deficits of this approach are summarised in this section.

The proposed approach uses road objects and context objects, in this case rows of trees, which are extracted from remotely sensed imagery to assess the quality of given road vector data: besides position and width, the shape and orientation are compared to the extracted objects.

In the literature review it was found that an exclusive use of extracted road objects in many cases does not deliver enough information for an adequate road data assessment. Therefore, in contrast to existing research a statistical modelling of roads, context objects and their relations is conducted in this thesis. The impact of the uncertainty inherent in geo-spatial data are identified and modelled.

The defined object model allows for a consistent geometric and statistical representation of medial axes and pointsets for roads and context objects. The conversion between object representations has been developed, including a propagation of statistical measures.

Geometric as well as topologic relations between the objects are defined in the so-called relationship model. Concerning geometry the relations *same shape* and *same orientation* are considered, whereas topology comprises the relations *contains* (with side condition *same width*) and *disjoint* (with a possibly required *minimum* and *maximum distance* between objects). The actual relations between extracted objects and the given database objects are calculated and compared to the model. This comparison results in probability measures, because the respective statistical properties of the objects are integrated.

Each observation of the object-based comparison which leads to probability values for the attainment of the required relations may contain ignorance about the correctness of the given database road object. The combination of all evidence related to one given database object is done using two different approaches. The first one is a traditional probabilistic combination, where the ignorance is not considered. The second one is based on the Evidence Theory where ignorance can be incorporated explicitly. Theoretical analyses show that the consideration of ignorance may lead to contradictory results compared to the probabilistic approach. In particular, this is the case when the evidence is conflicting. Whether this conceptual difference between both methods is relevant for the practical application will be analysed in the next chapter.

One deficit of the developed approach to road assessment concerns the modelling of roads in junction areas. Junctions may not be adequately represented by the medial axis. Therefore, the quality measures based on the medial axis representation, i.e. shape and orientation, may not constitute a reasonable means for the assessment. Compared to the overall length of an object, the junction area is relatively small. If the majority of a road object is incorrect, it does not matter if the junction can be assessed,

because the object will be rejected anyway. If on the contrary only the junction area is incorrect, the presented approach may fail and accept the road object.

The object-based assessment of road database objects is embedded in a graph-supported exploitation of the connection function of roads. If a road object was rejected but fulfils important network tasks, i.e. it connects roads which have been accepted through the shortest path, it may be accepted nevertheless. Two reasons may lead to acceptance. Either context objects – here: rows of trees – explain gaps in the road extraction, or enough evidence is given by a second, more tolerant, road extraction. Since the graph analysis is based on edges in the network, this approach is independent from object acquisition rules for database road objects.

4. Test of approach

This chapter reports on the tests which have been conducted with the developed approach. The used data and algorithms for road and context object extraction are presented in the next section, followed by a description of the test configurations. Each test focuses on different aspects of the assessment approach. Finally, the results of the tests are shown and evaluated.

4.1. Data and model parameters

The chosen test site is located in the German state North Rhine-Westphalia, near the city of Ibbenbüren. It has a size of $2 \times 8 \text{ km}^2$, mostly consisting of open landscape, refer to Figure 4.1.

ATKIS data: All 562 original ATKIS DLMBasis road objects were used for the tests. They have a total length of approximately 96.7 km : 89 *Roads* with a total length of approx. 13.2 km and 473 *Paths* with a total length of approx. 83.5 km . All *Paths* have a minimum width of 3 m and are therefore observable in the used imagery. The ATKIS data was revised in 1996 by the state survey office of North Rhine-Westphalia. The road data is plotted in Figure 4.1. One can observe some isolated road objects within the ATKIS road data. These are individual *Paths* connecting large agricultural facilities and surrounding fields.

According to Section 2.1.3 on the ATKIS DLMBasis and following the notations and definitions from the statistical modelling Section 3.2.1, the parameters for the ATKIS road objects are chosen as listed in Table 4.1.

Component	Variable/Value
Object modelling	$D_{Mo} = 3 \text{ m}$
Mapping object \rightarrow image	$D_O = 0$
Abstraction	$G_{\sigma A} = 0, D_A = 0$
Measurement	$G_{\sigma C} = 0$
Width	$G_{\sigma W} = 1 \text{ m}$

Table 4.1.: Statistical components and values for ATKIS road objects

Image data: The image flight took place on 2000/06/17; the parameters necessary for the estimation of statistical measures are:

- camera constant: 30 cm ,
- image scale: 1 : 12,500,
- film: RGB, analogue, image size: $23 \times 23 \text{ cm}^2$.

The film was scanned with a pixel size of $25 \mu\text{m}$, resulting in a ground sampling distance of approximately 0.3 m . The orthoimages used for the tests have been created using a digital terrain model, i.e. 3D-objects have not been incorporated. The producer of the images gives a nominal position accuracy in object space: $\Delta_I = \pm 1 \text{ m}$. This is interpreted as the 95%-confidence interval of a Gaussian distribution, resulting in a standard deviation for the accuracy of the image of $\sigma_I = 0.5 \text{ m}$. One orthoimage covers an area of $2 \times 2 \text{ km}^2$, four orthoimages have been merged for the tests. The image flight was conducted after the last revision of the database, therefore the images are considered up-to-date.

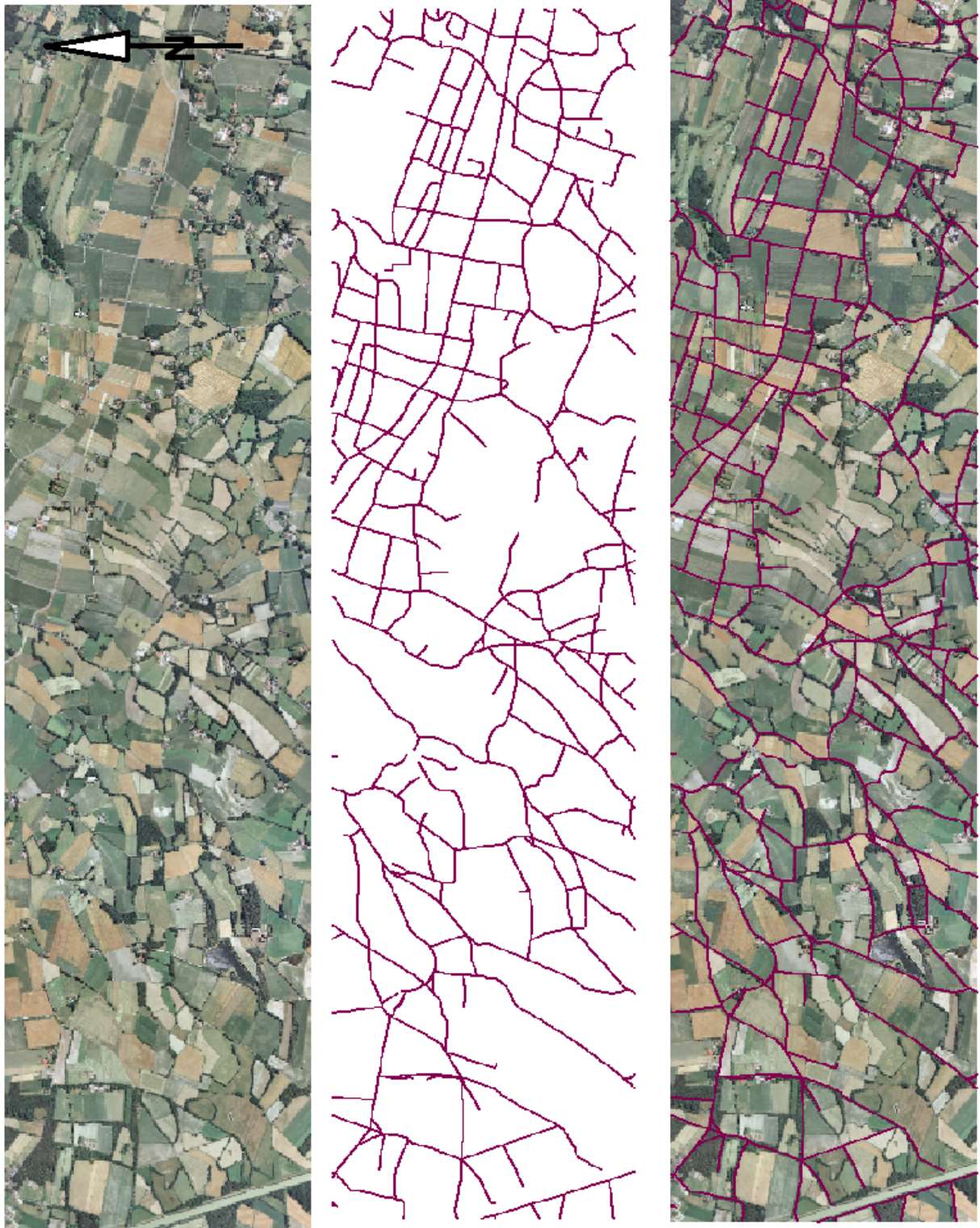


Figure 4.1.: Left hand image: orthoimage, centre image: road objects from ATKIS DLMBasis, right hand image: ATKIS road objects superimposed to orthoimage. Orthoimages and ATKIS DLMBasis ©LVA Nordrhein-Westfalen, Germany, 2006.

Extracted road objects: The road extraction algorithm of WIEDEMANN [2002] (refer to Section 2.2.1) was used for the tests. It models roads as linear objects in aerial or satellite imagery with a resolution of about 1 to 2m and uses one channel only for the extraction. Therefore, the images were resampled to a ground sampling distance of 1.6m and instead of using the three colour channels, intensity images have been computed. The underlying line extractor is introduced in [STEGER 1998]. The selection of the line extraction parameters, mainly the contrast between line and background, but also the maximum allowed grey value differences inside the line, are important means of controlling the behaviour of the road extraction. The initially extracted lines are evaluated by fuzzy values according to attributes defined in the road model, such as length, straightness, constancy in width and constancy in grey values. The individual evaluated lines are grouped to derive a topologically connected and geometrically optimal path between seed lines according to some predefined criteria: whether lines are merged into a road object is determined according to a collinearity criterion, which allows a maximum direction difference and a maximum gap length. Tuning those thresholds is a further means of influencing the sensitivity of the algorithm. Seed lines are the lines which reach a minimum evaluation score. The threshold is defined by the user and constitutes another important parameter to control the sensitivity of road extraction. Besides the medial axis, a mean width for each road object is estimated.

The prior knowledge given by the ATKIS road vector data is incorporated as follows. Firstly, according to the modelled topologic relation and the uncertainty measures, a region of interest (ROI) is defined for the extraction of roads for every database object separately. The ROI is the same as the buffer of interest as defined for the assignment, refer to Section 3.4.1. The definition of the ROI is reasonable, since road objects outside this region will not give evidence regarding the respective database object anyway. Secondly, the grouping of extracted lines is supported by the insertion of small seed lines derived from the respective ATKIS road object. This is motivated by the fact that in junction areas the line model is not valid. Two artificial seed lines from the ATKIS road object are created: they both start at the outermost vertices and point inward to the linestring. To avoid a misinterpretation of the possibly incorrect road vector data, the length of the seed lines is restricted: they have a maximum length of 2% of the overall length of the road object, and do not exceed an absolute length of 5m. These thresholds and the additional constraint that extracted lines must be part of a final road object prevent the algorithm from grouping only the two artificial lines into a complete road object. In Figure 4.2 the principle for the incorporation of ATKIS road objects into the grouping of extracted lines is shown. The fact that the proposed procedure for the incorporation of ATKIS road vector data actually enhances and does not negatively affect the quality assessment will be demonstrated with the tests.

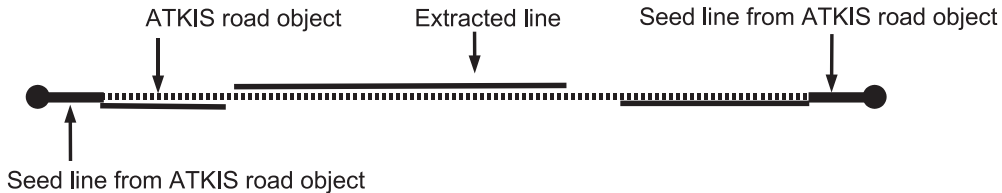


Figure 4.2.: Support of the ATKIS road object for the grouping of extracted lines

The statistical parameters for the road extraction are discussed next. The mapping from object to image space and the abstraction components are not considered for the following reasons: the first component is zero, because roads normally are not 3D-objects. Special cases such as roads on bridges are not taken into account here, moreover this kind of road does not occur in the given scene. The fuzziness of abstraction cannot be reasonably estimated, since it is not possible to predict cases where the extracted line does not correspond to a road object. In contrast, the imprecision inherent in the capture of the line can be estimated. In [STEGER 1998] a precision for the line extraction algorithm of 0.04 pixel has been achieved for artificial images. However, this is a very optimistic value for aerial images. From experience, the accuracy is defined as ± 0.3 pixel, i.e. $\pm 0.48m$ in object space, being again interpreted as the 95%-confidence interval: $\sigma_L = 0.24m$. The standard deviation for the accuracy is $\sigma_I = 0.5m$, but the images have been resampled to 1.6m. Therefore, by variance propagation the standard deviation for the accuracy of the used image is obtained as $\sigma'_I = \sqrt{1.6/0.3125} \cdot 0.5m \approx 1.1m$.

This is combined with $\sigma_L = 0.24$, yielding the standard deviation of a Gaussian for the measurement as $G_{\sigma C} = \sqrt{\sigma_I^2 + \sigma_L^2} = 1.12m \approx 1.1m$.

The width of the line is estimated as the Euclidean difference between two points on the edges bordering the line. The edge points are assumed to have the same accuracy measures as the line, therefore $G_{\sigma W} = \sqrt{2} \cdot G_{\sigma C} \approx 1.5m$. The parameters are summarised in Table 4.2.

Component	Variable/Value
Object modelling	$D_{Mo} = 0$
Mapping object \rightarrow image	$D_O = 0$
Abstraction	$G_{\sigma A} = 0, D_A = 0$
Measurement	$G_{\sigma C} = 1.1m$
Width	$G_{\sigma W} = 1.5m$

Table 4.2.: Statistical components and values for extracted road objects

Rows of trees: Two different sets of rows of trees have been acquired for the tests:

Automatically extracted rows of trees: The approach of GIMEL'FARB [1996], introduced in Section 2.2.4, was applied for the segmentation of the scene into the classes built-up, industrial, grassland, cropland and forest. The training data was defined by a human operator. Within the objects of the forest class rows of trees were delineated applying geometric constraints according to the definition of elongated objects in Section 2.1.1. Moreover, elongated regions having an average width larger than the average crown diameter observed in the scene were not further considered. The medial axes of the objects obtained by applying the named constraints were derived using the algorithm proposed in Section 3.2. Firstly, the long-side borders were separated from the pointset given for the individual segments. Then the medial axis was constructed from both long-side borders.

This procedure assumes implicitly that the medial axis of a row of trees segment is a good representation for the line connecting the trunks. Here, the fuzziness of abstraction becomes important: whether or not the trunk is centred beneath the crown can normally not be observed in aerial imagery. Therefore, the actual values for the distribution describing the fuzziness of abstraction need to be chosen adequately (see below).

Manually captured rows of trees: This set contains manually digitised medial axes of rows of trees observed in the imagery.

No prior information from ATKIS was used for the creation of both sets. Although the object *Row of Trees* is defined in the ATKIS object catalogue, no such object was available for the given scene.

Both sets of rows of trees are shown in Figure 4.3. The left hand image shows the manually captured objects, whereas the centre image shows the automatically extracted rows of trees. It can be observed that a lot of small (short) objects are amongst the automatically achieved rows of trees. In some cases these are short rows of trees which have not been captured by the human operator and thus are missing in the manually achieved set, a minority of them result from a wrong segmentation. Moreover, the automatically extracted rows of trees include more objects compared to the manually captured set, because the human operator mainly digitised rows of trees which cover roads.

The parameter *width* needs to be defined for all rows of trees objects. This value refers to the width of the trunks. As no further information is available, this value is set to $W = 1m$.

The statistical parameters are estimated based on the image flight information and general assumptions on the size of trees in the respective region of Germany. The average height of trees in this region is estimated as $H_{Tree} = 6m$, the average crown radius as observable in the image is $R_{Crown} = 3m$. The terrain in the scene is flat, therefore the inclination is set to $\alpha = 0$. Inserting $H_{Tree} = 6m$, $c = 30cm$, $\rho = 23 \cdot \sqrt{2}/2cm$ and $\alpha = 0$ into Equation 3.1, the maximum offset ΔR due to the mapping from a 3D-object to image space without the incorporation of the object's height is estimated and interpreted as the radius of the uniform distribution $D_O = \Delta R = 3.2m$. This is a pessimistic estimation, since it is

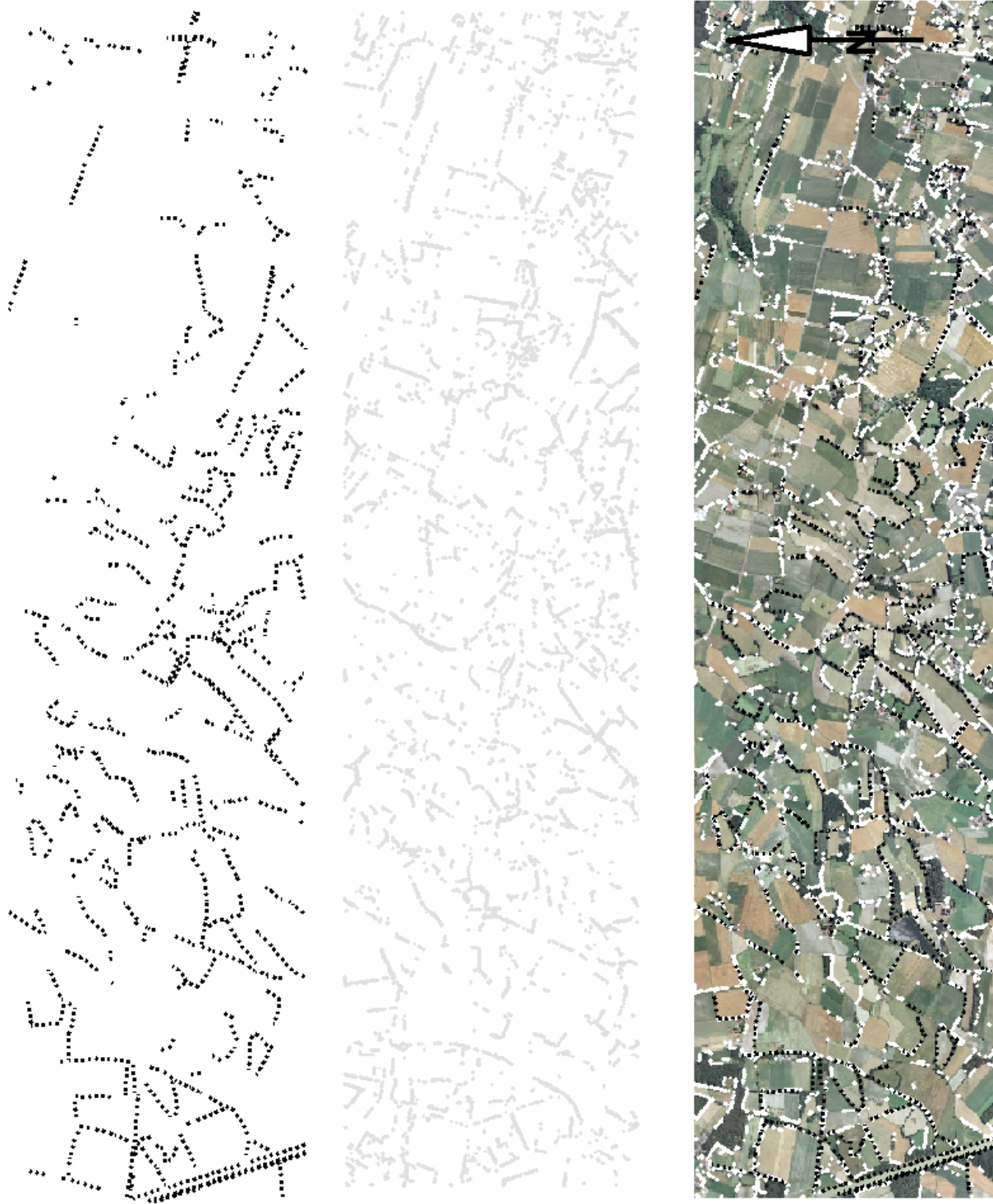


Figure 4.3.: Left hand image: manually captured rows of trees, centre image: automatically captured rows of trees, right hand image: both sets of rows of trees superimposed to orthoimage.

only valid for regions at the image border (at the nadir point it is zero). However, due to the creation of $2 \times 2km^2$ orthoimages the information on the original image position is not available.

The fuzziness of abstraction is related to the crown radius R_{Crown} , because the trunks are positioned underneath the crown, but without further information the position can only be roughly estimated through the medial axis. The chosen values are $D_A = 0.25 \cdot R_{Crown} = 0.75m$ and $G_{\sigma A} = 0.33 \cdot R_{Crown} = 1m$. The statistical measures reflect that it is most probable that the trunks are situated in an area of $\approx \pm 0.25 \cdot R_{Crown}$ around the medial axis. Besides, there is also a certain chance of having trees where the crown is not centred, for example trees being permanently subject to heavy winds from one direction. Therefore, an additional Gaussian PDF is considered. The convolution of the respective PDF leads to 99% confidence boundaries $\pm 2.8m$. Again, this is only a rough, but reasonable, estimation.

The accuracy of the positions in object space is given with $\sigma_I = 0.5m$ which is a reasonable estimate for the measurement accuracy: $G_{\sigma C} = 0.5m$. Finally, the accuracy of the width needs to be defined. The width of the trunks is defined as $W = 1m$. A standard deviation of $G_{\sigma W} = 0.25m$ fixes a 99% confidence area between $0.25m$ and $1.75m$, which are quite comprehensible values for the type of trees existing in the scene.

Component	Variable/Value
Object modelling	$D_{Mo} = 0$
Mapping object \rightarrow image	$D_O = 3.2$
Abstraction	$G_{\sigma A} = 1m, D_A = 0.75m$
Measurement	$G_{\sigma C} = 0.5m$
Width	$G_{\sigma W} = 0.25m$

Table 4.3.: Statistical components and values for rows of trees

Relationship model: The parameters of the relationship model have been given in Figure 3.4. Extracted road objects need to be *contained* in ATKIS road objects and have the *same width*. The constraint on identity of width will be modified during the tests. Rows of trees and ATKIS road objects have to be *disjoint* with $d_{min} = 1m$ and $d_{max} = 10m$. The constraint of *same shape* and *same orientation* holds for every object. The tolerance for the orientation is $\delta_t = 15^\circ$.

4.2. Test configurations

Three different kinds of tests have been carried out in order to evaluate the single components of the proposed approach to road database assessment.

1. **Assessment of geometric and topologic relations:** Here, the focus has been on the question of whether the developed algorithms for the assessment of geometric and topologic relations realistically reflect the existing relations between exemplary objects. The values for the statistical measures of the objects have been varied in order to evaluate their influence on the assessment result.
2. **Combination of evidence:** The ability to reasonably reflect the quality of an ATKIS object has been tested. Additionally, the empirical comparison between the probabilistic and the Evidential approach has been subject to this test, in particular the study of contradictory final quality indications.
3. **Graph analysis and overall approach:** Not individual objects have been assessed, but the whole set of ATKIS road data, introduced above. The impact of the graph analysis on the overall assessment result has been investigated as well as the benefit resulting from the incorporation of rows of trees. Here, the assessment result obtained with the manually captured rows of trees has also been compared to the result obtained with automatically extracted rows of trees. Besides the original ATKIS data some objects have been created manually to conduct several sensitivity analyses.

4.3. Results and evaluation

4.3.1. Assessment of geometric and topologic relations

The ATKIS road object shown in the left hand image of Figure 4.4 differs from a simple straight line. The extracted road object has a similar shape. The statistical parameters of the ATKIS road object are shown in Table 4.1: the width has been assumed as $w_A = 3m$, and the values for G_{σ_C} have been varied from $0.01m$ to $1m$, thus a logarithmic scale is used for the x-axis of Figure 4.4, right hand side. The width of the extracted object has been fixed to $w = 4m$, and its standard deviation to $G_{\sigma_W} = 1.5m$. The parameters for the relationship model have been adopted. To allow an easier comparison of the assessment result to the figure, the tolerance value for parallelism has been set to $\delta_t = 0$. The measures $P_{g-shape}$, P_{g-ori} and P_{t-top} as derived according to the individually assumed values for G_{σ_C} are shown in the right hand part of Figure 4.4. The measure $P_{t-width}$ has not been taken into account, because the statistical measures for the width have not been modified.

The identity of both shapes is reflected in a large value for $P_{g-shape}$: even for $G_{\sigma_C} = 0.1m$ the probability that both shapes are identical is 0.99. According to the theory of line moments this is a comprehensible result, because both objects are largely straight and parallel, i.e. deviations in the shape are restricted to some short segments which have no significant impact on the differences of line moments. Even the moments of higher order do not differ significantly if a standard deviation of $0.1m$ or larger is assumed.

The probability P_{t-top} does not grow arbitrarily, because the remaining possible topologic relations from cluster C_2 , i.e. *strong overlap*, *covered by*, *contained by* are not of interest for the modelled relation *contains*, refer to Figure 2.5 and Table 3.2. Since the imprecision of the objects has been supposed to be very small, the competing relation *strong overlap* is large compared to the requested relation *contains*.

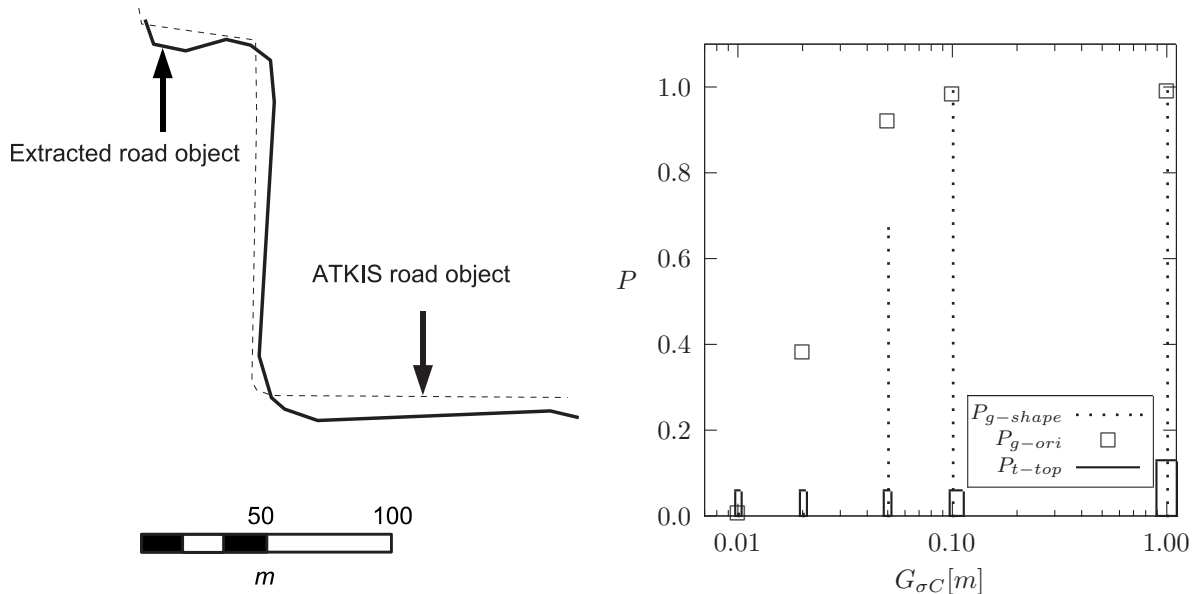


Figure 4.4.: Example II: good compliance of ATKIS road object and extracted road object

This example allows some conclusions. The developed approach to the assessment of geometric relations reasonably reflects the shape and orientation identity of two objects under consideration of imprecision. However, in certain circumstances the result from the analysis of shapes based on the proposed method may differ from subjective observations of a human operator. In the example the shape of both objects is identical, only some minor variations occur. These variations are not significant compared to the overall compliance of both objects, but a human operator might decide that due to these small variations both shapes are not identical. This problem is related to a missing explicit definition of the constraint *same shape* – the statistical and subjective decisions may be inconsistent.

The result from the assessment of topologic relations is as expected. The modelled and thus requested topologic relation is compared only to the relations in the same cluster. Therefore, it is reasonable that P_{t-top} does not grow arbitrarily.

4.3.2. Combination of evidence

The following examples which demonstrate the combination of evidence have been selected according to the scenarios defined for the theoretical comparison between both developed approaches in Section 3.4.4. The examples have been taken from real data (except for example IV). However, the underlying situation in the image is of no interest here, as an analysis of the road extraction and the ATKIS road data is given in the next section. The statistical measures of the objects can also be neglected, since the detailed examination of the algorithms to derive the individual probabilities related to one extracted object was subject to the preceding section. Therefore, only the final measures $P_{g_i}, P_{t_i}, qcov_i$ that are relevant for the combination of evidence are given.

Combination of evidence – Example I – Both objects confirm H^+ : In Figure 4.5, left hand image, a typical situation for a correct ATKIS road object, covered largely by extracted road objects is demonstrated. The relevant measures for the combination are shown in the right hand side of the figure and in Table 4.4. In that table additionally the values for P_i^+ and P_i^- are listed. The total coverage is given in the right hand column. The final probabilities and support values for both hypotheses H^+ and H^- are presented below the table.

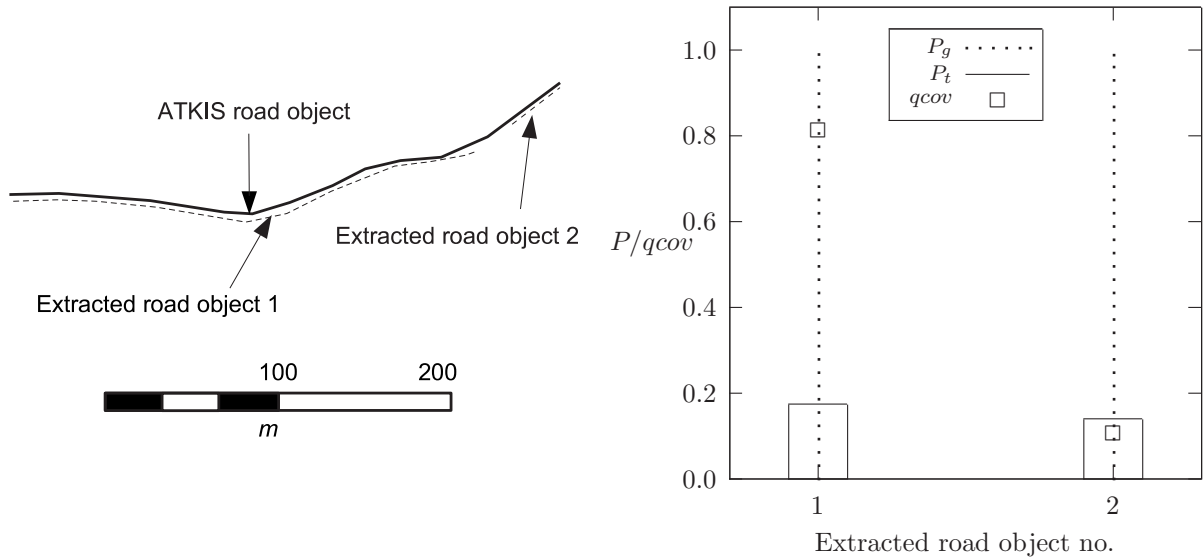


Figure 4.5.: Example for conformity of evidence: *correct* ATKIS road object

i	$P_{g_i} =$ $P_{g-shape_i} \cdot P_{g-ori_i}$	$\alpha_i =$ $P_{t_i} \cdot qcov_i$	$P_i^+ =$ $P_{g_i} \cdot \alpha_i$	$P_i^- =$ $(1 - P_{g_i}) \cdot \alpha_i$	cov.ERO
1	0.990	0.141	0.1396	0.0014	0.91
2	0.988	0.015	0.0148	0.0002	

$$P(\xi_1 + \xi_2 | H^+) = \mathbf{0.154}, P(\xi_1 + \xi_2 | H^-) = 0.002, \text{ confirms } H^+ \\ sp(H^+) = \mathbf{0.152}, sp(H^-) = 0.002, \text{ confirms } H^+$$

Table 4.4.: Conform Evidence: measures relevant for combination and its result, refer to Figure 4.5

According to the theoretical investigations in Section 3.4.4 on the combination of evidence, both approaches – the probabilistic and the Evidential – confirm H^+ , i.e. the hypothesis that the ATKIS object is correct. Thus, if the total coverage cov_ERO is larger than a predefined threshold cov_req , the ATKIS road object is accepted. One finding from this analysis has been that in the given case, namely strong confirmation of H^+ , the consideration of ignorance, i.e. of $(1 - \alpha_i)$ in the Evidential combination cannot lead to a contradictory combination result compared to the probabilistic approach.

Combination of evidence – Example II – Both objects confirm H^- : In this example a typical situation for an incorrect ATKIS object is given. The shapes of the extracted road objects and the ATKIS object shown in the left hand image in Figure 4.6 are not identical as expressed in low values for P_{g_i} , refer to Table 4.5.

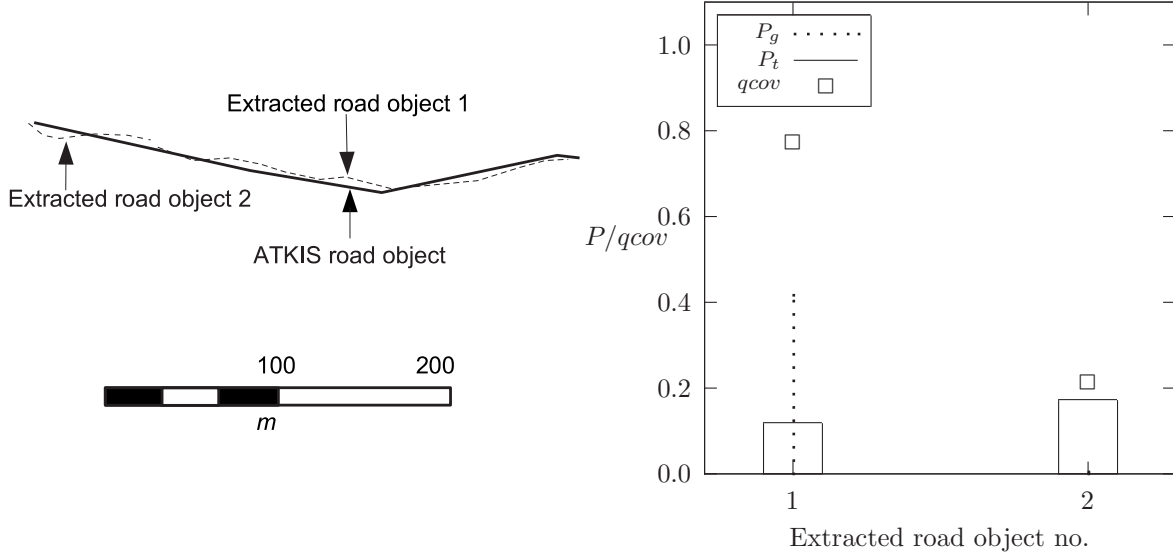


Figure 4.6.: Example for conformity of evidence: *incorrect* ATKIS road object

i	P_{g_i}	α_i	P_i^+	P_i^-	cov_ERO
1	0.416	0.093	0.0387	0.0543	0.98
2	0.005	0.037	0.0002	0.0368	

$$P(\xi_1 + \xi_2|H^+) = 0.0386, P(\xi_1 + \xi_2|H^-) = \mathbf{0.0907}, \text{ confirms } H^-$$

$$sp(H^+) = 0.0373, sp(H^-) = \mathbf{0.0874}, \text{ confirms } H^-$$

Table 4.5.: Conform Evidence: measures relevant for combination and its result, refer to Figure 4.6

The probability that extracted road object 1 and the ATKIS object have the same shape and same orientation, P_{g_1} , expresses some undetermined evidence, because the value of this parameter approaches 0.5. However, since the second extracted object gives full evidence for H^- (P_2^- is significantly larger than P_2^+), the ATKIS object has finally been rejected by both combination approaches.

Combination of evidence – Example III – Conflicting evidence: In this example conflicting evidence is combined. The extracted road objects 1 and 3 plotted in Figure 4.7 give evidence against the correctness of the ATKIS object, i.e. confirm H^- . The shortest extracted road object (no. 2) confirms the ATKIS object, since P_{g_2} is 0.99.

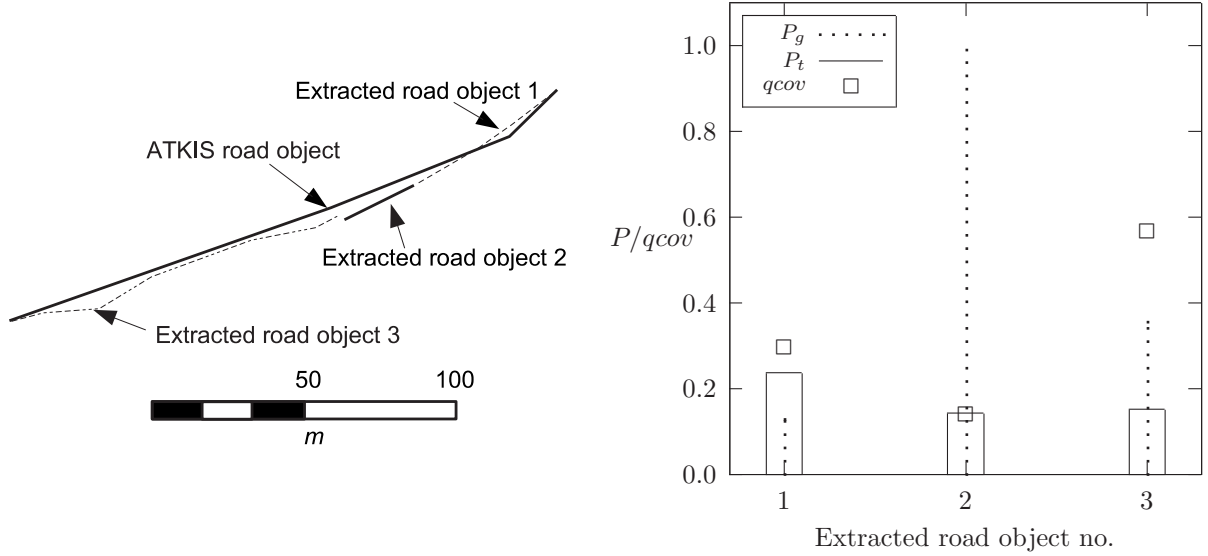


Figure 4.7.: Example for conflicting evidence: *incorrect* ATKIS road object

i	P_{g_i}	α_i	P_i^+	P_i^-	cov_ERO
1	0.129	0.070	0.0090	0.0610	1.00
2	0.990	0.020	0.0198	0.0002	
3	0.355	0.086	0.0305	0.0555	

$$P(\xi_1 + \xi_2 + \xi_3 | H^+) = 0.0593, P(\xi_1 + \xi_2 + \xi_3 | H^-) = \mathbf{0.1167}, \text{ confirms } H^-$$

$$sp(H^+) = 0.0541, sp(H^-) = \mathbf{0.1094}, \text{ confirms } H^-$$

Table 4.6.: Conflicting evidence: measures relevant for combination and its result, refer to Figure 4.7

Both approaches have finally confirmed H^- . This is a reasonable result as according to α_2 the influence of the extracted road object 2 to the overall result is marginal.

Combination of evidence – Example IV – Contradiction in quality indication: In the examples shown before no contradiction between the quality indication as derived from the maximum probability and maximum support rule occurred. In the following such a contradictory indication has been obtained. This example has not been taken from real data as such cases did not occur in the real data used for the tests in this thesis. The analysis of the result given below explains why it is unlikely that the final quality indications derived from the probabilistic and from the Evidential approach contradict in real situations.

In the left hand image in Figure 4.8 two extracted road objects are shown which cover the ATKIS road object by 99%, refer to cov_ERO in Table 4.7. The geometric evidence given by these objects is conflicting: $P_{g_1} = 0.191$ and $P_{g_2} = 0.990$.

Further

$$\begin{aligned}
 T_1 &< 0 \\
 \Leftrightarrow \alpha_1 + \alpha_2 - 2 \cdot (P_{g_1} \cdot \alpha_1 + P_{g_2} \cdot \alpha_2) &< 0 \\
 \Leftrightarrow \alpha_2 &> \left(\frac{\alpha_1 \cdot (2 \cdot P_{g_1} - 1)}{1 - 2 \cdot P_{g_2}} \right) \quad \text{if } (1 - 2 \cdot P_{g_2}) < 0. \quad (4.3) \\
 &< \left(\frac{\alpha_1 \cdot (2 \cdot P_{g_1} - 1)}{1 - 2 \cdot P_{g_2}} \right) \quad \text{if } (1 - 2 \cdot P_{g_2}) > 0.
 \end{aligned}$$

The values of Table 4.7 have been inserted into the Inequations 4.2 and 4.3 resulting in the constraint

$$0.0958 < \alpha_2 < 0.0986. \quad (4.4)$$

So, if α_2 takes values only within this very small range of $\pm 1.5\%$, a contradictory quality indication will be achieved. This demonstrates why it is unlikely that contradiction appears. Since the variables in the inequations are linearly dependent on each other, similar ranges may be expected if one of the other variables is chosen for this analysis.

Combination of evidence – Evaluation – Based on the examined examples the analysis permits to conclude that the explicit modelling of ignorance has no significant impact on the final reasoning result. The theoretically derived constraints for obtaining contradictory results are rarely satisfied in practical applications. According to the results it can be stated that in the application at hand the probabilistic combination approach is non-sensitive towards ignorance.

However, one interesting question remains: what is the correct decision if contradictions occur within the combination? Ignorance contained in observations means that there is a certain scope of interpretation, thus the final decision is quite subjective. In the examples I-III shown in the beginning of this section the evidence points towards a clear decision. In contrast, in example IV the mentioned freedom to interpret the observations leaves an open decision - even for a human operator. It is assumed that an interview of several human operators who are familiar with road verification would lead to a similar contradictory result in the given case. Thus, in practical applications any occurring contradiction should be considered in the final quality indication. For example a rejection of the respective road database object would urge the human operator to check the object.

4.3.3. Graph analysis and overall approach

In the following the approach as such and in particular the effect of the graph analysis on the result are evaluated. A confusion matrix has been used to rate the final assessment result, i.e. the *accept* and *reject* decision per object. In a confusion matrix reference decisions and the assessment result are compared. The types of error and their impact on a practical semi-automatic workflow are given in Table 4.8. The human operator who inspects the road assessment results only concentrates on the objects which have been rejected. The number of True Positives should be relatively high, since it indicates efficiency. The False Positive errors are undetected errors and thus should be minimised.

		<i>Assessment result</i>	
		<i>Acceptance</i>	<i>Rejection</i>
<i>Reference</i>	<i>Correct</i>	True Positive (Efficiency)	False Negative (Interactive final check)
	<i>Incorrect</i>	False Positive (Undetected errors)	True Negative (Interactive final check)

Table 4.8.: Confusion matrix

Two test series have been defined. In the first one the original ATKIS road objects have been used to demonstrate the performance of the approach applied to a typical open landscape scene in Germany. Since the original data only contain minor errors, a second test series using simulated data has been assembled to conduct additional sensitivity analyses.

Tests with original ATKIS data

The original ATKIS road objects were verified manually by a human operator using the imagery described above. The tolerance values for the relative position offset between an ATKIS object and the respective object observable in the image were $\Delta = \pm 4m$: the tolerance from ATKIS was defined by the modelling $D_{Mo} = 3m$, whereas the nominal accuracy from the orthoimage was $\Delta_I = \pm 1m$. The side condition *same width* was required for extracted objects.

It has to be kept in mind that the definition of reference data is a result of subjective decisions. For example no clear definition for the verification of the constraint *same shape* is given, refer to Section 4.3.1 on the examples for geometric assessment. During the presentation of the results, this topic will be discussed again.

Some details from the manual verification are listed below:

- 35 ATKIS road objects (total length $\approx 3.8km$) are **not in open landscape region**. These objects have not been considered for the evaluation of the results.
- 516 ATKIS road objects (total length $\approx 90.9km$) are **correct** with respect to all required quality measures: their medial axis is entirely positioned inside the $\pm 4m$ buffer of the correct object (according to the image). Their shape and orientation are also identical compared to the object observed in the imagery.
- The **width** of all observable and correct ATKIS road objects is **within the defined tolerance**. Therefore, the assessment of the side condition *same width* could not be evaluated with this data. However, in the tests with simulated data the width of all objects has been modified to evaluate the consequences of applying this constraint.
- 11 objects (total length $\approx 2.0km$) are **incorrect**. They do not satisfy the requirements defined for correct objects, i.e. their position, shape or orientation is incorrect.
- Approximately 130 ATKIS road objects (25%) are significantly **occluded by rows of trees**. This does not necessarily imply an invisibility of the road surface in the imagery. The percentage is obtained from the assignment algorithm, i.e. rows of trees have been assigned to the respective road objects.

Some parameters for the assessment have remained constant for all tests. The tolerance value δ_t for the angle between two objects has been defined as $\delta_t = 15^\circ$. The minimum required coverage `cov_req` is 0.8, i.e. besides the demand for maximum probability/support for H^+ at least 80% of an ATKIS road object needs to be covered by extracted objects in order to be accepted.

The tests have been carried out to analyse the performance of the overall approach. The confusion matrix is a reasonable means of evaluating the reliability as well as the efficiency. A major aspect has been to investigate the impact of the incorporation of rows of trees into the assessment. Here, one task has been to compare the results obtained with manually digitised rows of trees to the results from automatic image analysis. Additional sensitivity analyses were conducted in the second test series, because it turned out that the used ATKIS road database contains only few incorrect road objects which do not allow extensive tests on the reliability.

I. Strict vs. tolerant road extraction, no network exploitation: In the overall approach two parameter sets for the road extraction have been used: set 1 for the Initial object assessment (Phase 1) and set 2 for the Final object assessment (Phase 2). The strategy implemented in the approach requires a strict road extraction in Phase 1 compared to the tolerant road extraction in Phase 2.

In this first example only Phase 1 of the road database assessment was performed, firstly with roads extracted using set 1 and a second time with roads resulting from set 2. This means, the network function of roads was not exploited in the tests. The objective of these experiments was to analyse whether using roads extracted applying set 1 results in a more reliable but less efficient road assessment compared to roads extracted using set 2. The left column of the confusion matrix is an indicator for these properties: the larger the number of True Positives, the larger the efficiency, and the smaller the number of False Positives, the larger the reliability. No rows of trees were incorporated for this first test, but their impact to the assessment is discussed nevertheless.

Using parameter set 1, strict road extraction: In Table 4.9 the assessment results obtained with extracted roads resulting from parameter set 1 are shown. In the upper part the complete orthoimage is displayed. Individual road objects cannot be identified in detail. However, the spatial arrangement of True Positives, i.e. correct and accepted ATKIS road objects, drawn by thick continuous white lines and of False Positives, i.e. incorrect but accepted road objects, plotted by thick dashed white lines and of the True and False Negatives (thin continuous white lines) can be observed in this image. Below the

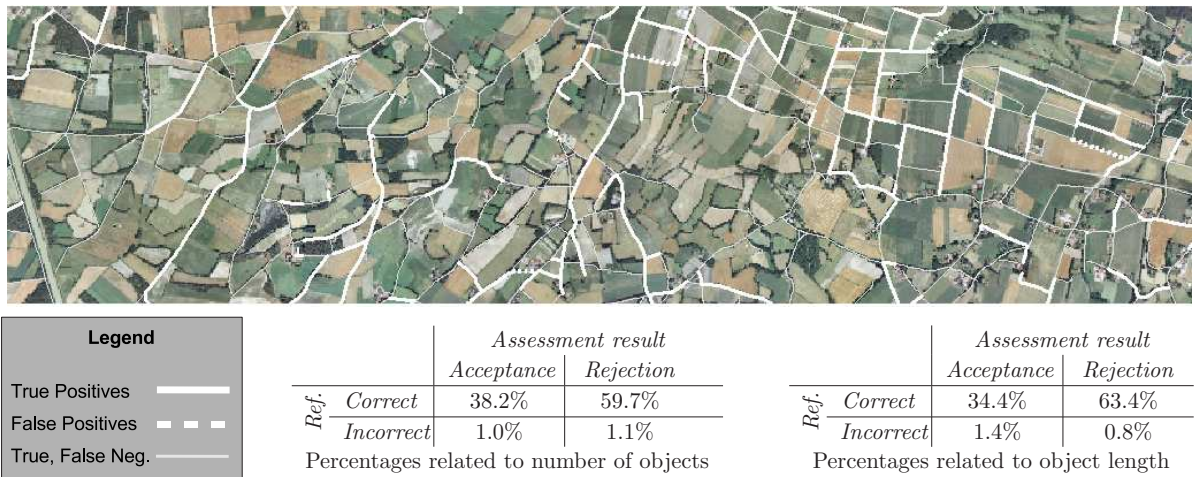


Table 4.9.: Confusion matrices and visualisation: assessment result incorporating extracted roads obtained with parameter set 1

orthoimage two confusion matrices are shown. The values in the left matrix are related to the number of objects, whereas the matrix on the right side lists percentages related to object length. For instance 38.2% of the ATKIS road objects are correct and have been accepted (True Positives), the overall length of these True Positives is 34.4% related to the overall length of all ATKIS road objects.

The comparison of the left and the right confusion matrix reveals that the percentage related to the length for True Positive decisions is smaller than the percentage related to the number of objects. As

will be seen below, apart from cases where the respective percentages are zero, these tendencies can be observed in all confusion matrices. This observation shows that mostly short correct objects are accepted.

Discussion of False Positives: The confusion matrices show that even the strict parameter setting



Figure 4.9.: Example for False Positive decision. Upper image: orthoimage detail showing a road under construction; lower image: superimposed extracted road (continuous line) and ATKIS road object (dashed line).

for road extraction leads to 1% False Positive decisions, i.e. 5 objects which are incorrect according to the decision from the human operator have been accepted by the automatic assessment algorithm. Two typical examples for those False Positive decisions are presented in Figures 4.9 and 4.10. The first figure shows a road object under construction, thus the human operator labelled this incorrect. However, the road extraction algorithm detected a valid road object which coincides well with the given ATKIS road object. It is obvious that such errors related to the actual usability of a road can only be avoided if additional information is provided to the road extraction algorithm, or to the assessment algorithm, respectively.

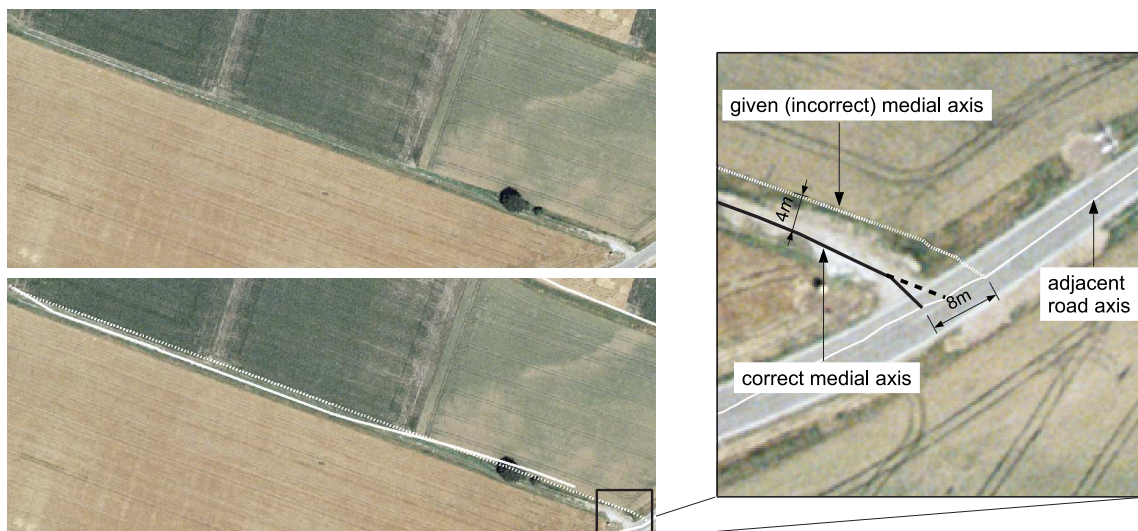


Figure 4.10.: Example for False Positive decision. Left, upper image: orthoimage detail showing a path leading to a field; left, lower image: superimposed extracted road (continuous line) and ATKIS road object (dashed line). The magnification (right) shows the correct road axis. The ATKIS road object is not correctly connected to the adjacent road at the right side.

The second example for a False Positive decision (refer to Fig. 4.10) reveals two problems inherent in the overall approach. The road object is correct, except for the junction area at the right image border: the geometric connection to the adjacent road is too far away from the correct medial axis. The actual offset measured in the image is about $8m$ (see magnification on the right hand side in the figure). The maximum offset apart from the junction area is only $4m$ and does not exceed the tolerance. Especially in junction areas a formal definition of the medial axis is difficult to give, resulting in possible different verification decisions. For instance, a second human operator would perhaps assume an extension of the straight line (dashed black line in the magnification), resulting in a maximum offset of $4m$ and thus would classify the ATKIS road object as correct. Similar to the evaluation of the requirement *same shape*, discussed in Section 4.3.1, a certain portion of uncertainty inherent in the preparation of reference data can be observed regarding the definition of junctions.

The second problem is visible in the lower image on the left side. It can be seen that the junction area has not been extracted at all. Therefore, one would expect a rejection decision. However, the major part – 85% – of the ATKIS road object has been covered by extracted road objects, and thus the required minimum overall coverage ($cov_req=80\%$) has been achieved. Since the covered part coincides well with the extracted road object, the object has finally been accepted. In other words, this False Positive results from the missing ability to explicitly incorporate evidence against the correctness of the road object. If in this example reliable evidence against the correctness of the junction area had been available, it would have been reasonable to reject the whole object. The problems and open questions related to this issue are discussed in the outlook provided in Chapter 5.

Discussion of True Negatives: An incorrect road which has been rejected, i.e. a True Negative decision, is exemplified in Figure 4.11. The road is currently under construction, but in contrast to the example for a False Positive decision given above, the majority of the visible road does not coincide with the road database object.



Figure 4.11.: Example for True Negative decision. Upper image: orthoimage detail showing a road under construction; lower image: superimposed extracted road (continuous line) and ATKIS road object (dashed line).

Discussion of True Positives and False Negatives: Altogether 98% of the assessed ATKIS road objects are correct. In this first example where the strict parameter setting has been applied for the road extraction, the major part of these correct objects has been rejected (False Negative decisions). A typical situation is given with Figure 4.12, showing two accepted road objects and one rejected. In this case the right road object (False Negative, FN) has been rejected due to bad contrast conditions. The road in the lower part and the field path in the upper part of the image have been successfully extracted and thus have been accepted (True Positive, TP). Further reasons for False Negative decisions, especially rows of trees occluding roads, will be discussed next.

To emphasise the influence of the trees regarding the assessment, the confusion matrices in Table 4.10 only relate to road objects which are significantly occluded by trees. Only approx. 30% of True Positives (compared to 38% above) are obtained, i.e. the occlusion leads to an insufficient road extraction in many



Figure 4.12.: Example for True Positive and False Negative decision, obtained with roads resulting from parameter set 1. The dashed lines show three road objects; two of them are correct and accepted (True Positive, TP), one is correct, but rejected (False Negative, FN).

cases. A further observation is that none of those road objects occluded by rows of trees has been labelled incorrect by the human operator.

		Assessment result				Assessment result	
		Acceptance	Rejection			Acceptance	Rejection
Ref.	Correct	30.4%	69.6%	Ref.	Correct	23.9%	76.1%
	Incorrect	0.0%	0.0%		Incorrect	0.0%	0.0%
Percentages related to number of objects				Percentages related to object length			

Table 4.10.: Confusion matrices: assessment result incorporating extracted roads obtained with parameter set 1, **only ATKIS objects being significantly occluded by trees**

Using parameter set 2, tolerant road extraction: Table 4.11 shows the assessment outcome which has been obtained with extracted roads resulting from parameter set 2, i.e. the tolerant settings. The number of False Positive decisions has remained constant compared to the results obtained with roads from the strict setting, while the percentage of True Positive decisions has increased from approximately 38% to 62%.

Discussion of True Positives and False Negatives: In Figure 4.13 the same road objects are shown as presented in Figure 4.12. The tolerant parameter settings, especially the contrast parameters, have led to a successful road extraction for the right object, which therefore has been accepted. However, approximately 36% of the correct road objects have still been rejected. Two main reasons for the failed road extraction are weak contrast conditions and secondly, significant occlusions caused by rows of trees.

In Figure 4.14 a typical field path is shown, which is composed of the same material as the adjacent fields. The contrast between the surface of the path and the surrounding is low, and thus it has not been extracted by the automatic algorithm. The image explains why a further tuning of parameters towards tolerant extraction is not successful: the more tolerant the parameters, the larger the risk of extracting structures in the field and interpreting them as road objects, see the continuous branch line in Figure 4.14.

The influence of occlusion on the assessment result is demonstrated with Figure 4.15. Altogether 25 road objects are visible in the scene, mainly occluded by rows of trees. Since in this test only extracted roads have been taken into account, the majority of road objects has been rejected, only 7 objects have been accepted. This image will be shown again when the rows of trees are incorporated into the assessment.

Again, only the roads significantly occluded by rows of trees have been taken into account for the calculation of the matrices in Table 4.12. As already observed for the tests with parameter set 1, the number

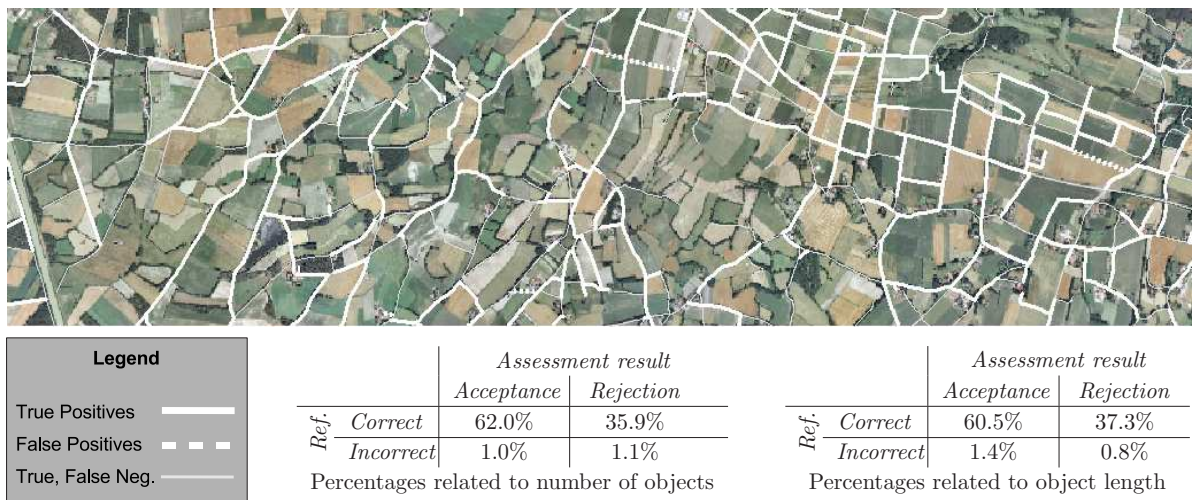


Table 4.11.: Confusion matrices and visualisation: assessment result incorporating extracted roads obtained with parameter set 2



Figure 4.13.: Example for True Positive decision obtained with roads extracted using tolerant setting



Figure 4.14.: Example for False Negative decision due to weak contrast



Figure 4.15.: Example for False Negative decisions resulting from occlusions caused by rows of trees

of True Positives decreases from 62% in the case that all objects are considered to less than 54% as in this case.

Summary: The presented results from the first tests allow some conclusions. First of all, compared to the result from the tolerantly tuned road extraction, the strict parameter setting for the road extraction does not result in a smaller amount of falsely accepted roads. Those False Positive decisions are the most critical ones in any automated quality assessment system. It has been found that in the given case some of these errors are related to a certain portion of uncertainty in the definition of correct and incorrect objects. Additionally, it may be expected and it will be shown below that an increase of the value for the parameter *cov_req* will lead to a further reduction of this kind of error. A deficit of the presented approach as already discussed in Section 3.5 was also identified. Since no explicit modelling and assessment of junction areas are integrated, false decisions related to incorrect junctions cannot be avoided.

Other incorrect road objects have been rejected because even the roads that have automatically been extracted with tolerant parameters do not give enough evidence for their correctness. Additional sensitivity analyses will be presented in the second test series.

		Assessment result				Assessment result	
		Acceptance	Rejection			Acceptance	Rejection
Ref.	Correct	53.6%	46.4%	Ref.	Correct	45.2%	54.8%
	Incorrect	0.0%	0.0%		Incorrect	0.0%	0.0%

Percentages related to number of objects Percentages related to object length

Table 4.12.: Confusion matrices: assessment result incorporating extracted roads obtained with parameter set 2, **only ATKIS objects being significantly occluded by trees**

One interesting observation concerns the assessment of the side condition *same width*. As pointed out above, the width of all ATKIS objects is within the defined tolerance. None of the objects has been rejected due to a wrong assessment of width, i.e. no False Negatives occurred from the calculation of the probability that an extracted object has the same width as the ATKIS road object. Whether the evaluation of this side condition leads to False Positive decisions will be tested in the second test series based on simulated data.

A prominent reason for False Negative decisions is given with the occlusion caused by dense vegetation in open landscape areas, particularly by rows of trees. To underline the role of rows of trees for the

assessment, the network function of roads is exploited next, but again no rows of trees are incorporated. The incorporation of rows of trees into the assessment workflow and its impact on the results will be demonstrated and discussed later.

II. Exploitation of network function – without rows of trees: Here, the network approach is

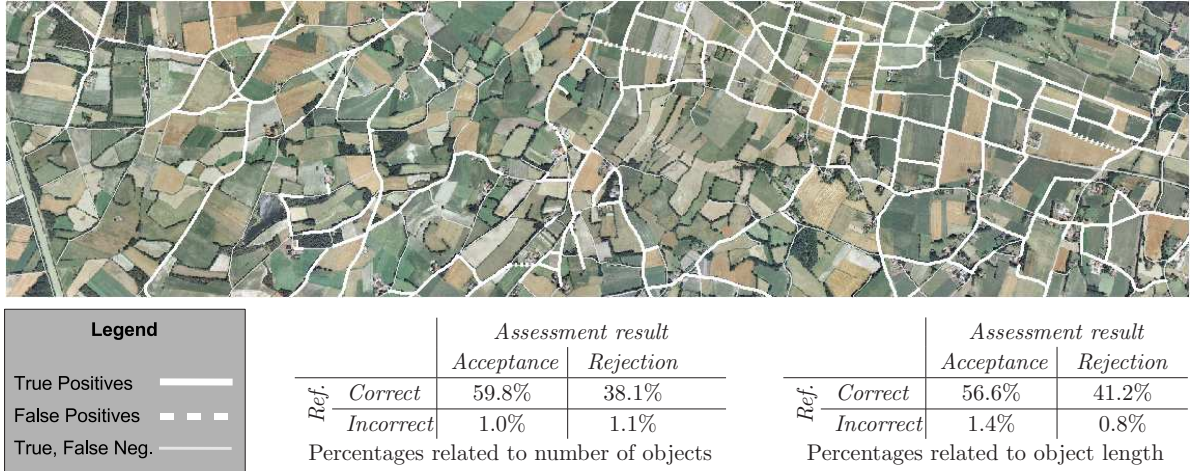


Table 4.13.: Confusion matrices and visualisation: assessment result, applying graph analysis without the incorporation of rows of trees

applied, but no rows of trees are incorporated. By this means, the impact of the graph analysis to the overall result can be evaluated. In Table 4.13 the image is shown as well as the confusion matrices. The left one is again related to the number of objects, and the right one is related to the length of objects.

The number of True Positive decisions increases compared to the tests where the graph analysis has not been applied (only parameter set 1), but it is less than the number observed if only parameter set 2, i.e. the tolerant one, has been applied. This is a quite reasonable result, because during the graph analysis dead end roads or roads at image borders are not chosen for the final assessment result: they can not be part of a shortest paths on principle. A further discussion regarding the impact of the graph analysis is given with the next test set.

The confusion matrices in Table 4.14 again show that the number of True Positives decreases when only road objects which are significantly occluded by rows of trees are considered (approximately 53% against 60% above). Another interesting issue relates to the statistics based on the length of object, i.e. the right hand side confusion matrix. The number of True Positives related to the object length is only approx. 40%, i.e. a hint that mainly long road objects are occluded by rows of trees.

		Assessment result	
		Acceptance	Rejection
Ref.	Correct	52.8%	47.2%
	Incorrect	0.0%	0.0%

Percentages related to number of objects

		Assessment result	
		Acceptance	Rejection
Ref.	Correct	39.5%	60.5%
	Incorrect	0.0%	0.0%

Percentages related to object length

Table 4.14.: Confusion matrices: assessment result, applying graph analysis without the incorporation of rows of trees, **only ATKIS objects being significantly occluded by trees**

III. Exploitation of network function – with manually captured rows of trees: In this test the complete workflow as proposed in this thesis has been adopted. During Phase 1 roads extracted by applying parameter set 1 are used to preliminarily assess the given ATKIS road network. The manually captured rows of trees are also incorporated, i.e. if a road is rejected, but connects two important network nodes (start-nodes), it will be accepted as far as rows of trees give enough evidence, otherwise it will be selected for the final object assessment (Phase 2). In Phase 2 the selected roads are assessed again, but parameter set 2 is used for road extraction.

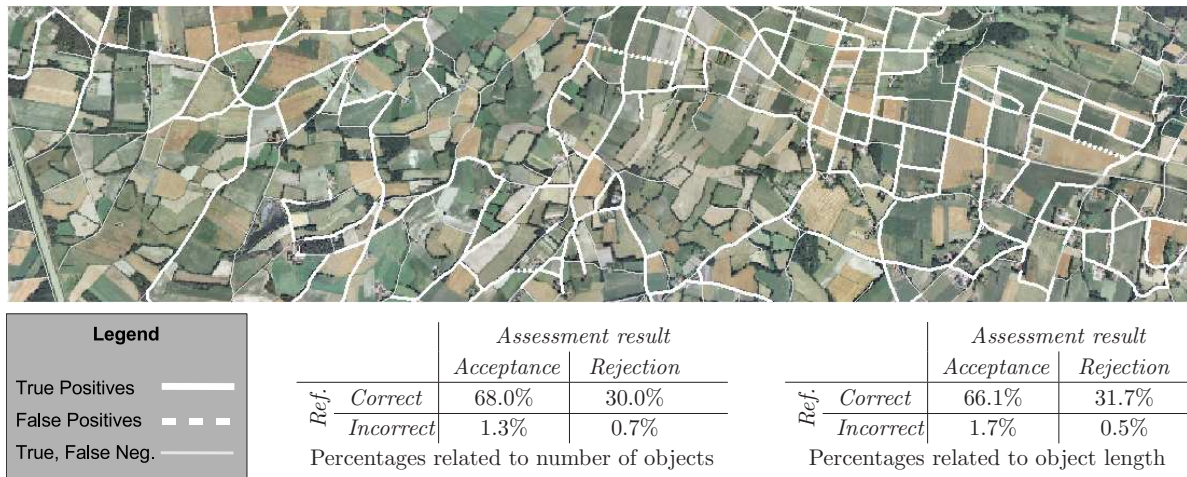


Table 4.15.: Confusion matrices and visualisation: assessment result, applying graph analysis and incorporating manually captured rows of trees

In Table 4.15 the complete image is shown as well as the confusion matrices, again related to the number of objects (left) and to the length of objects (right). The number of True Positive decisions has been increased from nearly 60% (network exploitation, without rows of trees) to 68%. Furthermore, one additional object has been classified as False Positive.

Discussion of influence of rows of trees and of graph analysis: The effect of both the use of the graph analysis and the incorporation of rows of trees into the assessment is demonstrated with the image presented in Figure 4.16, which displays the same scene as Figure 4.15. The 10 objects marked with ”+”



Figure 4.16.: Example for True Positive decisions because of incorporation of rows of trees

are additionally accepted road objects, compared to the results where only extracted roads have been incorporated. All the road objects marked with ”+” fulfil important network tasks as they link the road objects which have been accepted in Phase 1. Since the extracted road objects in conjunction with the rows of trees give enough evidence for the correctness of these important objects, they have finally been accepted.

One interesting issue is related to the road object marked with "1" in the figure. This object is entirely covered by trees. According to the strategy implemented in the presented approach, this object has been rejected, because no acceptance decision is possible without any evidence given by extracted roads.

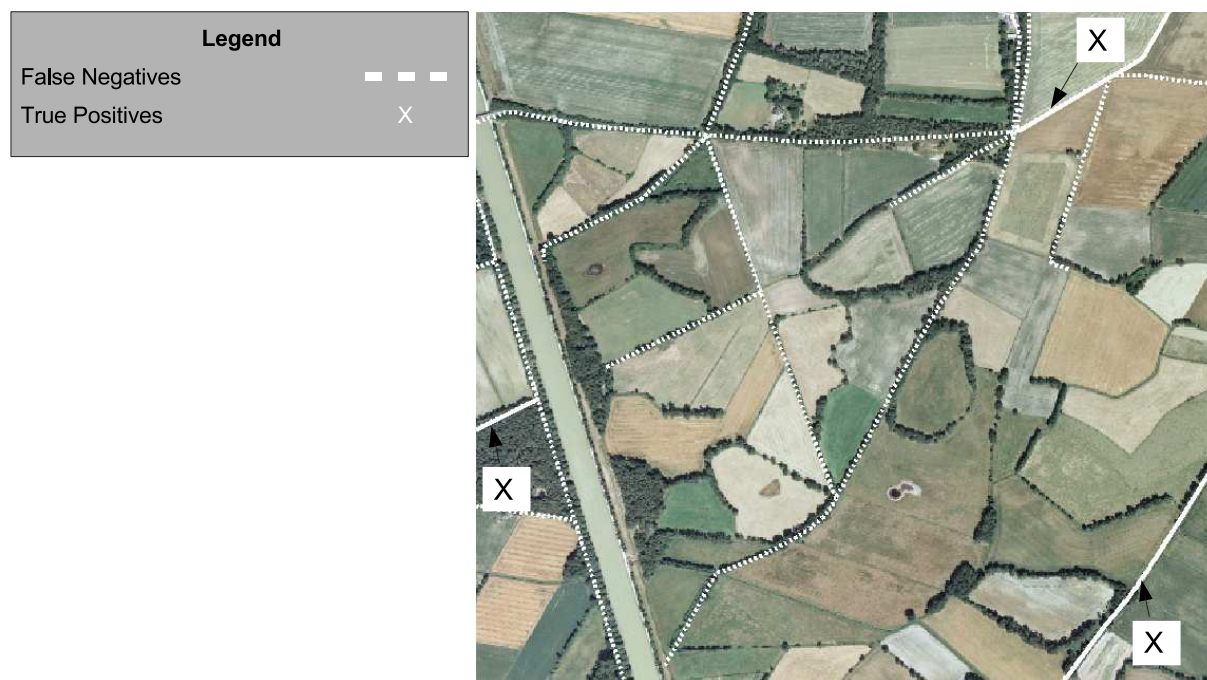


Figure 4.17.: Limits of approach: False Negative decisions for dead end roads, occluded by rows of trees

Limits of the presented approach are pointed out in Figure 4.17. This scene shows many road objects which are significantly occluded by trees, and which are connected to the network at only one node, i.e. they constitute dead end roads. One reason for this is the canal in the left part of the image: one single bridge leads to the opposite site. Additionally, the bridge is clipped by the image border. Only the objects marked with "X" have been accepted in Phase 1. Although the rows of trees give enough evidence for the correctness of some additional road objects, those have been rejected since they do not connect the accepted roads. This example clarifies that in practical applications the scenes need to overlap in order to avoid objects at the image border. If for instance a road object on the opposite side of the bridge had been accepted in Phase 1, at least the roads in the upper part connecting the bridge and the shown accepted object would have a certain chance to be labelled accepted.

Analysis of additional False Positive: One additional False Positive decision occurred during this test. The incorrect but accepted object is shown in Figure 4.18. This decision is related to the minimum required coverage. Although the offset between the road objects observable in the image and the given road database object exceeds the allowed threshold – at least in the curve – the object has been accepted. Compared to the assessment where only the extracted roads have been used, the required coverage measure is satisfied when the rows of trees are incorporated. Since this object connects two reliably extracted road objects, it has finally been accepted.

Again for the measures given in Table 4.16 only those ATKIS road objects have been considered which are significantly occluded by rows of trees. Compared to the experiments where the rows of trees have not been incorporated, the number of True Positives related to the number of objects does not decrease, it approximately remains constant. This result emphasises the importance of the rows of trees for the assessment. Again, the amount of True Positives with respect to the object length decreases because mainly long road objects are occluded by rows of trees.

In order to demonstrate the trade-off between reliability and efficiency which can be triggered by `cov_req`, an additional test has been conducted. All parameters remained constant, except for `cov_req`, which has been increased from `cov_req=0.80` to `cov_req=0.95`. In Table 4.17 the results are shown. In the given case

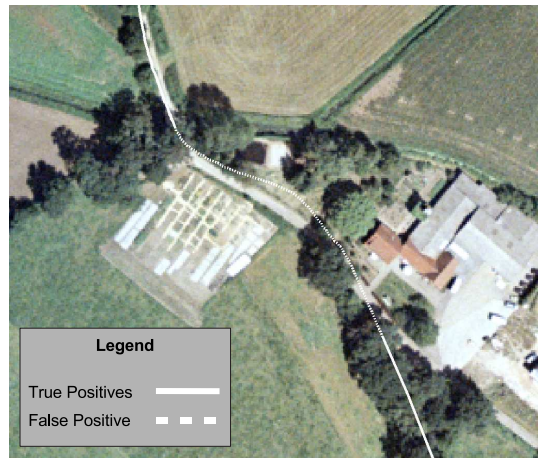


Figure 4.18.: Example for False Positive decisions because of incorporation of rows of trees

		Assessment result				Assessment result	
		Acceptance	Rejection			Acceptance	Rejection
Ref.	Correct	68.4%	31.6%	Ref.	Correct	56.5%	43.5%
	Incorrect	0.0%	0.0%		Incorrect	0.0%	0.0%

Percentages related to number of objects Percentages related to object length

Table 4.16.: Confusion matrices: assessment result, applying graph analysis and incorporating manually captured rows of trees, **only ATKIS objects being significantly occluded by trees**

the number of False Positives has decreased from 1.7 to 1.1%, but at the same time the number of True Positives has also decreased considerably: from 66.1% to 46.5%. The result shows that although some False Positive decisions can be avoided by this means, others remain. These remaining objects have been accepted because of undetected errors in junction areas.

		Assessment result				Assessment result	
		Acceptance	Rejection			Acceptance	Rejection
Ref.	Correct	50.0%	48.1%	Ref.	Correct	46.5%	51.3%
	Incorrect	0.9%	1.0%		Incorrect	1.1%	1.1%

Percentages related to number of objects Percentages related to object length

Table 4.17.: Confusion matrices: assessment result, applying graph analysis and incorporating manually digitised rows of trees, minimum required coverage: **cov_req=0.95**

Disregarding Paths: The analysis of False Negatives resulting from the first tests shows that a lot of False Negative decisions are related to bad contrast conditions which often occur at field paths. This observation is supported by the confusion matrices shown in Table 4.18. Here, only ATKIS *Road* objects have been taken into account, i.e. those objects which are mainly used for car and transportation traffic. The percentage of True Positive decisions has increased to nearly 80%, whereas True Negatives and False Positives do not occur at all, as no incorrect *Roads* are present in this dataset. A separate analysis of *Paths* has not been carried out, because the number of *Paths* is large compared to *Roads* (approximately 85%) and thus it may be expected that the percentages do not significantly differ from the numbers in the previous confusion matrices.

Summary: The examples presented above show that the exploitation of road network topology in conjunction with the incorporation of rows of trees leads to a significantly improved assessment result. However, if roads are not fully connected to the network they cannot benefit from the network-based optimisation. In practical applications adjacent scenes should overlap in order to assure that a minimum number of road objects is affected from these restrictions.

False Positive decisions related to undetected errors in junction areas cannot be avoided completely. Therefore, a large required overall coverage of extracted objects and road database objects does not lead

		Assessment result				Assessment result	
		Acceptance	Rejection			Acceptance	Rejection
Ref.	Correct	79.2%	20.8%	Ref.	Correct	74.8%	25.2%
	Incorrect	0.0%	0.0%		Incorrect	0.0%	0.0%

Percentages related to number of objects Percentages related to object length

Table 4.18.: Confusion matrices: assessment result, applying graph analysis and incorporating manually digitised rows of trees, **only ATKIS Roads, no Paths**

to a significant reduction of False Positives. In the shown examples the chosen threshold of $cov_req=0.80$ proved to be a reasonable trade-off between efficiency and reliability.

The increased efficiency encountered for the assessment of *Road* objects confirms the statement that roads determined for car transportation are easier to identify in aerial imagery than field paths. Reasons for this are for instance their larger width and more consistent surface conditions.

IV. Exploitation of network function – with automatically extracted rows of trees: The scope of the test presented in the following has been to demonstrate the influence of the automatically extracted rows of trees to the assessment results. In Table 4.19 the results are shown. Compared to

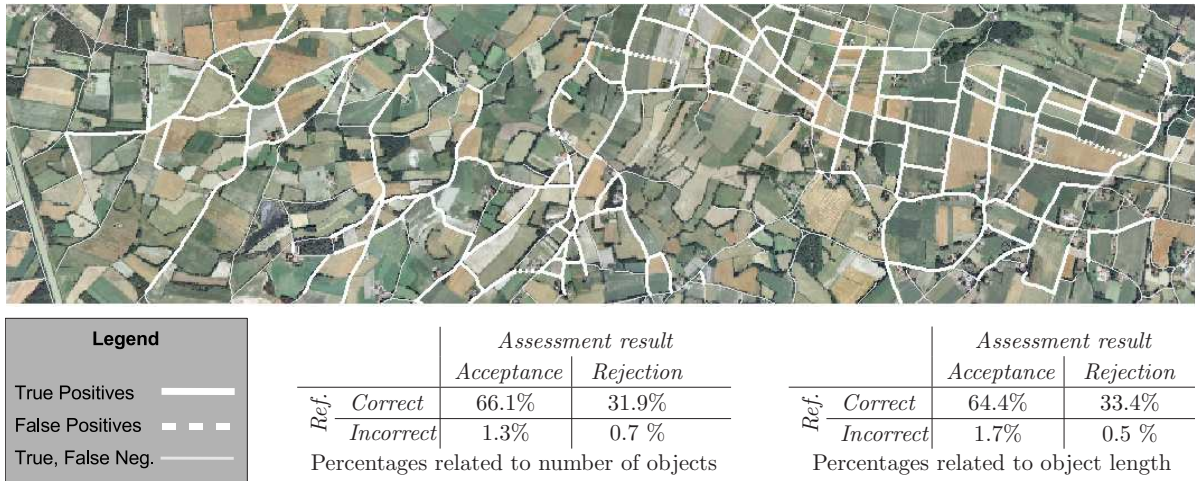


Table 4.19.: Confusion matrices and visualisation: assessment result, applying graph analysis and incorporating automatically extracted rows of trees

the results obtained with manually captured rows of trees, the number of False Positives has remained constant, but the percentage of True Positive decisions has decreased from 68% to approximately 66%. This decrease corresponds to 8 objects. These missing True Positives can be traced back to missing rows of trees. An example is shown in Figure 4.19. The dashed lines represent the manually captured rows of trees, whereas the continuous lines show automatically extracted objects. Under certain circumstances the segmentation of the scene into the classes built-up, industrial, grassland, cropland and forest is not correct. As described above, the rows of trees have been derived from forest areas through the application of geometric constraints.

In the example shown the small settlement area and the surrounding cropland areas lead to a number of pixels with uncertain class assignment. The area of pixels which possibly belong to forest is small against the area of the remaining classes. Therefore, these pixels have been labelled cropland or settlement, respectively.

Altogether, the result obtained with those automatically extracted rows of trees is comparable to the result obtained with the manually digitised set.

V. Road extraction without incorporation of seeds from ATKIS objects: In the beginning of this section the used road extraction algorithm was described in some detail. The means of incorporating the prior information from the ATKIS road database into the road extraction is to use the ATKIS roads

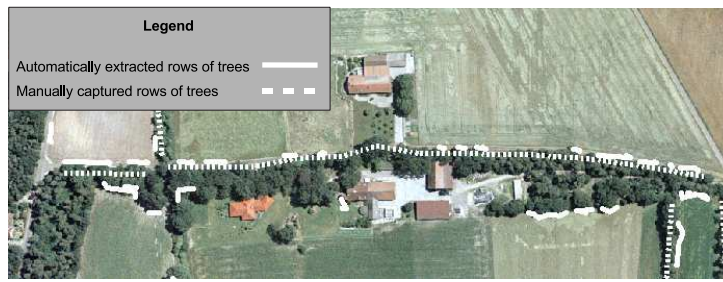


Figure 4.19.: Example for automatic extraction of rows of trees: missing object

as seed lines (refer to Figure 4.2) and to define regions of interest for the road extraction from the existing data. The road extraction which has been conducted for the preceding experiments applied these methods.

Table 4.20 shows the results from the road database assessment where seed lines from the existing road data have not been incorporated into the road extraction. All data and parameters were identical to the information used in test III, therefore the numbers can be compared to Table 4.15.

The number of False Positives has remained the same as in the preceding test where the seed lines from the road database objects have been incorporated into the road extraction. However, the number of True Positives, i.e. the measure for the efficiency, has decreased from 68% to approximately 63%. This result allows the conclusions that the incorporation of the existing road data into the road extraction enhances the overall assessment performance, and has no negative effect on the reliability.



Legend	
True Positives	—
False Positives	- - -
True, False Neg.	—

		Assessment result	
		Acceptance	Rejection
Ref.	Correct	62.8%	35.2%
	Incorrect	1.3%	0.7 %

Percentages related to number of objects

		Assessment result	
		Acceptance	Rejection
Ref.	Correct	59.4%	38.4%
	Incorrect	1.7%	0.5 %

Percentages related to object length

Table 4.20.: Confusion matrices and visualisation: assessment result, applying graph analysis and incorporating manually digitised rows of trees. The roads have been extracted without incorporation of the ATKIS road objects.

Tests with simulated ATKIS data: sensitivity analyses

Some issues have not been treated sufficiently so far. The width of all given ATKIS road objects is correct, thus the side condition *same width* could not be evaluated adequately. For this reason the value for the attribute *width* has been set to incorrect values for all ATKIS road objects for the next test.

Moreover, the question of whether the graph analysis supports the reduction of False Positive decisions could not be checked. It was found that the False Positive decisions in the tests with real data occurred mainly due to a missing clear definition of what is correct or due to the lacking assessment of junction areas. Therefore, an artificial set of incorrect ATKIS road data has been prepared.

VI. Modified width of ATKIS road objects:

The ATKIS data used for the first test series is assessed here again. The only modification concerns the attribute *width*. The value of this attribute has been set to $w_A = 25m$ for all objects. The test configuration is identical to test III., i.e. the manually captured rows of trees have been incorporated. Table 4.21 shows that all objects have been rejected. This is a quite convincing result, since it demonstrates on the one hand that the road extraction operator obviously does not make any gross errors in the calculation of the road width. On the other hand the procedure to calculate the probability that the widths are identical achieves reasonable results.

		Assessment result	
		Acceptance	Rejection
Ref.	Correct	0.0%	0.0 %
	Incorrect	0.0%	100.0 %

Table 4.21.: Confusion matrix: artificially ATKIS data: width of all ATKIS roads= $25m$

VII. Wrong set of road data: In this case all objects from the manually captured set of road data are incorrect with respect to the roads observable in the image, refer to the detail of the orthoimage in the upper row of Table 4.22.



Legend	
True Negatives	———
False Positives	- - - -

		Assessment result	
		Acceptance	Rejection
Ref.	Correct	0.0%	0.0%
	Incorrect	0.0%	100.0 %

Percentages related to number of objects

		Assessment result	
		Acceptance	Rejection
Ref.	Correct	0.0%	0.0%
	Incorrect	0.0%	100.0 %

Percentages related to object length

Table 4.22.: Confusion matrices and visualisation: assessment result incorporating extracted roads obtained with parameter set 1

The tests which have been conducted with this data are similar to test I., i.e. firstly the whole data has been assessed only using roads extracted with parameter set 1. In a second test extracted roads have been used which have been obtained with parameter set 2. No graph approach has been applied, however, some conclusions regarding the benefit from the graph analysis are possible.

The assessment which only incorporates roads extracted using the strict parameter setting (refer to Table 4.22) results in a rejection of the complete data, i.e. the ratio of True Negatives is 100%. The assessment test where only extracted roads obtained with the tolerant set 2 are incorporated leads to a False Positive ratio of 26.0% (refer to Table 4.23). The False Positives occur where the artificial road object is placed right on a field, coinciding well for instance with paths caused by tractors. These errors will not lead to False Positive decisions in a complete assessment run, where the graph analysis is included: in Phase 1 where set 1 is used, all objects will be rejected and thus no roads will be chosen for Phase 2.

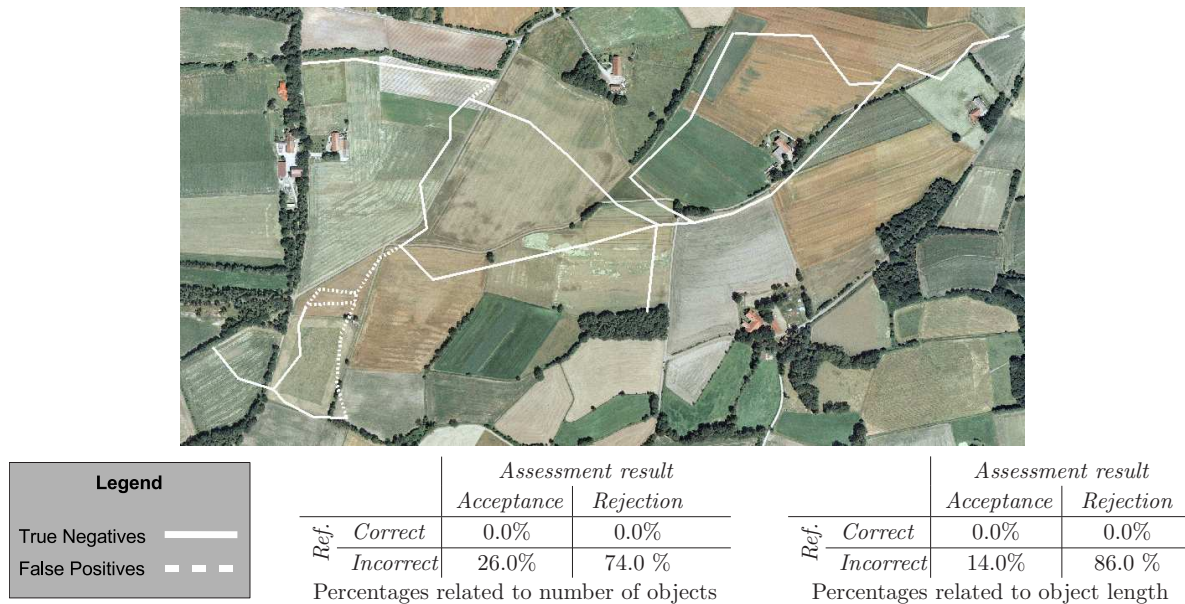


Table 4.23.: Confusion matrices and visualisation: assessment result incorporating extracted roads obtained with parameter set 2

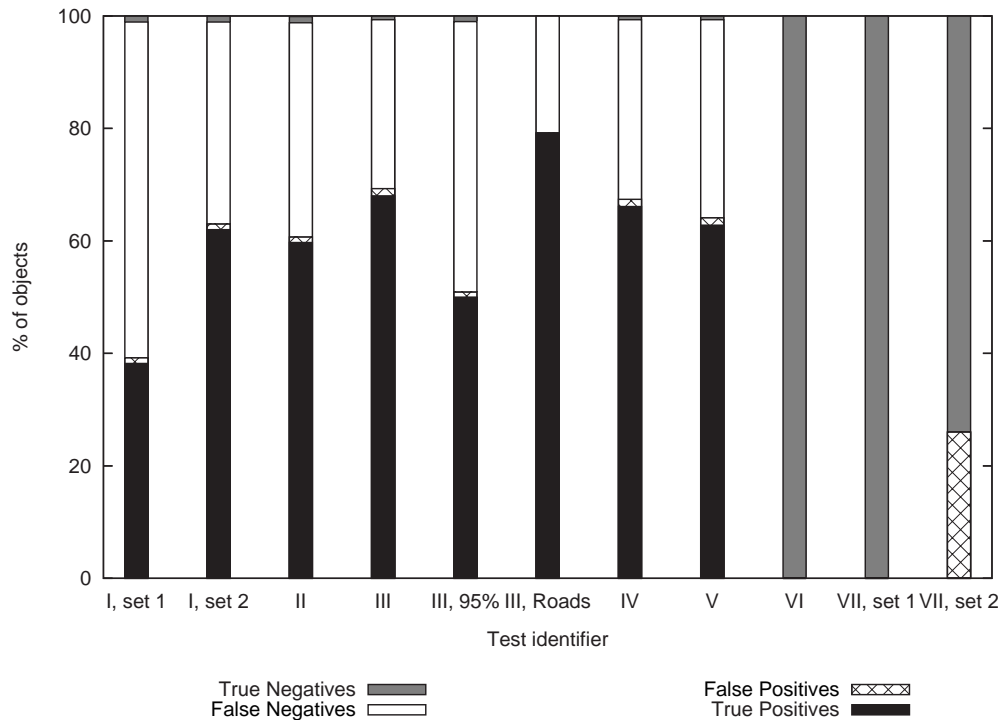
Graph analysis and overall approach – Evaluation –

The chart in Figure 4.20 shows the content of all confusion matrices (percentages related to number of objects). The labels on the x-axis refer to the tests which have been conducted.

Some findings can be summarised:

- The graph analysis, including the incorporation of rows of trees which explain gaps in road extraction, enhances the efficiency of the quality assessment (compare True Positives of (I, set 1) and (I, set 2) to III in the chart and II to III).
- Roads which constitute dead ends are not integrated in the network-based optimisation. This property of the approach leads to a minimisation of False Positives, but also to a reduced number of True Positive decisions.
- The correct non-dead end objects which have been rejected (i.e. False Negatives) when the rows of trees are incorporated, can be explained by an unsuccessful road extraction, for instance due to weak contrast, or the objects are entirely occluded by vegetation.
- The False Positive decisions which occurred with the original dataset are mostly related to undetected errors in junction areas. These errors could not be avoided through the graph analysis. However, the experiments with simulated data show that in most other cases the False Positive errors are reduced (compare (VII, set 1) to (VII, set 2)).
- The increase of required coverage of ATKIS road objects with extracted objects did not result in significantly increased reliability, but in a reduced efficiency (compare (III, 95%) to III).
- In a test where only ATKIS *Roads* were considered, a substantial increase of True Positives was registered (compare (III, Roads) to III).
- Incorporating the existing road database into the road extraction turned out to increase the efficiency of the whole approach, but not to have a negative effect on the reliability (compare III to V).
- Although some false and some missing objects are amongst the automatically extracted rows of trees, the applied algorithm for the extraction of rows of trees proved to be helpful. The segmentation algorithm as such, as well as the derivation of the centre axis using the approach developed in Section 3.2.1 seems to be useful for practical applications (compare IV to III).
- The assessment of the attribute *width* turned out to be reliable (see VI).

- In all confusion matrices the percentage for True Positive decisions related to the length is smaller than the percentage related to the number. This observation shows that mainly short objects are accepted.



Test identifier	Description
I, set 1	Application only of strict road extraction, no network exploitation
I, set 2	Application only of tolerant road extraction, no network exploitation
II	Exploitation of network function – without rows of trees
III	Exploitation of network function – with manually captured rows of trees
III, 95%	Exploitation of network function – with manually captured rows of trees, requirement of a 95%-coverage
III, Roads	Exploitation of network function – with manually captured rows of trees, only consideration of ATKIS <i>Roads</i> , no <i>Paths</i>
IV	Exploitation of network function – with automatically extracted rows of trees
V	Same as III, but road extraction without incorporation of seeds from ATKIS objects
VI	Modified width of ATKIS road objects (completely incorrect)
VII, set 1	Wrong set of road data, application only of strict road extraction, no network exploitation
VII, set 2	Wrong set of road data, application only of tolerant road extraction, no network exploitation

Figure 4.20.: Overview on assessment results

5. Conclusions and outlook

This thesis describes a new approach to the assessment of road databases. In contrast to existing research work it includes a detailed statistical and relational modelling of all involved objects. Not only extracted road objects but also context objects which are able to explain deficient road extraction are incorporated into the quality assessment. The developed approach results in an acceptance and rejection decision for every object from the given road database. The core of this thesis is an adequate modelling of objects and their relations, a statistically founded assessment of relations between objects and a reasonable combination of the obtained measures in conjunction with a network exploitation strategy. The approach has been developed for open landscape regions, and the ATKIS DLMBasis has been used as an example of geo-spatial data source.

In the following the main issues are discussed.

- Object modelling

The influences on the precision of geo-spatial objects have been identified and categorised. They are modelled by probability density functions, in particular by Gaussian and uniform functions. The parameters for the respective functions are derived based on the used image data or algorithms.

The object modelling includes elongated objects, which are represented by their medial axes and as area objects. A conversion between geometric representations has been developed which includes a consistent propagation of statistical measures. The derivation of the medial axis from the area representation is based on an enhanced skeletonisation which provides an appropriate description of elongated objects.

The obtained results allow the conclusion that the chosen representation meets the requirements. However, the modelling of junction areas by means of the medial axis has been found to be insufficient in some cases.

- Model of the geometric and topologic relations between road objects and local context objects

One basic idea pursued in this thesis is that objects represented in the geo-spatial database must maintain the same spatial relations as the respective object in reality. To this end the geometric relations *same shape* and *same orientation* as well as the topologic relations *disjoint* and *contains* are defined in the so-called relationship model.

The evaluation of experimental results shows that these relations are a satisfactory means of describing similarity of the considered objects. However, the disregard of junction areas in this model led to some false assessment decisions.

- Assessment of existing relations between a road database object and extracted objects

The identity of shape is assessed by applying an approach based on geometric moments, which are used as shape descriptors. It is exploited that the moment invariants of objects with the same shape are identical. The uncertainties inherent in each object are propagated for the moments and therefore the question of whether moments are identical is formulated as a statistical test. The probability that two objects have the same orientation is also calculated using error propagation for the orientation, followed by a statistical test on the identity of the respective orientations. Topologic relations are assessed using a method which analyses the minimum and maximum difference between intersection sets of the respective objects. It considers the statistical measures of the objects and results in a probability that the existing topologic relation meets the required one.

Altogether, the developed algorithms to assess the geometric and topologic relations lead to comprehensive results. The uncertainties inherent in the objects are adequately considered by the obtained probability measures. The automatic assessment is solely based on statistical measures. Particularly, the missing explicit definition of the property *same shape* may lead to diverging results compared to a manual and therefore subjective assessment.

The pursued strategy of incorporating the existing road database into the road extraction algorithm turned out to contribute to a efficient and reliable assessment result.

- Collection and balancing of evidence given by the extracted objects and quality indication for database object

Each observation from the object-based comparison which leads to probability values for the attainment of the required relations may contain ignorance about the correctness of the given database road object. The combination of all evidence related to one given database object is done using two different approaches. The first one is a traditional probabilistic combination not considering the ignorance. The second one is based on the Evidence Theory, where ignorance can be incorporated explicitly. Theoretical considerations concerning possible contradictory final quality indications resulting from both methods are irrelevant for practical results. The findings imply that for the application at hand the probabilistic combination is non-sensitive towards ignorance.

As mentioned above no detailed modelling of junction areas is provided with the presented approach. In the test with real data some False Positive decisions occurred due to the unclear definition of medial axes in junction areas. However, it has to be kept in mind that the reference data has been created based on very stringent rules. The ATKIS object catalogue does not define precise rules for the capture of junction areas. This issue will be discussed again in the outlook below.

A second problem may arise from the fact that it is not foreseen to explicitly consider conflicts with the current model concerning topologic relations. Only the probability for an attainment of the modelled topologic relation is integrated. If for instance it is likely that a row of trees is placed right on the surface of a road object from the database, this observation will give no evidence for the correctness of the road object. This is reasonable. Yet, it will raise no evidence for the incorrectness of the database object, either. One means of approaching this problem in such cases is to consider the complement to 1 of the probability that the topologic relation is maintained ($1 - P_t$) to support the hypothesis H^- .

Another type of False Positive decisions, i.e. the acceptance of incorrect objects, concerns properties which are not necessarily observable in images. An interesting example has been shown by the road under construction. Since the road visible in the image corresponds to the model implemented in the road extraction algorithm, it was successfully extracted and therefore has been accepted. Such False Positive decisions can only be avoided if additional knowledge is incorporated either in the road extraction algorithm or in the approach to the assessment.

- Exploitation of road network topology and incorporation of rows of trees

The developed strategy of exploiting the connection functionality of roads in conjunction with the incorporation of context objects proved to be a means of enhancing the overall assessment performance. Even the results obtained with automatically extracted rows of trees only differ marginally from results obtained with manually captured objects. To reduce the risk of False Positive decisions a key constraint for the application of a tolerant road extraction and for the incorporation of context objects is that roads to be assessed need to be entirely connected to the network. Therefore, dead end roads or roads at image borders cannot benefit from the possible evidence given in Phase 2 or by context objects. In practical applications the number of objects affected by this constraint can be reduced by overlapping the investigated scenes.

The presented approach to road database assessment using remotely sensed imagery shows that a modelling of objects and their relations, including a consistent statistical processing is essential for the comparison of vector datasets from different origins. The evaluation of the algorithms for geometric and topologic relation assessment demonstrates that it is worth incorporating error propagation methods to obtain reasonable results.

The effectiveness of the assessment also depends on the performance of the used road extraction operator. If correct road objects are not extracted or if non-road objects which appear as roads in the imagery lead to false extractions, errors in assessment decisions cannot be avoided. However, by means of the chosen graph-based strategy which also uses context objects to explain gaps in road extraction, the number of this kind of errors is reduced considerably.

Outlook

The incorporation of further objects into the assessment seems to be an interesting and promising means of improvement. The relationship model can easily be extended towards new object classes. For instance,

the edges of forests are not considered up to now. Similar to rows of trees, they may occlude roads and therefore hamper the automatic extraction of roads. The geometric and topologic relations can be modelled similarly to those for rows of trees. One issue is related to such an extension: the consideration of elongated objects is not sufficient for this object class. Forests are normally not elongated, but arbitrarily shaped. However, the method for the assessment of topologic relations remains the same as long as the region is regularly closed and singularly connected as requested in [WINTER 1996]. The geometric relations can be assessed using the same methodology when the edge of the forest as such is represented as a linestring.

To integrate additional object classes is also interesting for the graph-based optimisation. In the current approach only reliably extracted roads are considered for the definition of start-nodes. Especially for dead end roads other object classes may give rise to implication that a road object is important in the sense of connection functionality. For example a large agricultural facility needs to be connected to the road network. If according to the road database there is only one road object leading to such a facility, but this has not been accepted in the first assessment phase, the existence of the facility may justify that the object is checked again in the second phase.

Two subjects are closely related: the improved consideration of junction areas and the ability to explicitly bring in evidence against the correctness of a road database object. The geometric modelling of crossings and their automatic extraction from remotely sensed imagery is a current topic which is tackled by many research groups. The most important issue related to the assessment of a junction present in a geo-spatial database is to determine those properties which are suitable to reasonably compare it to an extracted junction. Another question arises regarding the incorporation of evidence delivered by the junction assessment. It must be taken into consideration that the evidence given by a junction may lead to a rejection of the whole adjacent road objects, regardless of the remaining evidence. Obviously, this option puts high demands on the junction extraction and assessment algorithm – the triggering of this algorithm towards a minimisation of False Negative and False Positive decisions seems to be a great challenge. One means of reducing the complexity is to regard junctions as separate object class and therefore assess them independently from the road objects.

The statistical properties of the extracted objects are estimated according to experience and the characteristics of the used data and algorithm. However, whether the given parameters reflect the actual object properties is not ensured. If an adequate sample of objects is present, the parameters can be learnt automatically, for instance using Bayesian estimation, where the estimated parameters can be introduced as prior knowledge.

Additional significant improvements concern the extension of the approach regarding quality assessment in settlement areas and the update of existing road data. The assessment of road vector data in built-up areas requires an enhancement of the relationship model and further investigations on the incorporation of the existing data into automatic road extraction. Object classes to be included into the relationship model are for instance buildings, or rows of buildings, respectively, and objects on the road like vehicles. Recent research on road extraction in built-up areas shows that more detailed data is required for a satisfactory result. In [HINZ 2004] surface models are used to restrict the search space for road extraction. An interesting question in conjunction with the approach in the present thesis is whether the existing road vector data can be used sufficiently and reliably for such a search space restriction instead. Similar to the method to incorporate the existing road data into the extraction applied for open landscape it needs to be ensured that incorrect road vector data does not lead to false extractions.

The problem of updating the road network, i.e. of the detection of roads that are currently not contained in the database, is subdivided. Omission errors can be caused by two main reasons: firstly, the road already existed when the database was created or last updated, but the (human) operator forgot to capture the road or did not see the necessity of doing so. The important fact here is that the missing road is part of an existing network; its age is probably similar to that of the adjacent roads. The second reason for omission errors is that the road was not built or completed when the road database was last updated, i.e. the road is newer than the database.

In the first case a graph-based search in conjunction with a knowledge-driven road extraction is a means of detecting potentially missing roads. Hypotheses for gaps in the existing network can be found applying distance and collinearity criteria for edges and nodes in the graph. For instance, two supposed dead end roads which only have a distance of a few metres and which are collinear may be connected. A further

road extraction in the region of interest defined by the hypothesis then needs to be applied to confirm or reject the assumption. Such a procedure reflects a typical model-driven strategy, i.e. to define hypotheses and then to verify them using available data.

In the second case the road network by itself is not enough to define hypotheses for new roads. If information on newly built-up areas is available, the hypothesis that those regions need to be connected to the existing road network may be formulated and thus a similar method as presented in the last paragraph is possible. If no such additional information exists, a data-driven strategy is possible, i.e. to extract roads in the image and afterwards to link them to the existing road network. The constraint that new roads need to be connected to the existing road network allows for a reduction of false extractions.

In this regard a property of the developed approach to road database assessment can be exploited. So far, an object-based accept and reject decision is derived, but the information on the quality of individual segments is also available: it is used for the transition from objects to network edges. The information on the segment-based quality is a means of detecting those road objects which have only partially been modified.

The approach to road database assessment presented in this thesis has been developed in the framework of the WiPKA-QS project. The majority of the algorithms is integrated in the workflow at the German Federal Agency for Geodesy and Cartography (BKG) where a system for the automated verification and quality control of the ATKIS DLMBasis is installed.

A. Appendix

A.1. Distance transforms and skeletons

In \mathbb{R}^2 the Euclidean distance between two points p and q is given by $d_\epsilon = \sqrt{(x_q - x_p)^2 + (y_q - y_p)^2}$. In principle this distance can also be used in discrete space, but it is more common to use distances defined in discrete space instead. The discrete distance d_G between two pixels p and q is defined as the smallest length L of the path P in raster G [SOILLE 1999]:

$$d_G(p, q) = \min\{L(P) | P \text{ path linking } p \text{ to } q \text{ in } G\}. \quad (\text{A.1})$$

The path to be taken depends on the chosen *metric*. Using the N_4 metric (*city-block*) just the four horizontal and vertical neighbours are considered, whereas in the N_8 metric (*chessboard*) all eight adjacent pixels are involved. In Figure A.1 these concepts are illustrated by means of a *discrete distance transform*.



Figure A.1.: Distances from the central pixel using different metrics in \mathbb{Z}^2

The *skeleton* of a 2D-object is a 1D-line representation resulting from thinning the object, starting at its boundary. The skeleton represents the shape of the object and preserves its initial connectivity; it is also known as medial axis [BLUM 1967, LEE 1982, ROSENFELD 1986]. A common means of illustrating the skeletonisation is the so-called *grassfire process*: the object is imagined as a grassland lit along its whole boundary. If it is assumed that the fire progresses uniformly, the fire fronts will meet at points belonging to the skeleton. In \mathbb{R}^2 the skeleton is unique (refer to [SOILLE 1999]), whereas in \mathbb{Z}^2 no straightforward definition is known. The two facts mainly responsible for this are: a) a discrete skeletal line is not infinitely thin, b) the centre skeleton cannot always be realised (consider for example the skeleton of a 2 pixel thick discrete line). Refer to [OGNIEWICZ and KÜBLER 1995] for an overview of different techniques to obtain

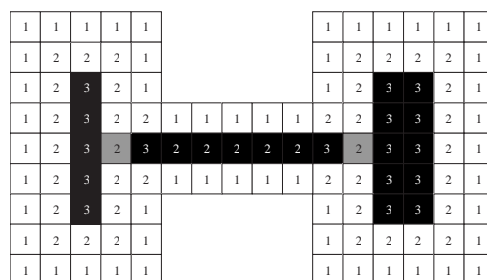


Figure A.2.: Skeletonisation applying discrete distance transform using City-block-Metric

a discrete skeleton. One means of calculating the discrete skeleton is to use the distance transform introduced above: the local maxima of the distance transform of the boundary points represent points of the skeleton. Since the points are not necessarily connected (which is required) and the skeleton line

may be thicker than one pixel at some locations, post processing steps need to be applied. In Figure A.2 an example is given. In black the local maxima of the distance transform using the N_4 metric are shown. This initial skeleton needs to be thinned using standard operators from morphological image processing, the grey pixels are not local maxima, but need to be assigned to the skeleton in order to derive a closed representation.

The discrete skeleton is an approximation of the skeleton as derived through geometric construction in \mathbb{R}^2 , refer to Figure A.3: the discrete skeleton is smoothed. From both Figures A.2 and A.3 one can see that the raster size has a significant influence on the amount of smoothing.

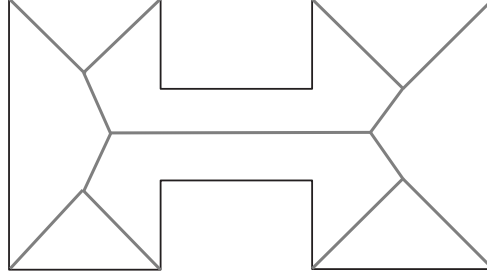


Figure A.3.: Skeleton constructed according to [LEE 1982]

A.2. Line moments and their statistical properties

In the following the symbols according to [LAMBERT and GAO 1995] are used. Given a two-dimensional object B , whose domain $D(B)$ is known, the moment (p, q) of order $=(p + q)$ is calculated by

$$m_{pq} = \int \int_{(x,y) \in D(B)} x^p y^q f(x, y) dA \quad p, q = [0, 1, \dots, \infty], \quad (\text{A.2})$$

where $f(x, y)$ is a continuous image function. In this thesis a linestring representation in \mathbb{R}^2 is assumed. If an elongated object is given, the linestring representation is derived from the medial axis, reflecting the object's shape (refer to Appendix A.1)¹. The uncertainty inherent in the geometric position of the vertices is modelled by a Gaussian distribution and assumed to be identical for all vertices as well as for the x and y coordinate directions, i.e. variance $\sigma_x^2 = \sigma_y^2 = \sigma_{x,y}^2$ for all vertices.

The line is represented by an n -side polygon with vertices (x_i, y_i) where $i = 1, 2, \dots, n$. In [LAMBERT and GAO 1995] the moments m_{pq} for line objects are derived. They are given with Equation A.3.

$$m_{pq} = \sum_{i=1}^{n-1} \left[\begin{cases} \sqrt{1 + a_i^2} \sum_{k=0}^q \binom{q}{k} a_i^k (y_i - a_i x_i)^{q-k} \frac{x_{i+1}^{p+k+1} - x_i^{p+k+1}}{p+k+1} & \text{if } x_i \neq x_{i+1} \\ x_i^p \frac{y_{i+1}^{q+1} - y_i^{q+1}}{q+1} & \text{if } x_i = x_{i+1} \end{cases} \right], \quad (\text{A.3})$$

where a_i is the slope of the i . segment: $a_i = (y_{i+1} - y_i)/(x_{i+1} - x_i)$.

In case of line moments the zeroth moment m_{00} is the length of the line.

The *central moments* μ , i.e. translation invariants, are calculated considering the centre of gravity \bar{x}, \bar{y} :

$$\mu_{pq} = \sum_{i=1}^{n-1} \left[\begin{cases} \sqrt{1 + a_i^2} \sum_{k=0}^q \binom{q}{k} a_i^k ((y_i - \bar{y}) - a_i(x_i - \bar{x}))^{q-k} \frac{(x_{i+1} - \bar{x})^{p+k+1} - (x_i - \bar{x})^{p+k+1}}{p+k+1} & \text{if } x_i \neq x_{i+1} \\ (x_i - \bar{x})^p \frac{(y_{i+1} - \bar{y})^{q+1} - (y_i - \bar{y})^{q+1}}{q+1} & \text{if } x_i = x_{i+1} \end{cases} \right]. \quad (\text{A.4})$$

The centre of gravity is obtained from the zeroth and first order moments:

$$\bar{x} = \frac{m_{10}}{m_{00}}, \quad \bar{y} = \frac{m_{01}}{m_{00}}. \quad (\text{A.5})$$

¹A more specific algorithm for the derivation of the medial axis from an object is given in the modelling part (Section 3.2.1).

Rotation invariance is obtained applying the *method of principal axis* [HU 1962]. Here, firstly the orientation θ of the principal axis is calculated using second-order moments:

$$\theta = \frac{1}{2} \arctan \frac{2\mu_{11}}{\mu_{20} - \mu_{02}}. \quad (\text{A.6})$$

Two problems concerning the orientation calculation need to be considered. If the dimension of the object becomes similar in both x and y directions, θ is not defined. This problem does not occur in this thesis, because only elongated objects are treated. The second issue about θ is its ambiguity concerning the correct choice of the major axis. The correct orientation is $\theta = \theta + n\pi/2$. According to [SARDANA et al. 1994] the application of the following constraints is used to find the correct moments:

1. $\mu_{20} > \mu_{02}$, otherwise add $\pi/2$ to θ .
2. $\mu_{30} > 0$, otherwise change the signs of all moments μ_{pq} with odd order $p+q$.

The object is then rotated by $-\theta$ using the centre of gravity as fixed point. The orthogonal transformation of rotation is:

$$\begin{bmatrix} x' \\ y' \end{bmatrix} = \begin{bmatrix} \cos \theta & \sin \theta \\ -\sin \theta & \cos \theta \end{bmatrix} \begin{bmatrix} x - \bar{x} \\ y - \bar{y} \end{bmatrix}. \quad (\text{A.7})$$

The central moments calculated from the rotated object are *translation and rotation invariant*. In the following these moments are symbolised by μ'_{pq} .

As pointed out in Section 3.4 on the realisation of the approach, only translation and rotation invariant moments are used. However, *scale invariance* could be derived by a normalisation by the length of the object:

$$\eta_{pq} = \mu_{pq} (\mu_{00})^{-(p+q+1)}. \quad (\text{A.8})$$

Variance propagation for line moments: The variance of a moment $\sigma_{\mu'_{pq}}^2$ is obtained applying variance propagation. The intermediate steps to calculate the variances are given below.

The slope a_i is a function of the segment defined by x_i, x_{i+1}, y_i and y_{i+1} . Its partial derivatives are

$$\begin{aligned} \frac{\partial a_i}{\partial x_i} &= \frac{y_{i+1} - y_i}{(x_{i+1} - x_i)^2}, \\ \frac{\partial a_i}{\partial x_{i+1}} &= -\frac{y_{i+1} - y_i}{(x_{i+1} - x_i)^2}, \\ \frac{\partial a_i}{\partial y_i} &= \frac{1}{x_i - x_{i+1}}, \\ \frac{\partial a_i}{\partial y_{i+1}} &= \frac{1}{x_{i+1} - x_i}, \end{aligned} \quad (\text{A.9})$$

leading to the variance

$$\sigma_{a_i}^2 = \left(\frac{\partial a}{\partial x_i} \right)^2 \sigma_{x_i}^2 + \left(\frac{\partial a}{\partial x_{i+1}} \right)^2 \sigma_{x_{i+1}}^2 + \left(\frac{\partial a}{\partial y_i} \right)^2 \sigma_{y_i}^2 + \left(\frac{\partial a}{\partial y_{i+1}} \right)^2 \sigma_{y_{i+1}}^2. \quad (\text{A.10})$$

The central moment of the i . segment (μ_{pq_i}) is a function of \bar{x}, \bar{y} and x_i, y_i, x_{i+1} (and of a_i , which is a function of x_i, y_i, x_{i+1} , and y_{i+1}), $\forall i = 1, 2, \dots, n-1$. The partial derivatives for the case $x_i \neq x_{i+1}$ are

$$\begin{aligned}
\frac{\partial \mu_{pq_i}}{\partial a_i} &= \sqrt{1 + a_i^2} \sum_{k=0}^q \left[\left(\binom{q}{k} a_i^k ((y_i - \bar{y}) - a_i(x_i - \bar{x}))^{(q-k)} \right) \cdot \right. \\
&\quad \left. \left(\frac{a_i}{1 + a_i^2} + \frac{k}{a_i} + (q-k) \frac{-(x_i - \bar{x})}{(y_i - \bar{y}) - a_i(x_i - \bar{x})} \right) \cdot \mathbf{g} \right], \\
\frac{\partial \mu_{pq_i}}{\partial \bar{x}} &= \sqrt{1 + a_i^2} \sum_{k=0}^q \binom{q}{k} a_i^k \left[((q-k) ((y_i - \bar{y}) - a_i(x_i - \bar{x}))^{(q-k-1)} a_i) \cdot \mathbf{g} + \right. \\
&\quad \left. \mathbf{f} \cdot ((x_i - \bar{x})^{p+k} - (x_{i+1} - \bar{x})^{p+k}) \right], \\
\frac{\partial \mu_{pq_i}}{\partial \bar{y}} &= \sqrt{1 + a_i^2} \sum_{k=0}^q \binom{q}{k} a_i^k (q-k) ((y_i - \bar{y}) - a_i(x_i - \bar{x}))^{(q-k-1)} (-1) \cdot \mathbf{g}, \\
\frac{\partial \mu_{pq_i}}{\partial x_i} &= \sqrt{1 + a_i^2} \sum_{k=0}^q \binom{q}{k} a_i^k \left[((q-k) ((y_i - \bar{y}) - a_i(x_i - \bar{x}))^{(q-k-1)} (-1) a_i) \cdot \mathbf{g} + \right. \\
&\quad \left. \mathbf{f} \cdot ((-1)(x_i - \bar{x})^{p+k}) \right], \\
\frac{\partial \mu_{pq_i}}{\partial x_{i+1}} &= \sqrt{1 + a_i^2} \sum_{k=0}^q \binom{q}{k} a_i^k \mathbf{f} (x_{i+1} - \bar{x})^{p+k}, \\
\frac{\partial \mu_{pq_i}}{\partial y_i} &= \sqrt{1 + a_i^2} \sum_{k=0}^q \binom{q}{k} a_i^k (q-k) ((y_i - \bar{y}) - a_i(x_i - \bar{x}))^{(q-k-1)} \cdot \mathbf{g}, \tag{A.11}
\end{aligned}$$

using the additional variables

$$\begin{aligned}
\mathbf{f} &= ((y_i - \bar{y}) - a_i(x_i - \bar{x}))^{q-k}, \\
\mathbf{g} &= \frac{(x_{i+1} - \bar{x})^{p+k+1} - (x_i - \bar{x})^{p+k+1}}{p+k+1}.
\end{aligned}$$

If $x_i = x_{i+1}$, μ_{pq} only depends on \bar{x}, \bar{y} and x_i, y_i, y_{i+1} , leading to the simplified derivatives

$$\begin{aligned}
\frac{\partial \mu_{pq_i}}{\partial \bar{x}} &= -p \mu_{pq_i} (x_i - \bar{x})^{-1}, \\
\frac{\partial \mu_{pq_i}}{\partial \bar{y}} &= (x_i - \bar{x})^p (-(y_{i+1} - \bar{y})^q + (y_i - \bar{y})^q), \\
\frac{\partial \mu_{pq_i}}{\partial x_i} &= p \mu_{pq_i} (x_i - \bar{x})^{-1}, \\
\frac{\partial \mu_{pq_i}}{\partial y_i} &= (x_i - \bar{x})^p (-1) (y_i - \bar{y})^q, \\
\frac{\partial \mu_{pq_i}}{\partial y_{i+1}} &= (x_i - \bar{x})^p (y_{i+1} - \bar{y})^q, \tag{A.12}
\end{aligned}$$

The variance is again given by the sum

$$\sigma_{\mu_{pq}}^2 = \sum_{i=1}^{n-1} \left[\left[\left(\frac{\partial \mu_{pq_i}}{\partial a_i} \right)^2 \sigma_{a_i}^2 + \left(\frac{\partial \mu_{pq_i}}{\partial \bar{x}} \right)^2 \sigma_{\bar{x}}^2 + \left(\frac{\partial \mu_{pq_i}}{\partial \bar{y}} \right)^2 \sigma_{\bar{y}}^2 + \dots \quad \text{if } x_i \neq x_{i+1}, \right. \right. \\
\left. \left[\left(\frac{\partial \mu_{pq_i}}{\partial \bar{x}} \right)^2 \sigma_{\bar{x}}^2 + \left(\frac{\partial \mu_{pq_i}}{\partial \bar{y}} \right)^2 \sigma_{\bar{y}}^2 + \dots \quad \text{if } x_i = x_{i+1} \right] \right]. \tag{A.13}$$

For moments not being invariant under any translation (m_{pq}), the variance is obtained when \bar{x} and \bar{y} are omitted in equation A.13. This is necessary to calculate the variances $\sigma_{\bar{x}}^2$ and $\sigma_{\bar{y}}^2$: they are obtained from $\sigma_{m_{00}}^2$, $\sigma_{m_{10}}^2$ and $\sigma_{m_{01}}^2$, refer to eq. A.5. The respective partial derivatives are

$$\begin{aligned}\frac{\partial \bar{x}}{\partial m_{00}} &= -\frac{m_{10}}{m_{00}^2}, \\ \frac{\partial \bar{y}}{\partial m_{00}} &= -\frac{m_{01}}{m_{00}^2}, \\ \frac{\partial \bar{x}}{\partial m_{10}} &= \frac{\partial \bar{y}}{\partial m_{01}} = \frac{1}{m_{00}},\end{aligned}\tag{A.14}$$

finally leading to the variance of the centre of gravity:

$$\begin{aligned}\sigma_{\bar{x}}^2 &= \left(\frac{\partial \bar{x}}{\partial m_{00}}\right)^2 \sigma_{m_{00}}^2 + \left(\frac{\partial \bar{x}}{\partial m_{10}}\right)^2 \sigma_{m_{10}}^2, \\ \sigma_{\bar{y}}^2 &= \left(\frac{\partial \bar{y}}{\partial m_{00}}\right)^2 \sigma_{m_{00}}^2 + \left(\frac{\partial \bar{y}}{\partial m_{01}}\right)^2 \sigma_{m_{01}}^2.\end{aligned}\tag{A.15}$$

The orientation θ is a function of the second order rotation invariant moments, the partial derivatives are

$$\begin{aligned}\frac{\partial \theta}{\partial \mu_{11}} &= \frac{1}{1 + \tan^2 2\theta} \cdot \frac{1}{\mu_{20} - \mu_{02}}, \\ \frac{\partial \theta}{\partial \mu_{20}} &= -\frac{\mu_{11}}{(1 + \tan^2 2\theta) \cdot (\mu_{20} - \mu_{02})^2}, \\ \frac{\partial \theta}{\partial \mu_{02}} &= \frac{\mu_{11}}{(1 + \tan^2 2\theta) \cdot (\mu_{20} - \mu_{02})^2},\end{aligned}\tag{A.16}$$

leading to the variance of θ :

$$\sigma_{\theta}^2 = \left(\frac{\partial \theta}{\partial \mu_{11}}\right)^2 \sigma_{\mu_{11}}^2 + \left(\frac{\partial \theta}{\partial \mu_{20}}\right)^2 \sigma_{\mu_{20}}^2 + \left(\frac{\partial \theta}{\partial \mu_{02}}\right)^2 \sigma_{\mu_{02}}^2.\tag{A.17}$$

When the object is rotated by θ (eq. A.7) the variance of the points must be propagated. Afterwards, the formula given in A.13 applies to the rotation invariant moment.

A rotated point $p'(x, y)$ has the derivatives

$$\begin{aligned}\frac{\partial x'}{\partial \theta} &= y', \\ \frac{\partial y'}{\partial \theta} &= -x', \\ \frac{\partial x'}{\partial x} &= \frac{\partial y'}{\partial y} = \cos \theta, \\ \frac{\partial x'}{\partial \bar{x}} &= \frac{\partial y'}{\partial \bar{y}} = -\cos \theta, \\ \frac{\partial x'}{\partial y} &= \frac{\partial y'}{\partial \bar{x}} = \sin \theta, \\ \frac{\partial x'}{\partial \bar{y}} &= \frac{\partial y'}{\partial x} = -\sin \theta,\end{aligned}\tag{A.18}$$

leading to the variances

$$\begin{aligned}\sigma_{x'}^2 &= \left(\frac{\partial x'}{\partial \theta}\right)^2 \sigma_{\theta}^2 + \dots, \\ \sigma_{y'}^2 &= \left(\frac{\partial y'}{\partial \theta}\right)^2 \sigma_{\theta}^2 + \dots.\end{aligned}\tag{A.19}$$

To summarise, the procedure to derive the translation and rotation invariant moment μ'_{pq} and its variance is:

1. Calculate m_{00}, m_{10}, m_{01} , applying eq. A.3. The variances are obtained from eq. A.13, with $\bar{x} = \bar{y} = 0$.
2. Calculate the centre of gravity (eq. A.5) and its variances (eq. A.15).
3. Calculate θ (eq. A.6) using second order translation invariant moments. The variance of θ is obtained from eq. A.17.
4. Rotate the object using the centre of gravity as fixed point and $-\theta$ as rotation angle (eq. A.7), leading to x' and y' with variances as obtained from eq. A.19.
5. Finally, the translation and rotation invariant moment μ'_{pq} is obtained from eq. A.4 using x', y', \bar{x}, \bar{y} . The respective variance is calculated when the correct variances are inserted into A.13.

Example: A line object with an assumed length of approximately $134m$ is shown in Figure A.4. The moments of the zeroth and first order are given as well as the central moments of the second order. The orientation θ is calculated from them, including a variance measure (based on the assumed variance of the object coordinates $\sigma_{x,y} = 0.8m$). In Table A.1 the rotation and translation invariant moments of this object from the third up to the eighth order are listed. The last three columns show the ratio $\mu'_{pq}/\sigma_{\mu'_{pq}}$, assuming different variances of the object coordinates ($\sigma_{x,y} = 0.5m, 0.8m$ and $3.0m$). An absolute ratio larger than 2.96 indicates that a moment is significantly larger than zero (i.e. it is not within the 99%-confidence interval). In the example shown only three moments (assuming $\sigma_{x,y} = 0.5m$) are larger than zero, refer to * in the table. When $\sigma_{x,y}$ increases to $0.8m$, only one moment is significant and finally, for $\sigma_{x,y} = 3m$ none of the moments is different from zero, i.e. in that case the line object does not differ significantly from a straight line.



Measure	Value
m_{00} (length)	134.05
m_{10}	6562.9
m_{01}	5842.1
μ_{11}	95572
μ_{20}	105370
μ_{02}	88118
θ	0.5299 (30.36°)
σ_{θ}^2	8.7E-3 (0.50°)

Figure A.4.: Examples of line moments: zeroth and first order: normal moments; second order: translation invariants and θ derived from them. The variance of θ is based on an assumed variance of the object coordinates $\sigma_{x,y} = 0.8m$.

p	q	order	μ'_{pq}	$\sigma_{x,y} = 0.5m$ $\mu'_{pq}/\sigma_{\mu'_{pq}}$	$\sigma_{x,y} = 0.8m$ $\mu'_{pq}/\sigma_{\mu'_{pq}}$	$\sigma_{x,y} = 3.0m$ $\mu'_{pq}/\sigma_{\mu'_{pq}}$
3	0	3	$7.094 \cdot 10^4$	0.05	0.03	0.01
2	1	3	$-1.409 \cdot 10^5$	-0.31	-0.19	-0.05
1	2	3	$-5.748 \cdot 10^4$	-0.08	-0.05	-0.01
0	3	3	$-1.623 \cdot 10^4$	-0.04	-0.03	-0.01
4	0	4	$4.443 \cdot 10^8$	4.79*	3.00*	0.80
3	1	4	$8.632 \cdot 10^7$	3.43*	2.14	0.57
2	2	4	$1.753 \cdot 10^7$	0.46	0.29	0.08
1	3	4	$3.763 \cdot 10^6$	0.17	0.11	0.03
0	4	4	$8.670 \cdot 10^5$	0.10	0.06	0.02
5	0	5	$2.640 \cdot 10^8$	0.05	0.03	0.01
4	1	5	$-2.839 \cdot 10^8$	-0.19	-0.12	-0.03
3	2	5	$-1.243 \cdot 10^8$	-0.06	-0.04	-0.01
2	3	5	$-3.958 \cdot 10^7$	-0.03	-0.02	-0.01
1	4	5	$-1.132 \cdot 10^7$	-0.02	-0.01	0.00
0	5	5	$-3.049 \cdot 10^6$	-0.02	-0.01	0.00
6	0	6	$1.303 \cdot 10^{12}$	3.69*	2.31	0.61
5	1	6	$2.444 \cdot 10^{11}$	2.78	1.73	0.46
4	2	6	$4.698 \cdot 10^{10}$	0.39	0.24	0.06
3	3	6	$9.312 \cdot 10^9$	0.13	0.08	0.02
2	4	6	$1.918 \cdot 10^9$	0.07	0.04	0.01
1	5	6	$4.140 \cdot 10^8$	0.05	0.03	0.01
0	6	6	$9.464 \cdot 10^7$	0.03	0.02	0.01
7	0	7	$7.790 \cdot 10^{11}$	0.03	0.02	0.01
6	1	7	$-5.520 \cdot 10^{11}$	-0.10	-0.06	-0.02
5	2	7	$-2.456 \cdot 10^{11}$	-0.03	-0.02	-0.01
4	3	7	$-7.768 \cdot 10^{10}$	-0.02	-0.01	0.00
3	4	7	$-2.218 \cdot 10^{10}$	-0.01	-0.01	0.00
2	5	7	$-6.094 \cdot 10^9$	-0.01	-0.01	0.00
1	6	7	$-1.652 \cdot 10^9$	-0.01	-0.01	0.00
0	7	7	$-4.449 \cdot 10^8$	-0.01	-0.01	0.00
8	0	8	$4.158 \cdot 10^{15}$	2.93	1.82	0.49
7	1	8	$7.695 \cdot 10^{14}$	2.34	1.46	0.39
6	2	8	$1.445 \cdot 10^{14}$	0.36	0.22	0.06
5	3	8	$2.762 \cdot 10^{13}$	0.12	0.07	0.02
4	4	8	$5.397 \cdot 10^{12}$	0.06	0.04	0.01
3	5	8	$1.084 \cdot 10^{12}$	0.04	0.02	0.01
2	6	8	$2.256 \cdot 10^{11}$	0.02	0.02	0.00
1	7	8	$4.900 \cdot 10^{10}$	0.02	0.01	0.00
0	8	8	$1.119 \cdot 10^{10}$	0.02	0.01	0.00

Table A.1.: Translation and rotation invariant moments from the third up to the eighth order of the object from Figure A.4, including the ratio $\mu'_{pq}/\sigma_{\mu'_{pq}}$ with assumed $\sigma_{x,y} = 0.5m, 0.8m$ and $3.0m$. Ratios with an absolute value smaller than 0.01 are shown as 0.00. Moments marked with a * are significantly larger than zero.

References

- ADV, ed. (1989). *ATKIS-Gesamtdokumentation*, Hannover.
- ADV (2006). *ATKIS-Objektartenkatalog*. <http://www.atkis.de> (2006/01/31).
- ALTMANN, D. (1994). *Fuzzy Set Theoretic Approaches for Handling Imprecision in Spatial Analysis*. *International Journal of Geographical Information Systems*, 8:271–289.
- AMBLER, S. W. (2005). *The Elements of UML 2.0 Style*. Cambridge Univ. Press, Cambridge.
- BACHER, U. and H. MAYER (2005). *Automatic Road Extraction from Multispectral High Resolution Satellite Images*. In *International Archives of Photogrammetry, Remote Sensing and Spatial Information Sciences*, vol. 36, part B3/W24, pp. 29–34.
- BALTSAVIAS, E. P. (2004). *Object Extraction and Revision by Image Analysis Using Existing Geodata and Knowledge: Current Status and Steps Towards Operational Systems*. *ISPRS Journal of Photogrammetry and Remote Sensing*, 58(3-4):129–151.
- BARTELME, N. (2005). *Geoinformatik*. Springer, Berlin, 4. ed.
- BAUMGARTNER, A. (2003). *Automatische Extraktion von Straßen aus digitalen Luftbildern*. PhD thesis, Deutsche Geodätische Kommission. Series C, vol. 564.
- BAUMGARTNER, A., S. HINZ and C. WIEDEMANN (2002). *Efficient Methods and Interfaces for Road Tracking*. In *International Archives of Photogrammetry, Remote Sensing and Spatial Information Sciences*, vol. 34, part B3A, pp. 28–31.
- BAUMGARTNER, A., C. STEGER, H. MAYER, W. ECKSTEIN and H. EBNER (1999). *Automatic Road Extraction Based on Multi-Scale, Grouping, and Context*. *Photogrammetric Engineering & Remote Sensing*, 65(7):777–785.
- BLAKE, A. and M. ISARD (1998). *Active Contours*. Springer, London.
- BLOCH, I. (1999). *On Fuzzy Distances and Their Use in Image Processing Under Imprecision*. *Pattern Recognition*, 32(11):1873–1895.
- BLUM, H. (1967). *A Transformation for Extracting New Descriptors of Shape*. In *Models for the Perception of Speech and Visual Form*, pp. 362–380. MIT Press, Cambridge MA.
- BORDES, G., G. GIRAUDON and O. JAMET (1997). *Automatic Road Extraction from Grey-Level Images Based on Object Database*. In *Integrating Photogrammetric Techniques with Scene Analysis and Machine Vision III*, vol. 3072, pp. 110–118. SPIE.
- BOXER, L. (1997). *On Hausdorff-Like Metrics for Fuzzy Sets*. *Pattern Recognition Letters*, 18:115–118.
- BUSCH, A., M. GERKE, D. GRÜNREICH, C. HEIPKE, C.-E. LIEDTKE and S. MÜLLER (2004). *Automated Verification of a Topographic Reference Dataset: System Design and Practical Results*. In *International Archives of Photogrammetry, Remote Sensing and Spatial Information Sciences*, vol. 35, part B2, pp. 735–740.
- BUTENUTH, M., B.-M. STRAUB, C. HEIPKE and F. LANG (2003). *Tree Supported Road Extraction from Aerial Images Using Global and Local Context Knowledge*. In *Lecture Notes in Computer Science*, vol. 2626, pp. 162–171. Springer, Berlin.
- CLEMENTINI, E. and P. DI FELICE (1996). *An Algebraic Model for Spatial Objects with Undetermined Boundaries*. In *Geographic Objects with Indeterminate Boundaries*, vol. 2 of *GIS Data*, pp. 155–169. Taylor and Francis, London.

- DEMPSTER, A. (1967). *Upper and Lower Probabilities Induced by a Multivalued Mapping*. *Annals of Mathematical Statistics*, 38:325–339.
- DIAL, G., L. GIBSON and R. POULSEN (2001). *IKONOS Satellite Imagery and its use in Automated Road Extraction*. In *Automatic Extraction of Man-Made Objects from Aerial and Space Images*, vol. 3, pp. 357–367. Balkema, Lisse.
- DOUCETTE, P., P. AGOURIS, M. MUSAVI and A. STEFANIDIS (1999). *Automated Extraction of Linear Features from Aerial Imagery Using Kohonen Learning and GIS Data*. In *Lecture Notes in Computer Science*, vol. 1737, pp. 20–33. Springer, Berlin.
- DOUCETTE, P., P. AGOURIS and A. STEFANIDIS (2004). *Automated Road Extraction from High Resolution Multispectral Imagery*. *Photogrammetric Engineering & Remote Sensing*, 70(12):1405–1416.
- DUDA, R. O. and P. E. HART (1973). *Pattern Classification and Scene Analysis*. Wiley, New York.
- EGENHOFER, M. J. and R. D. FRANZOSA (1991). *Point-Set Topological Spatial Relations*. *International Journal of Geographical Information Systems*, 5(2):161–174.
- EGENHOFER, M. J. and J. R. HERRING (1990). *Categorizing Binary Topological Relations Between Regions, Lines, and Points in Geographic Databases*. Technical Report, Department of Surveying Engineering, University of Maine.
- FISCHLER, M. A., J. M. TENENBAUM and H. J. WOLF (1981). *Detection of Roads and Linear Structures in Low-Resolution Aerial Imagery Using a Multisource Knowledge Integration Technique*. *Computer Graphics and Image Processing*, 15:201–223.
- FÖRSTNER, W. (1996). *10 Pros and Cons Against Performance Characterization of Vision Algorithms*. In *Workshop 'Performance Characteristics of Vision Algorithms'*, Cambridge.
- GERKE, M. (2002). *Scene Analysis in Urban Areas Using a Knowledge-Based Interpretation System*. In *International Archives of Photogrammetry, Remote Sensing and Spatial Information Sciences*, vol. 34, part 3, pp. 63–66.
- GERKE, M., M. BUTENUTH, C. HEIPKE and F. WILLRICH (2004). *Graph Supported Verification of Road Databases*. *ISPRS Journal of Photogrammetry and Remote Sensing*, 58(3-4):152–165.
- GIBSON, L. (2003). *Finding Road Networks in IKONOS Satellite Images*. In *ASPRS Annual Convention*, Anchorage.
- GIMEL'FARB, G. L. (1996). *Texture Modelling by Multiple Pairwise Pixel Interactions*. *IEEE Transactions on Pattern Analysis and Machine Intelligence*, 18(11):1110–1114.
- GLEMSER, M. (2001). *Zur Berücksichtigung der geometrischen Objektunsicherheit in der Geoinformatik*. PhD thesis, Deutsche Geodätische Kommission. Series C, vol. 539.
- GORDON, J. and E. H. SHORTLIFFE (1990). *The Dempster-Shafer Theory of Evidence*. In [SHAFER and PEARL 1990], pp. 529–539.
- GUNST, M.E. DE (1996). *Knowledge-Based Interpretation of Aerial Images for Updating of Road Maps*. PhD thesis, Netherlands Geodetic Commission Publications on Geodesy, TU Delft. No. 44.
- HAKE, G., D. GRÜNREICH and L. MENG (2002). *Kartographie*. de Gruyter, Berlin, 8. ed.
- HARALICK, R. M. and L. G. SHAPIRO (1993). *Computer and Robot Vision*, vol. 2. Addison Wesley, Reading, MA.
- HEDMAN, K., B. WESSEL and U. STILLA (2005). *A Fusion Strategy for Extracted Road Networks from Multi-Aspect SAR Images*. In *International Archives of Photogrammetry, Remote Sensing and Spatial Information Sciences*, vol. 36, part B3/W24, pp. 185–190.
- HEIPKE, C., A. ENGLISCH, T. SPEER, S. STIER and R. KUTKA (1994). *Semi-Automatic Extraction of Roads from Aerial Images*. In *International Archives of Photogrammetry and Remote Sensing*, vol. 30, part B3/1, pp. 353–360.

- HINZ, S. (2004). *Automatische Extraktion urbaner Straßennetze aus Luftbildern*. PhD thesis, Deutsche Geodätische Kommission. Series C, vol. 580.
- HU, M.-K. (1962). *Visual Pattern Recognition by Moment Invariants*. IRE Transactions on Information Theory, 8:179–187.
- KASS, M., A. WITKIN and D. TERZOPOULUS (1988). *Snakes: Active Contour Models*. International Journal of Computer Vision, 1(4):321–331.
- KOCH, K. R. (1997). *Parameterschätzung und Hypothesentests*. Dümmler, Bonn, 2. ed.
- KOENDERINK, J. (1984). *The Structure of Images*. Biological Cybernetics, 50:363–370.
- KOHLAS, J. and P. A. MONNEY (1995). *A Mathematical Theory of Hints. An Approach to Dempster-Shafer Theory of Evidence*, vol. 425 of *Lecture Notes in Economics and Mathematical Systems*. Springer, Berlin.
- KRAUS, K. (1993). *Photogrammetry*, vol. 1. Dümmler, Bonn, 4. ed.
- KUTTERER, H. and S. SCHÖN (2004). *Alternativen bei der Modellierung der Unsicherheit beim Messen*. Zeitschrift für Vermessungswesen, 129(6):389–398.
- LAMBERT, G. and H. GAO (1995). *Line Moments and Invariants for Real Time Processing of Vectorized Contour Data*. In *Image Analysis and Processing, ICIAP*, vol. 8, pp. 347–352, Berlin. Springer.
- LEE, D. T. (1982). *Medial Axis Transformation of a Planar Shape*. IEEE Transactions on Pattern Analysis and Machine Intelligence, 4(4):363–369.
- LINDBERG, T. (1994). *Scale-Space Theory in Computer Vision*. Kluwer, Boston.
- LOHMANN, G. (1991). *An Evidential Reasoning Approach to the Classification of Satellite Images*. PhD thesis, DLR-Forschungsbericht 91-29.
- MAYER, H. (1998). *Automatische Objektextraktion aus digitalen Luftbildern*. professoral dissertation, Deutsche Geodätische Kommission. Series C, vol. 494.
- MCKEOWN, D. M. and J. L. DENLINGER (1988). *Cooperative Methods For Road Tracking in Aerial Imagery*. Computer Vision and Pattern Recognition, pp. 662–672.
- NIEMEIER, W. (2002). *Ausgleichsrechnung. Eine Einführung für Studierende und Praktiker des Vermessungs- und Geoinformationswesens*. de Gruyter, Berlin.
- OGNIEWICZ, R. L. and O. KÜBLER (1995). *Hierarchic Voronoi Skeletons*. Pattern Recognition, 28(3):343–359.
- PLIETKER, B. (1997). *Automatisierte Methoden zur ATKIS-Fortführung auf der Basis von digitalen Orthophotos*. In *Photogrammetric Week*, pp. 135–146. Herbert Wichmann, Heidelberg.
- QUINT, F. (1997). *Kartengestützte Interpretation monokularer Luftbilder*. PhD thesis, Deutsche Geodätische Kommission. Series C. vol. 477.
- REQUICHA, A. A. G. (1977). *Mathematical Models of Rigid Solids*. Technical Report 28, University of Rochester, New York.
- ROCHERY, M., I. H. JERMYN and J. ZERUBIA (2004). *Gap Closure in (Road) Networks Using Higher-Order Active Contours*. In *Proc. IEEE International Conference on Image Processing (ICIP)*, Singapore.
- ROSENFELD, A. (1986). *Axial Representations of Shape*. Computer Vision, Graphics and Image Processing, 33:156–173.
- ROTTENSTEINER, R., G. SUMMER, J. TRINDER, S. CLODE and K. KUBIK (2005). *Evaluation of a Method for Fusing LIDAR Data and Multispectral Images for Building Detection*. In *International Archives of Photogrammetry, Remote Sensing and Spatial Information Sciences*, vol. 36, part B3/W24, pp. 15–22.

- RUSKONÉ, R. (1996). *Road Network Automatic Extraction by Local Context Interpretation: Application to the Production of Cartographic Data*. PhD thesis, Université de Marne-La-Vallée, Noisy-le-Grand, France.
- SARDANA, H. K., M. F. DAEMI and M. K. IBRAHIM (1994). *Global Description of Edge Patterns Using Moments*. *Pattern Recognition*, 27(1):109–118.
- SHAFER, G. (1976). *A Mathematical Theory of Evidence*. Princeton University Press, Princeton.
- SHAFER, G. and J. PEARL, eds. (1990). *Readings in Uncertain Reasoning*. Morgan Kaufmann, San Mateo, CA.
- SOILLE, P. (1999). *Morphological Image Analysis*. Springer, Berlin.
- SOLBERG, R. (1992). *Semi-Automatic Revision of Topographic Maps from Satellite Imagery*. In *International Archives of Photogrammetry and Remote Sensing*, vol. 29, part B4, pp. 549–556.
- STEGER, C. (1998). *An Unbiased Detector of Curvilinear Structures*. *IEEE Transactions on Pattern Analysis and Machine Intelligence*, 20(2):311–326.
- STOICA, R., X. DESCOMBES and J. ZERUBIA (2004). *A Gibbs Point Process for Road Extraction from Remotely Sensed Images*. *International Journal of Computer Vision*, 57(2):121–136.
- STRAUB, B.-M. (2003). *Automatische Extraktion von Bäumen aus Fernerkundungsdaten*. PhD thesis, Deutsche Geodätische Kommission. Series C. vol. 572.
- STRAUB, B.-M., C. WIEDEMANN and C. HEIPKE (2000). *Towards the Automatic Interpretation of Images for GIS-Update*. In *International Archives of Photogrammetry and Remote Sensing*, vol. 33, part B2, pp. 525–532.
- TEH, C.-H. and R. T. CHIN (1988). *On Image Analysis by the Methods of Moments*. *IEEE Transactions on Pattern Analysis and Machine Intelligence*, 10(4):496–513.
- TÖNJES, R. (1999). *Wissensbasierte Interpretation und 3D-Rekonstruktion von Landschaftsszenen aus Luftbildern*. PhD thesis, Düsseldorf, Germany. VDI-Fortschrittberichte 10, No. 575.
- TUPIN, F., I. BLOCH and H. MAÎTRE (1999). *A First Step Toward Automatic Interpretation of SAR Images Using Evidential Fusion of Several Structure Detectors*. *IEEE Transactions on Geosciences and Remote Sensing*, 37(3):1327–1343.
- VOSSELMAN, G. (1996). *Uncertainty in GIS Supported Road Extraction*. In *International Archives of Photogrammetry and Remote Sensing*, vol. 31, part B3, pp. 909–916.
- WALLACE, S. J., M. J. HATCHER, R. G. LEY, G. PRIESTNALL and R. D. MORTON (2002). *Automatic Differentiation of Linear Features Extracted From Remotely Sensed Imagery*. In *International Archives of Photogrammetry, Remote Sensing and Spatial Information Sciences*, vol. 34, part 3.
- WALTER, V. (2000). *Automatic Change Detection in GIS Databases Based on Classification of Multi-spectral Data*. In *International Archives of Photogrammetry and Remote Sensing*, vol. 33, part B4/3, pp. 1138–1145.
- WIEDEMANN, C. (2002). *Extraktion von Straßennetzen aus optischen Satellitenbildern*. PhD thesis, Deutsche Geodätische Kommission. Series C. vol. 551.
- WIEDEMANN, C., C. HEIPKE, H. MAYER and O. JAMET (1998). *Empirical Evaluation of Automatically Extracted Road Axes*. In *Empirical Evaluation Methods in Computer Vision*, pp. 172–187, Los Alamitos, CA. IEEE Computer Society Press.
- WINTER, S. (1996). *Unsichere topologische Beziehungen zwischen ungenauen Flächen*. PhD thesis, Deutsche Geodätische Kommission. Series C, vol. 465.
- WINTER, S. (1998). *Uncertain Topological Relations between Imprecise Regions*. Technical Report, Fachbereich Geoinformation, TU Wien, Austria.

-
- WORBOYS, M. F. (1998). *Imprecision in Finite Resolution Spatial Data*. *Geoinformatica*, 2(3):257–279.
- WORBOYS, M. F. and P. BOFAKOS (1993). *A Canonical Model for a Class of Areal Spatial Objects*. In *Lecture Notes in Computer Science*, vol. 692, pp. 36–52. Springer, Berlin.
- ZADEH, L. (1965). *Fuzzy Sets*. *Information and Control*, 3(8):338–353.
- ZHANG, C. (2004). *Towards an Operational System for Automated Updating of Road Databases by Integration of Imagery and Geodata*. *ISPRS Journal of Photogrammetry and Remote Sensing*, 58(3-4):166–186.
- ZHANG, C. and E. P. BALTSAVIAS (2002). *Improving Cartographic Road Databases by Image Analysis*. In *International Archives of Photogrammetry, Remote Sensing and Spatial Information Sciences*, vol. 34, part B3, pp. 400–405.
- ZHANG, J. and M. F. GOODCHILD (2002). *Uncertainty in Geographical Information*. Taylor and Francis, New York.

Curriculum vitae – Markus Gerke

Beruf und Ausbildung

Seit Januar 2001	Wissenschaftlicher Mitarbeiter am Institut für Photogrammetrie und GeoInformation, Universität Hannover
Mai 1999 bis Mai 2000	Zivildienst beim Paritätischen Wohlfahrtsverband, Hannover
Oktober 1994 bis Dezember 2000	Studium des Vermessungswesens an der Universität Hannover
Juli 1994 bis September 1994	Praktikum bei den Öffentlich bestellten Vermessungsingenieuren Dr. Fleischer & Doms, Göttingen
August 1981 bis Juni 1994	Schulbesuch, Abitur am Felix-Klein-Gymnasium, Göttingen

Privat

Juni 2004	Geburt Sohn Till
August 2002	Heirat mit Susanne Gerke, geb. Rieke
26. August 1974	Geboren in Göttingen Eltern: Wolfgang Gerke und Vera Gerke, geb. Richter

Acknowledgement – Dank

Dieses abschließende Kapitel möchte ich gerne nutzen, um einigen Menschen einen ganz herzlichen Dank auszusprechen. Die vielen Helfer – sowohl aus dem privaten als auch aus dem fachlichen Bereich – haben die Entstehung dieser Arbeit erst ermöglicht.

Meiner Frau Susanne gilt mein aufrichtiger Dank, vor allem für ihre Unterstützung durch Motivation, Verständnis, Korrekturlesen und das Opfern vieler Feierabende und Wochenenden.

Mein besonderer Dank richtet sich außerdem an ...

meinen Doktorvater, Prof. Dr.-Ing. Christian Heipke, der durch seine erfahrene Anleitung und die zahlreichen wertvollen Diskussionen nicht nur meine fachliche Weiterentwicklung gefördert hat. Ihm habe ich zu verdanken, dass ich während meiner Zeit am IPI, und insbesondere während der Fertigstellung dieser Arbeit, meine Forschungsschwerpunkte nach eigenen Interessen gestalten konnte.

die Korreferenten Prof. Dr.-Ing. Helmut Mayer und Prof. Dr.-Ing. Claus-Eberhard Liedtke, sowie den Gutachter Prof. Dr.-Ing. Dietmar Grünreich, die sich trotz ihrer hohen Arbeitsbelastung bereit erklärt haben, diese Arbeit zu bewerten. Ganz besonders danke ich Helmut Mayer, durch dessen konstruktive Kritik und fachkundigen Rat ich sehr große Hilfe erfahren habe.

meine Kollegen am IPI. Die positive Atmosphäre am Institut ist durch gegenseitige Unterstützung und Rücksichtnahme geprägt. So waren die Diskussionen innerhalb der Bildanalysegruppe stets sehr ergiebig und nützlich für diese Arbeit. Ferner möchte ich mich bei Ulla Wissmann und Adelheid Elmhurst für die Erstellung von Referenzdaten bedanken. Von meinen Ex-Kollegen, Dr.-Ing. Felicitas Willrich und Dr.-Ing. „Benz“ Wolf, habe ich sehr viel gelernt – von der Bildanalyse bis zum Projektmanagement. Dieses Wissen dient immer als wesentliche Grundlage für meine Arbeit.

die Kollegen vom Bundesamt für Kartographie und Geodäsie (BKG) und vom Institut für Informationsverarbeitung (TNT) an der Universität Hannover als Beteiligte am WiPKA-QS-Projekt für die gute Zusammenarbeit. Bei den Kollegen der Technischen Universität München, Fachgebiet Photogrammetrie und Fernerkundung, und dem Landesvermessungsamt Nordrhein-Westfalen möchte ich mich für die Bereitstellung der Straßenextraktionssoftware bzw. der Luftbild- und ATKIS-Daten bedanken.

Anne Menis für die Korrektur des englischen Textes.

meine Eltern und meine Schwiegereltern. Meine Eltern haben mich stets in all meinen Bestrebungen und in jeglicher Hinsicht unterstützt. Außerdem verdanke ich allen vieren durch ihr promptes und flexibles Einspringen als Till-Sitter und „Rund-um-Hilfe“ viel Zeit für diese Arbeit.